

# **Elucidation of the Reinforcement Mechanism of Functionalized Nanoparticles in Silica Loaded Rubber Compounds**

Von der Naturwissenschaftlichen Fakultät der  
Gottfried Wilhelm Leibniz Universität Hannover

zur Erlangung des Grades

Doktorin der Naturwissenschaften (Dr. rer. nat.)

genehmigte Dissertation

von

Minghan Xu, M. Sc. (China)

2017

Referent: Prof. Dr. U. Giese  
Korreferentin: Prof. Dr. C. Vogt  
Tag der Promotion: 22.08.2017

# Elucidation of the Reinforcement Mechanism of Functionalized Nanoparticles in Silica Loaded Rubber Compounds

Minghan Xu, Dissertation, Leibniz University of Hanover, 2017

## Abstract

Nano-sized rubber particles (trade name Nanoprene®) improve the performance of silica loaded tread compounds. Hydroxylated particles show a more beneficial effect than particles with other functional groups (-carboxyl, -dimethyl amino, -pyridine, or -epoxy). For an elucidation of the reinforcement mechanism of the hydroxyl containing nanoparticles compound studies were performed and the silanization rates were determined.

In unvulcanized rubber compounds filler flocculation was reduced by either silanization or by hydroxyl modified nanoparticles. By the combination of both measures the best results were obtained. Also in vulcanizates these measures resulted in an improvement of silica distribution. As a consequence, the mechanical and dynamic mechanical properties were improved. As the silanization of the hydroxyl groups present in the nanoparticles occurred at a significantly lower rate than the silanization of the more acid silanol groups of silica. In model experiments the conversion of the silanol groups was very low (7 – 8 %). It is to conclude that the improvement of silica dispersion is caused by hydrogen bonding of unsilanized silanol groups on the silica surface with the hydroxyl groups of the nanoparticles.

In a second part of the thesis the influence of water swelling was investigated relating to the weight increase, the damping performance, and the Payne effect of the vulcanizates. The weight increase (80 °C/16 weeks) was 22.1 wt.% for the unfilled, 18.5 wt.% for the carbon black filled, and 27.5 wt.% respectively 32.3 wt.% for the silica filled vulcanizates (silanized respectively unsilanized). Only in the silica loaded vulcanizates water caused an additional  $\tan \delta$  peak in the temperature range -5 to 0 °C. It is apparent that this peak was caused by the adsorption of water on the silica surface. At temperatures < 0 °C water is frozen and caused a stiffening of the rubber chains which were chemically bound on the silica surface. In addition, adsorbed water caused a reduction of the Payne-effect which is consistent with a break down of the filler network.

This result shows that there is further potential for the performance improvement of silica loaded tire treads if water can be replaced by an appropriate nonvolatile compounding ingredient.

**Keywords:** functionalized nanoparticles, silanization, filler dispersion, reinforcing mechanism, water swelling

# Untersuchung der Verstärkungswirkung funktionalisierter Nanopartikel in kiesel säure gefüllten Kautschukmischungen

Minghan Xu, Dissertation, Universität Hannover, 2017

## Zusammenfassung

Nanoskalige Kautschukpartikel (Handelsname: Nanoprene®) verbessern die Eigenschaften kiesel säure haltiger Laufflächenmischungen, wobei mit hydroxylmodifizierten Teilchen eine bessere Wirkung als mit Partikeln, die andere funktionelle Gruppen wie -Carboxyl, -Dimethylamino, -Pyridin und -Epoxid enthalten, erzielt wird. Zur Untersuchung der Verstärkungswirkung hydroxylhaltiger Nanopartikel wurden Mischungsstudien durchgeführt und die Kinetik und der Umsatz der Silanisierung bestimmt.

In unvulkanisierten Kautschukmischungen wird die Füllstoffflokulation sowohl durch Silanisierung als auch durch den Zusatz hydroxylmodifizierter Nanopartikel reduziert, wobei eine Kombination beider Maßnahmen den größten Effekt zeigt. Auch in Vulkanisaten führen diese Maßnahmen zu einer Verbesserung der Füllstoffverteilung. Als Konsequenz werden die mechanischen und die mechanisch dynamischen Eigenschaften verbessert. Da die Silanisierung der hydroxyl-modifizierten Nanopartikel sehr viel langsamer als die der aciden Silanolgruppen erfolgt und da der Silanisierungsgrad der Silanolgruppen in Modellexperimenten nur sehr niedrig war (7 – 8 %), ist zu vermuten, dass die Verbesserung der Silicaverteilung durch Wasserstoffbrücken zwischen unsilanisierten Silanolgruppen auf der Silicaoberfläche und Hydroxylgruppen der Nanoteilchen verursacht wird.

In einem zweiten Teil der Arbeit wurde der Wassereinfluß auf die Gewichtszunahme, das Dämpfungsverhalten und den Payne-Effekt von Vulkanisaten untersucht. Die Gewichtszunahme (80 °C/16 Wochen) betrug bei einem ungefüllten (22.1 %), bei einem rußgefüllten (18.5 %) und bei den silicagefüllten Vulkanisaten 27.5 % bzw. 32.3 % (silanisiert bzw. nicht silanisiert). Nur bei den silicagefüllten Vulkanisaten verursacht Wasser ein zusätzliches  $\tan \delta$  Signal im Temperaturbereich vor -5 bis 0 °C. Es ist davon auszugehen, dass dieses Signal durch Wassereinlagerungen auf der Silicaoberfläche verursacht wird. Da Wasser bei Temperaturen < 0 °C als Eis vorliegt, führt es zu einer Versteifung der auf der Silicaoberfläche chemisch gebundenen Polymerketten. Zusätzlich findet die Wasserquellung zu einer Abnahme des Payne-Effekts, d. h. zu einem Abbau des Füllstoffnetzwerks.

Dieses Ergebnis zeigt, dass es für die Eigenschaftsverbesserung silicagefüllter Reifenlaufflächen weiteres Potential gibt, wenn Wasser durch geeignete nichtflüchtige Zusätze ersetzt werden kann.

**Schlüsselwörter:** Funktionalisierte Nanoteilchen, Silanisierung, Füllstoffdispersion, Verstärkungsmechanismen, Wasserquellung

---

**Table of contents**

<b>1</b>	<b>Introduction.....</b>	<b>1</b>
1.1	Historical review .....	1
1.2	Motivation and aim of this thesis.....	3
1.3	Structure of this thesis .....	5
<b>2</b>	<b>Theoretical background .....</b>	<b>9</b>
<b>2.1</b>	<b>Functionalized nano-sized polymer particles.....</b>	<b>9</b>
2.1.1	Characteristics of the nanoparticles .....	9
2.1.2	Synthesis of functionalized nano-sized particles .....	11
2.1.3	Determination of the hydroxyl number .....	15
2.1.4	Nanoparticles with different functional groups.....	16
<b>2.2</b>	<b>Properties and characterization of fumed and precipitated silica.....</b>	<b>17</b>
<b>2.3</b>	<b>Silanization.....</b>	<b>19</b>
2.3.1	Silane coupling agents.....	19
2.3.2	Mechanism and kinetics of silanization reaction.....	21
2.3.3	Factors affecting silanization reaction .....	22
<b>2.4</b>	<b>Filler reinforcement of elastomers .....</b>	<b>24</b>
2.4.1	Contribution of the polymer network .....	25
2.4.2	Hydrodynamic effects .....	25
2.4.3	Polymer-filler interaction .....	26
2.4.4	Filler-filler interaction.....	27
2.4.5	Filler flocculation in a filled compound.....	28
<b>2.5</b>	<b>Crosslinked polymer networks.....</b>	<b>30</b>
2.5.1	Vulcanization process.....	30
2.5.2	Effect of silane on the crosslink density .....	34
2.5.3	Determination of crosslink densities.....	37
2.5.4	Swelling of filler-reinforced vulcanizates .....	40
<b>2.6</b>	<b>Dynamic mechanical properties of vulcanizate.....</b>	<b>41</b>
2.6.1	Energy loss during dynamic load .....	41
2.6.2	Rolling resistance and wet skid performance .....	43
2.6.3	Temperature dependence of moduli and $\tan \delta$ .....	44
<b>3</b>	<b>Results and discussion.....</b>	<b>46</b>
<b>3.1</b>	<b>Silanization of the functionalized nanoparticles .....</b>	<b>46</b>
3.1.1	Features of Nanoprene® grades with different functional monomers.....	46
3.1.2	Test method development using headspace gas chromatography.....	49

---

3.1.3	Silanization of silica and Nanoprene® .....	49
3.1.4	Kinetics of silanization reaction .....	50
<b>3.2</b>	<b>Reinforcing mechanisms of hydroxyl modified nanoparticle in silica hybrid systems .....</b>	<b>57</b>
3.2.1	Filler flocculation and break-down of filler network structure .....	58
3.2.2	Tensile testing .....	60
3.2.3	Dynamic mechanical properties .....	61
3.2.4	Characterization of vulcanizates by transmission electron microscopy (TEM).....	64
3.2.5	Equilibration swelling experiments .....	65
3.2.6	Reinforcement mechanism of silica and Nanoprene® BM75OH.....	68
<b>3.3</b>	<b>Influence of different functionalized nanoparticles on silica hybrid systems.....</b>	<b>70</b>
3.3.1	Influence of different functionalized nanoparticles on silica flocculation .....	71
3.3.2	Properties of unvulcanized compounds .....	73
3.3.3	Tensile testing .....	74
3.3.4	Dynamic mechanical properties.....	76
3.3.5	The other mechanical properties.....	78
<b>3.4</b>	<b>Influence of water on silica loaded vulcanizates.....</b>	<b>80</b>
3.4.1	Features of the silane-activated and silane-free reference vulcanizate .....	81
3.4.2	Influence of water on the weight increase of vulcanizates.....	83
3.4.3	Influence of silane on dynamic mechanical properties after water storage.....	84
3.4.4	Temperature dependence of the rate of water uptake.....	87
3.4.5	Reversibility of water swelling/drying on dynamic mechanical properties .....	88
3.4.6	Hydrolysis of the silanized silica vulcanizate .....	90
<b>3.5</b>	<b>Influence of water on vulcanizates which contain other fillers .....</b>	<b>94</b>
3.5.1	Influence of water on the weight increase of vulcanizates.....	94
3.5.2	Dynamic mechanical properties of the original vulcanizates .....	96
3.5.3	Influence of water on dynamic mechanical properties.....	97
3.5.4	Influence of water on the Payne effect.....	102
<b>4</b>	<b>Conclusions .....</b>	<b>108</b>
<b>5</b>	<b>Experimental part .....</b>	<b>112</b>
<b>6</b>	<b>Literature .....</b>	<b>125</b>
<b>7</b>	<b>Annexes .....</b>	<b>133</b>
	<b>Abbreviations .....</b>	<b>137</b>
	<b>Acknowledgments.....</b>	<b>140</b>
	<b>Curriculum vitae .....</b>	<b>141</b>

# 1 Introduction

## 1.1 Historical review

Rubber is an elastic polymer that has a widely use in today's society. As a result of its economic importance, rubber consumption and/or the growth of rubber consumption is an indicator for the state of the economy of a country and its growth. The earliest natural rubber was identified and collected by the Native Americans in the form of a milky, colloidal suspension (known as latex) from the sap of several varieties of plants which was mainly used for rubber balls and toys<sup>[1]</sup>. The first use of reinforced rubber products was flat cotton composites such as waterproof garments, gloves, shoes, inflatable cushions<sup>[2]</sup>, and it gained considerable importance soon after the discovery of vulcanization with sulfur by Charles Goodyear in 1839<sup>[3]</sup>. In 1895, the first pneumatic tires for automobiles were introduced by Michelin<sup>[4]</sup>. The pneumatic tires were initially based on layers of woven cotton canvas and rubber, and later on, the canvas was replaced by cord fabrics. After the discovery of the reinforcing effect of carbon black in the beginning of the nineteenth century<sup>[5]</sup>, natural rubber started to be used in tire industry. By the use of carbon black modulus, tear strength and wear characteristics of the vulcanizates were significantly enhanced. Besides, the service life of a tire was doubled by applying carbon black as a reinforcing filler, ultimately increasing the demand for carbon black.

A huge improvement of tire performance was the development of precipitated silica by the Columbian Chemical Corporation in 1948<sup>[6]</sup>. Silica was first used in tire technology to improve the adhesion of the rubber compound to steel and cord since the early fifties<sup>[7]</sup>. At a later stage silica was also used as an additive for truck tread compounds and for agricultural tires which are exposed to heavy abrasion in order to reduce chipping and chunking<sup>[8, 9]</sup>. But due to the presence of silanol groups and its high polarity, silica has a strong tendency to agglomeration in non-polar rubber matrices such as natural rubber (NR)<sup>[10]</sup>, polybutadiene rubber (BR)<sup>[11]</sup>, and poly(styrene-co-butadiene) rubber (SBR)<sup>[12]</sup> which are used for the production of tires. As a result, the dispersion of untreated silica in a non-polar rubber matrix is rather poor. In the late 1960s, 3-mercaptopropyl-trimethoxy silane was introduced. By the use of this silane silica agglomeration could be reduced. Unfortunately 3-mercaptopropyl-trimethoxy silane had a short scorch time. In 1972 the more scorch resistant silane bis[3-(triethoxysilyl)propyl] tetrasulfide (TESPT, Si 69<sup>®</sup>) was introduced by Evonik Industries AG (formerly Degussa AG)<sup>[13]</sup>. At sufficiently high temperatures (> 125 °C) Si 69<sup>®</sup> reacts with the silanol groups of silica and renders the silica surface hydrophobic. In addition, the tetrasulfide moiety of Si 69<sup>®</sup> creates sulfur linkages between the unsaturated polymer and the silica

surface. As the crosslinking reaction of the tetrasulfide moiety starts at temperatures  $> 135\text{ }^{\circ}\text{C}$  the temperature window, in which the compounding bis[3-(triethoxysilyl)-propyl] tetrasulfide has to be performed, is rather narrow. As of today a whole range of scorch-resistant bifunctional organosilanes have been developed and are commercially available from different suppliers. The basic chemistry of these silanes, however, is essentially the same as for Si 69®. With the advent of the scorch resistant silanes silica had become an active, high-performance ingredient for the preparation of rubber compounds<sup>[14-18]</sup>.

The use of silica for tires was first mentioned in a Degussa patent<sup>[19]</sup>. The technology was further developed by Bridgestone<sup>[20]</sup> and Michelin<sup>[21, 22]</sup> and was commercially introduced by Michelin in 1992 named as the “green tire technology”. The green tires, however, were still black as the carbon black was not completely substituted by silica. A small portion of carbon black was left in the compound as carbon black is a good protector against UV-radiation and carbon black effects electric conductivity which is need to avoid static loading of the tire during service. The introduction of silica tires into the market resulted in a significant increase of silica consumption.

As of today, silica-based tire treads have a great importance particularly in Europe as these treads are superior over carbon black loaded tire treads regarding the “magic triangle” of the three tire tread properties: rolling resistance, wet skid resistance and abrasion resistance. The “magic properties” depend on each other in a complicated manner. It is not possible to improve one of these properties without the deterioration of one or two of the other properties. Due to the interdependence of these properties they are referred to as “magic”.

The silica technology demands for higher performing raw materials (e.g. polymer and silica) and for a good control of the mixing process. Compared to conventional carbon black tires, the silica-silane system makes tires more energy efficient and provides a higher safety on wet roads. Although green tire technology allowed for a considerable breakthrough, silica adversely affects the abrasion resistance in comparison to tires with carbon black.

For a prospective car purchaser the parameters of the magic triangle work out as hard economic facts and are nearly as significant as the price of a new car. The impact of rolling resistance on the overall economy of a car can be demonstrated by the following simple calculation. It is assumed that the total mileage of a new car is 300,000 km. At an average fuel consumption of 7 l/100 km the total fuel consumption of this car will be 21,000 l. At a price of 1.20 €/l the petrol consumption during the life time of the car amounts to 25,200 €. According to expert estimates, the rolling resistance of tires accounts for about 20 % of the fuel consumption of a car<sup>[23]</sup>. On this basis of the total petrol consumption during the life time



of the car the bill to overcome the total rolling resistance of the tires amounts to 5,040 €. A similar calculation about the impact of abrasion resistance on the overall economy of a car is based on the assumption that the average lifetime of a tire is 40,000 km. For a total mileage of 300,000 km this converts into  $7.5 \times 4$  tires = 30 tires. At tire costs of 100 € per tire the total cost of tires converts into 3,000 €. By these simple calculations it becomes evident that the economic impact of rolling resistance is higher than that of abrasion resistance. Anyway both factors should not be ignored if the overall economy of a car is considered.

The wet grip of tires is mainly associated with safety. Unfortunately a similar calculation about the economic impact of wet grip on the overall economy of a car cannot be performed in a similar straightforward manner. As safety is a major issue in Europe since the 2000s almost all passenger car treads in Europe were equipped with silica and silane<sup>[24]</sup>. It has to be also mentioned in this context that the establishment of ABS braking technology was only possible on the basis of silica-based tire treads<sup>[25]</sup>.

The latest progress in the performance improvement of silica-based tire treads was achieved when functionalized nanoscale polymer additives became commercially available. A series of products was developed by Lanxess<sup>[26]</sup> and commercialized under the trade name Nanoprene®. In addition to the positive effect of silane Nanoprene® further reduces filler agglomeration in silica loaded tire treads. As a result the rolling resistance and the wear resistance are improved.

For the first time, the use of functionalized nanoscale polymer particles enabled an improvement in all three parameters of the magic triangle without any deterioration in a particular property<sup>[27]</sup>.

## **1.2 Motivation and aim of this thesis**

Silica in combination with a silane coupling agent is widely used as a reinforcing filler for passenger car tire treads. Regarding rolling resistance and wet traction the performance of silica tires is superior over that of carbon black loaded compounds. Although as of today, silica is a well-established filler in the tire industry in particular since the introduction of the silanization with scorch resistant silanes there are still some flaws which need to be improved. Improvements are needed regarding a further reduction of silica agglomeration, an improvement in abrasion resistance and a reduction of the complexity of the silanization reaction. As outlined above, the use of functionalized nanoscale polymer particles in particular the hydroxylated Nanoprene® BM75OH grade allows for an improvement of some of these properties. In spite of a vast amount of literature on Nanoprene® most of which is

patent literature<sup>[28, 29]</sup>, there is a lack in the understanding of the reinforcing mechanism of Nanoprene<sup>®</sup>. In order to elucidate the role of Nanoprene<sup>®</sup> in silanized silica compounds from a scientific point of view the following set of questions are addressed in this thesis:

(1) As outlined above, the functionalized nanoscale polymer additive (Nanoprene<sup>®</sup> BM75OH) is used for the improvement of the mechanical and physical properties of silica containing rubber compounds. From the patent literature it is clear that the most beneficial effects are obtained when silica and Nanoprene<sup>®</sup> are present during the silanization reaction. Also a sequential silanization process during which the total amount of silane is distributed between two mixing stages is superior over a mixing process in which the total amount of silane is present in the first mixing stage<sup>[30-32]</sup>. From these observations it is evident that the silanization of a compound which contains silica and Nanoprene<sup>®</sup> is important for the achievement of good mechanical and dynamic properties. Up to today, however, it is not clear if the silanization of the hydroxyl groups of Nanoprene<sup>®</sup> BM75OH occurs under the conditions which are used in a standard mixing and silanization procedure. If the hydroxyl groups of Nanoprene<sup>®</sup> are silanized the next question is about the ratio of the silanization rates of Nanoprene<sup>®</sup> and silica. From a qualitative point of view it is clear that the silanol groups of silica which have a significantly higher acidity than hydroxyl groups will be silanized at a much higher rate. The relative reaction rates of these two silanization reactions, however, are not yet known. This knowledge about the difference in reaction rates could help to understand the reinforcing mechanism of Nanoprene<sup>®</sup>.

(2) The second set of questions refers to the influence of Nanoprene<sup>®</sup> on the filler network of silica loaded compounds. As there is a large polarity difference between silica and the hydrophobic rubber matrix, silica flocculation occurs during the heating up of unvulcanized compounds and also during the early stages of vulcanization before the rubber network is formed. The physical performance of silica filled rubber is significantly impacted by the flocculation process. As a consequence, insight into the impact of Nanoprene<sup>®</sup> on silica flocculation could help to understand the role of Nanoprene<sup>®</sup>.

(3) As the filler/filler network and filler aggregates have an important influence on the dynamic properties and the energy dissipation of vulcanizates the third set of questions is concerned with the influence of Nanoprene<sup>®</sup> on the physical properties of the silica/Nanoprene<sup>®</sup> hybrid systems. The properties, regarding the stress/strain-performance, the dynamic properties, etc., depend to a high extent on filler dispersion. A compound study in which the impacts of Nanoprene<sup>®</sup>, silica, and silane are systematically investigated will

yield information about the efficiency of silica dispersion by either silanization, or by the use of Nanoprene® or by a combination of both measures.

(4) Up to now it is not clear to which extent silica preserves its hydrophilic nature in a vulcanizate and how water influences the polymer-filler interaction and the vulcanizate properties. There are some publications on the interaction of water with silica surfaces<sup>[33]</sup>. From these publications it is well known that the interaction between silanol groups and adsorbed water occurs by hydrogen bonds<sup>[34]</sup>. There is just one publication which addresses the influence of water on the dielectric properties of silica loaded rubber compounds by Schwartz et al.<sup>[35]</sup>. In this publication it was demonstrated by dielectric spectroscopy that water generates a new response with a lower frequency than the main segmental relaxation of the polymer chains. The low frequency peak was assigned to a hydration layer around the silica particles. However, the influence of water on the dynamic mechanical properties of the vulcanizates has not been investigated, so far.

From this background the influence of water on the mechanical properties of vulcanizates which are either filled with silica or with silica and Nanoprene® (without and with silanization) will be investigated. Another question which is also addressed in this context is whether hydrolysis of the  $-\text{CH}_2-\text{O}-\text{Si}(\text{OR})_2-\text{CH}_2-$  bonds which are (possibly) formed by the silanization of Nanoprene® has an impact on the mechanical properties of silica/Nanoprene® composites. In these studies silanized silica compounds (without Nanoprene®) which contain  $\equiv\text{Si}-\text{O}-\text{Si}(\text{OR})_2-\text{CH}_2-$  bonds are included as a reference as these bonds are known to be significantly more stable towards hydrolysis than  $-\text{CH}_2-\text{O}-\text{Si}(\text{OR})_2-\text{CH}_2-$  bonds.

(5) As outlined above the standard Nanoprene® grade BM75OH contains hydroxyl groups. In the fifth aspect of this thesis nanoscale particles with other functional groups are evaluated. The question to be answered is: are there functional groups which will render the nanoscale polymer particles a better performance than the established hydroxyl modified nanoparticles.

### 1.3 Structure of this thesis

The research work which was performed in the context of the present thesis is focused on the following major topics:

(1) The silanization kinetics and turnover rates of hydroxyl modified nano-sized particles and of silica.

(2) Characterization of unvulcanized and vulcanized rubber compounds which are loaded with different filler systems.

(3) The influence of water on the filler-polymer interactions and the dynamic mechanical properties of vulcanized compounds

(4) The evaluation of a new range of nanoparticles which contain other functional groups than hydroxyl groups

In chapter 1 an introduction is given in which a historical review is included. Subsequently the motivation and aim of the thesis are outlined.

In chapter 2, an overview on the theoretical background of the following topics is given: nano-sized polymer particles, types of silica and characteristic properties, chemistry of silanization, reinforcing mechanisms, crosslinking chemistry, the characterization of crosslinked rubber networks, and the dynamic mechanical properties of filler reinforced vulcanizates.

In chapter 3 the results of the thesis are presented and discussed.

In chapter 3.1 a new analytical method for the determination of the silanization rates is described. For the silanization reactions the model compound triethoxy(octyl)silane is used. Rates are determined by the evolution of ethanol which is monitored by head space gas chromatography. The amount of ethanol evolved is quantified with an internal standard method. In the first step the silanization of nano-additives (Nanoprene®) which contain different functional groups is studied. The silanization rates are important to the further understanding of the reinforcing mechanism of the functionalized nano-additives in a rubber compound.

In chapter 3.2 there is a focus on a better understanding of the reinforcing mechanisms of hydroxyl modified nanoscale rubber particles. In this context first the silanization kinetics of the hydroxyl modified Nanoprene® grade BM75OH and of silica are determined. Subsequently the results of a comparative compounding study are presented. The study includes a blank compound without any filler, a compound with silica, and a compound which contains silica plus Nanoprene®. The filler loaded compounds are studied with silanization and without. The results allow conclusions about the reinforcing mechanism of hydroxyl modified nanoscale particles (Nanoprene® BM75OH) in a silanized silica hybrid filler system.

As continuation of this section filler flocculation and the subsequent break-down of the filler network are studied with a Rubber Process Analyzer (RPA). Furthermore, the filler dispersion is investigated by stress/strain tests, by dynamic measurements (temperature and strain sweeps), and also by transmission electron microscopy (TEM). In order to determine the

crosslink density and to evaluate the matrix-filler interaction, equilibrium swelling experiments are performed on vulcanized samples. For the swelling experiments toluene is used as a solvent.

In another aspect of this thesis the performance of nanoparticles which were synthesized with other functional monomers are evaluated in chapter 3.3. The functional monomers comprise acrylic acid, 2-vinylpyridine, 4-vinylpyridine, glycidyl methacrylate, and 2-dimethylamino ethyl methacrylate. With the hydroxyl modified nanoparticles as a reference a comparative study is performed in which the silanized silica compounds are evaluated. The properties of the unvulcanized compounds are first investigated by rheometrical properties, scorch, Mooney viscosity and Mooney relaxation. Further, the vulcanizates are characterized by strain-stress measurements, dynamic mechanical analysis, hardness, rebound resilience, compression set and abrasion resistance.

In chapter 3.4 the influence of water on two silica loaded compounds is investigated. Only one of these compounds is silanized. For the determination of the water uptake the temperature and the time of water storage are varied and an Arrhenius plot is established. Gas chromatography with mass spectrometry detection is used in order to find out if hydrolysis occurs during water exposure. Also TEM is applied in order to find out if the morphology of the silica compound changes by the exposure to water. The influence of water on the damping process is studied prior to water storage, after water storage and after drying of the water swollen vulcanizates. In this part of the study many aspects on the influence of water are covered.

As the dynamic properties of silica-loaded vulcanizates are significantly affected by the amount of absorbed water, the investigations on the influence of water are extended and vulcanizates which are loaded with other fillers are included. These fillers comprise carbon black, and Nanoprene® BM75OH. As a reference the unfilled system is included. The dependence of the different filler systems on the influence of water is studied with a particular emphasis on the Payne effect.

Chapter 4 gives the overall conclusions of this thesis.

The experimental part is found in chapter 5 and literature quotations are given in chapter 6.

Parts of this thesis have already been published. Other parts are under preparation for publication:

- [1] Minghan Xu, Ulrich Giese, Werner Obrecht, Thomas Frueh, Influence of Water on Dynamic Mechanical Properties of Silica Loaded Tire Tread Vulcanizates, *Kautschuk Gummi Kunststoffe*, 2017, 4 (17), 47-53.
- [2] Minghan Xu, Ulrich Giese, Thomas Frueh, Werner Obrecht, Reinforcing Mechanisms of Filler Hybrid Systems Based on Nanoscale Rubber Particles and Silica (publication under preparation).
- [3] Minghan Xu, Ulrich Giese, Werner Obrecht, Thomas Frueh, Effect of Water on Dynamic Mechanical Properties of Vulcanizates Which Contain Different Fillers (publication under preparation).
- [4] Minghan Xu, Ulrich Giese, Werner Obrecht, Thomas Frueh, Evaluation of the Reinforcement Mechanism of Different Functionalized Nanoparticles in Silica Loaded Rubber Compounds (publication under preparation).

## 2 Theoretical background

According to the structure of this thesis in the present chapter an overview on the following topics is given: functionalized nano-sized polymer particles, silica, silanization chemistry, rubber reinforcement, rubber networks, and dynamic mechanical properties of vulcanizates.

### 2.1 Functionalized nano-sized polymer particles

#### 2.1.1 Characteristics of the nanoparticles

As outlined before, the functionalized nano-sized polymer particles were developed by Lanxess as an additive for silica containing rubber compounds. A range of hydroxylated grades which differ in the monomer composition, respectively the glass transition temperature ( $T_g$ ) is commercially available under the trade name Nanoprene<sup>®</sup>. According to Lanxess the most common grade is designated as Nanoprene<sup>®</sup> BM75OH which is mainly based on polybutadiene. This grade is hydroxyl modified and has a glass transition temperature ( $T_g$ ) of about  $-75\text{ °C}$ <sup>[27]</sup>.

According to Lanxess Nanoprene<sup>®</sup> is prepared by emulsion polymerization. At the end of the polymerization process a polymer latex is obtained. The latex consists of spherical polymer particles which are dispersed in the aqueous phase. The diameter of one particle is about 50 nm and the particle size distribution is very narrow<sup>[27]</sup>. In order to avoid aggregation respectively agglomeration of the nanoscale particles which occurs during the separation of the particles from the latex and the subsequent drying Lanxess characterizes the nanoparticles in the latex stage by the use of analytical ultracentrifugation. The particle size<sup>[36]</sup> and the particle size distribution<sup>[37]</sup> are determined by methods which are well documented in the literature.

As there are crosslinking and hydroxylating monomers present during the emulsion process the latex particles which are obtained at the end of the polymerization process consist of a highly crosslinked core and a hydroxylated shell. The following scheme of the chemical structure of Nanoprene<sup>®</sup> is given by Lanxess (Figure 1). In the dry stage the interaction of the hydroxyl groups by hydrogen bonding occurs between neighbouring nano-sized particles<sup>[38]</sup>. As a result of hydrogen bonding between the particles Nanoprene<sup>®</sup> bales are quite stable and there is no formation of nano dust during the processing of Nanoprene<sup>®</sup>. The tendency of Nanoprene<sup>®</sup> particles to aggregate is well demonstrated in an electron micrograph by Cataldo<sup>[39]</sup>. In this micrograph not a single particle with a diameter of 50 nm can be detected. The particles form aggregates with aggregate diameters well over 50 nm. In silica compounds hydrogen bonds form between the hydroxyl groups of Nanoprene<sup>®</sup> and the

silanol groups of silica. According to Lanxess the dispersion of silica in a nonpolar rubber compound is significantly improved by the addition of Nanoprene® and the resulting interaction of the silanol groups of silica with the hydroxyl groups of the nano-sized particles.

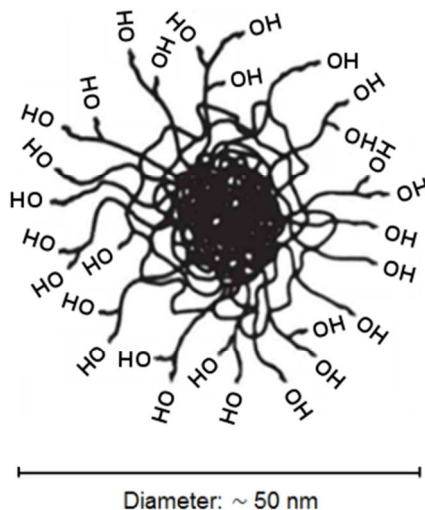


Figure 1. General structure of Nanoprene® with a highly crosslinked core and a hydroxylated surface (the diameter of the rubber particle is around 50 nm)<sup>[27]</sup>

In a rubber compound all sorts of polar groups can be present with which the hydroxyl groups of Nanoprene® can interact principally. The interaction with the polar groups of a carboxylated SBR rubber results in particularly beneficial vulcanizate properties<sup>[40]</sup>. As the respective properties, such as rolling resistance, wet-slip, abrasion resistance, and  $\tan \delta$  maximum in the amplitude sweep, are inferior if the carboxylated SBR is replaced by a standard unmodified SBR this is another indication for the formation of hydrogen bonds between the hydroxyl groups of Nanoprene® and the carboxyl groups of SBR.

According to Lanxess the classification of Nanoprene® as a “filler” or a “rubber” is not as straightforward as it seems<sup>[41]</sup>. As a result of the bulk monomers on the basis of which Nanoprene® is synthesized Nanoprene® has a distinct  $T_g$  which for some of the grades is well below ambient temperature. From this point of view these grades look like rubber. In a compound, however, the performance of Nanoprene® is distinctively different from that of a rubber. As a consequence of the high degree of crosslinking Nanoprene® is unmixable with other rubbers. Also the particle morphology of Nanoprene® is preserved during the mixing process even when exposed to high shear. At the end of the mixing process Nanoprene® forms a separate phase, which shows an identical  $T_g$  in comparison with the nameplate  $T_g$  of the respective Nanoprene® grade. From these perspectives Nanoprene® looks more like a filler. As Nanoprene® preserves its distinct and well defined nameplate  $T_g$  during mixing and



vulcanization it is easy to design rubber compounds with a desired  $T_g$ . Also as a consequence from the high degree of crosslinking compound ingredients such as mineral oil, sulfur, and accelerators are not absorbed by the Nanoprene<sup>®</sup> phase. As Nanoprene<sup>®</sup> is significantly softer than a standard inorganic filler the overall performance of Nanoprene<sup>®</sup> is between that of a “rubber” and a “filler”. As a result, by introducing Nanoprene<sup>®</sup> into the formulation it should be considered as an additive rather than a filler or a rubber. In the formulation it should be added on top of the other compound ingredients<sup>[39]</sup>. Silica based tire compounds which are silanized and which also contain Nanoprene<sup>®</sup> show a series of advantageous properties such as the improvement of wear resistance and the reduction of rolling resistance as indicated by a reduction of  $\tan \delta$  at temperatures  $> 30$  °C. If a Nanoprene<sup>®</sup> grade with  $T_g$  around  $-20$  °C is used a separate  $\tan \delta$  peak shows in the dynamic mechanical spectrum and the expected improvement of wet skid resistance is found in many tread compounds.

### 2.1.2 Synthesis of functionalized nano-sized particles

According to patents which are assigned to Lanxess two synthetic routes are available for the production of Nanoprene<sup>®</sup>. Initially, the so called peroxide route was used<sup>[42, 43]</sup>. In this route the readily available rubber latices which are based on BR, SBR and NBR were used as a latex feedstock. Depending on the different applications the latex feedstocks differ in the degree of crosslinking. Latices which are used for the production of SBR- and NBR-rubbers do not contain crosslinked rubber particles. Other latices which are used for carpet backing, paper coating, or the rubber toughening of thermoplastics etc. contain slightly crosslinked rubber particles. For example, a slightly crosslinked BR-latex is available from the emulsion ABS-production. As the crosslink densities of these feedstocks are not sufficient for the use as additives in tire tread compounds the crosslink densities of these latices have to be increased. This target is achieved by post crosslinking (vulcanization) in the latex stage, which is performed with dicumyl peroxide at a temperature of  $150$  °C. The increase in crosslink densities can be monitored by an increase of the gel content and a decrease of the swelling index. Appropriate solvents for the determination of both properties (gel content and swelling index) are toluene for nonpolar polymers (BR and SBR) and methyl ethyl ketone or acetone for polar polymers (NBR). The swelling index is determined by the weight ratios of wet (solvent swollen) polymer over dry polymer. Subsequent to the crosslinking of the latices they are grafted with functional monomers in order to obtain the different nanorubber grades. Due to the homogenous dispersion of dicumyl peroxide in the bulk of the latices the crosslink structure of these particles is homogeneously distributed over the whole particle and there is no gradient in the crosslink density from the gel core to the outer shell. Due to the limited

amount of residual double bonds which are present after the crosslinking with dicumyl peroxide the subsequent grafting reaction with functional monomers is inefficient and the resulting content of functional groups on the particle surface is low.

Without latex finishing the synthesis of nanoscale rubber particles by the peroxide route involves three distinct process steps:

- Preparation of a slightly crosslinked or uncrosslinked latex feedstock
- Crosslinking reaction with an organic peroxide e.g. dicumyl peroxide
- Grafting of the crosslinked latex with functional monomers

As a consequence of these distinct process steps each of which can be performed in a well-defined manner, the peroxide route is very flexible. It allows the synthesis of nano-sized polymer particles which differ in particle size, chemical composition, degree of crosslinking and the chemistry of grafted functional monomers. On the other hand, due to the high number of process steps the peroxide route is not economic.

For the reduction of manufacturing costs a more economic synthetic route was developed by Lanxess. This route involves one process step in which all necessary monomers including crosslinking and functional monomers are copolymerized in a single process step. This production route is being referred to as “direct polymerization”<sup>[44]</sup>. During the direct polymerization process the size of the particles can no longer be adjusted as crosslinking occurs simultaneously with the polymerization of the other monomers. Within very narrow limits the final diameter of the particles is constantly around 50 nm. On the other hand, the efficiency of the chemical binding of the functional groups is higher than in the peroxide route<sup>[45]</sup>. By the introduction of direct polymerization for the manufacturing of Nanoprene® the number of process steps and also the production costs were considerably reduced.

The direct emulsion polymerization is a free radical polymerization<sup>[46]</sup>. The reaction process involves the emulsification of hydrophobic monomers in water by an oil-in-water emulsifier followed by the initiation reaction with either an oil soluble initiator or a water soluble initiator<sup>[47]</sup>. The oil soluble initiators which are mainly used comprise redox systems on the basis of organic hydroperoxides e.g. tert-butyl hydroperoxide, or p-menthane hydroperoxide in the presence of a reducing agent and Fe<sup>2+</sup>. The ion salt is combined with sequestering agents in order to avoid the precipitation of iron hydroxide in a basic environment. Also oil soluble initiators such as azo-based initiators can be used. The most commonly used water soluble initiators are the ammonium, sodium or potassium salts of peroxydisulfate or peroxydiphosphate. The aims which are pursued during the emulsion polymerization process

are to obtain a stable latex during the whole course of the polymerization, and to achieve a fairly high polymerization rate. The polymerization rate is firstly controlled by the amount of initiator and the polymerization temperature; secondly the initiator or an ingredient of the initiator system is incrementally or continuously added during the course of the polymerization. The emulsifier systems are based on sulfonic acids, fatty acid, modified resin acids and mixtures of the same. In order to achieve good latex stabilities the carboxyl groups of the emulsifier are neutralized with an equimolar amount of alkali metal hydroxide. As high degrees of crosslinking are to be achieved, the emulsion polymerization is not short-stopped at low monomer conversions but the polymerization is allowed to proceed to high monomer conversions. Finally short stopping agents, which are usually reducing agents e.g. hydroxyl amine, diethyl hydroxyl amine, phenols etc. are added to the latex. Subsequently the residual monomers and volatile side products are removed by steam stripping (water distillation).

As a consequence from the direct polymerization process the distribution of crosslinks over the bulk of the latex particle is not homogenous. Contrary to the crosslinked nanoparticles which are obtained from the peroxide route, direct emulsion polymerization yields latex particles which have a gradient of the crosslink density along the radius of the particle. The crosslink density is high in the core of the particle and low at the surface of the particle. In the direct polymerization also high contents of functional monomers can be incorporated.

After the synthesis of the functionalized nano size particles they have to be isolated from the aqueous phase. This process step is referred to as “finishing of the latex” or “latex finishing”. The finishing process does not depend on the route by means of which the latex is obtained (peroxide route or direct polymerization). The isolation can be either achieved by spray drying or by coagulation, washing and drying (Figure 2).

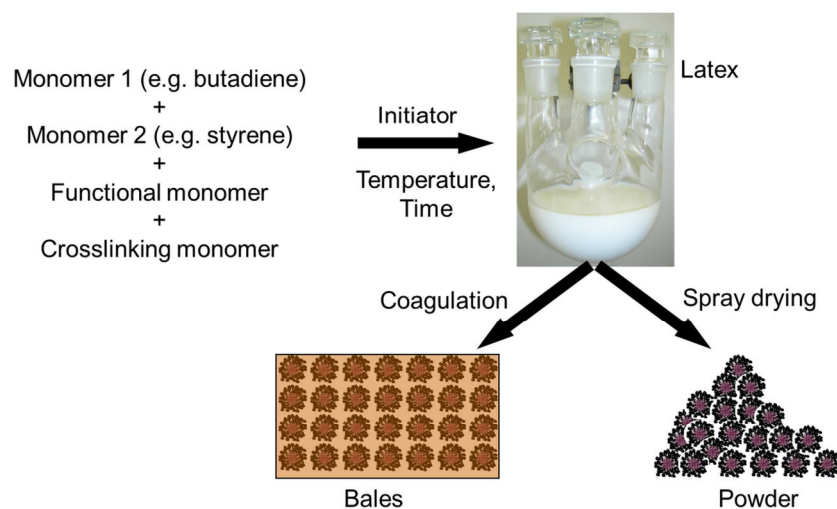


Figure 2. Scheme of latex production and latex finishing<sup>[48]</sup>

As shown in Figure 2 the nano size particles are isolated from the aqueous phase alike other emulsion rubbers. For the coagulation of the latices electrolytes are used. Subsequent to coagulation, the crumbs are washed, mechanically dewatered, thermally dried and baled. Another option is latex finishing by spray drying. In this case free flowing powders of functionalized nano-sized particles are obtained. It has to be emphasized, however, that also in the spray drying process the nano-sized particles aggregate and no single particles are obtained. In the spray drying process huge amounts of water have to be evaporated. Therefore this finishing method is more expensive than latex finishing by electrolyte coagulation. Due to the higher price of spray dried powders they are used for other applications than the manufacturing of tires. The powder applications include the rubber modification of thermoplastics (e.g. polyamides) and of thermoset resins (e.g. epoxy resins, phenol/formaldehyde resins, urea/formaldehyde resins).

It is noteworthy that the glass transition temperature of Nanoprene® mainly depends on the ratio of the copolymerized monomers. As a consequence the glass transition temperature ( $T_g$ ) can be calculated by means of the Fox-Flory equation<sup>[49]</sup>.

$$\frac{1}{T_g} = \frac{w_1}{T_{g1}} + \frac{w_2}{T_{g2}} \quad \text{Equ. (1)}$$

where  $T_{gi}$  is the glass transition temperatures of the homopolymers, and  $w_i$  is the proportion by weight of the monomers. The weight ratio of the bulk components (without crosslinking and functional monomers) is the decisive factor for the approximate calculation of the glass transition temperature of Nanoprene®<sup>[46]</sup>. The Fox-Flory equation does not account for the increase of  $T_g$  by crosslinking. Therefore the Fox-Flory equation yields a  $T_g$  which is lower than the experimentally determined  $T_g$ . In the case of weakly crosslinked gels, the experimentally determined glass transition temperature is higher by about 1 °C than the  $T_g$  which is calculated on the basis of the Fox-Flory equation. For the highly crosslinked gels, the glass transition temperatures can be up to 10 °C higher than the calculated value. Depending on the monomer composition the glass transition temperatures of the nanogels produced by the emulsion polymerization process are usually in the range from -78 to +150 °C. The nanogels which contain the bulk monomer butadiene have a  $T_g$  in the range of -78 to -70 °C. Nanogels which are based on styrene and butadiene cover the  $T_g$ -range from -70 to +100 °C. The  $T_g$ -range > 100 °C is accessible with sterically hindered vinyl monomers like divinylbenzene.

Several thermal analysis techniques are used to determine the glass transition temperature. The  $T_g$  of Nanoprene® can be measured by differential scanning calorimetry (DSC) which is

widely used for investigating the thermal transitions of materials. DSC monitors the difference in heat flow between a sample and an amorphous reference when the sample is heated or cooled. The glass transition of the polymer can be detected by DSC as a stepwise change in the thermal capacity and directly shown in the DSC thermogram.

### 2.1.3 Determination of the hydroxyl number

The content of hydroxyl groups is determined on dried nanogels by the reaction of the hydroxyl groups with a known amount of acid anhydride e.g. acetic anhydride or phthalic anhydride. The respective reaction equation for the determination of the hydroxyl number is given in Figure 3.

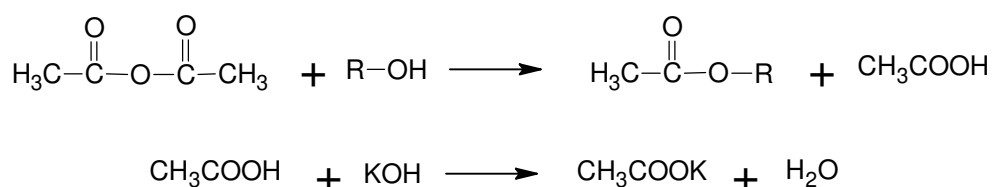


Figure 3. Reaction of hydroxyl groups with acid anhydride and titration of the acid formed<sup>[50]</sup>

In this figure R-OH indicates the standard grade of hydroxylated Nanoprene®. By the reaction of the hydroxyl groups with the acid anhydride a stoichiometric amount of acid is formed. The acid is titrated with an alcoholic KOH (potassium hydroxide) solution under non-aqueous conditions, according to DIN 53240.

The KOH consumption is equivalent to the hydroxyl number of the nanorubber and is termed as hydroxyl number with the dimension mg KOH per gram of polymer. The hydroxyl number can be calculated by the following equation:

$$HN = [(blank - EP1) \times CONC \times TITER \times 56.106 / Sample\ size] + TAN \quad \text{Equ. (2)}$$

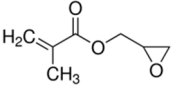
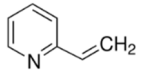
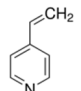
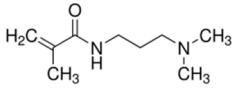
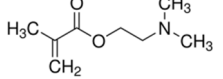
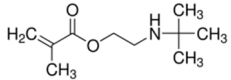
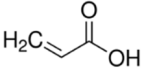
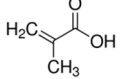
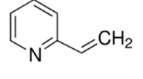
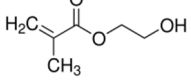
in which HN represents the hydroxyl number [mg KOH/g sample]; blank indicates the blank value of solvent and reagents [ml]; EP1 is the titrant consumption up to the first potentiometric endpoint [ml]; TITER indicates the titer of titrant used [-]; 56.106 is the molecular weight of KOH [g/mol]; TAN is the previously determined acid number of sample [mg KOH/g]. The unit of sample size is in g.

The hydroxyl group is an important functional group and the method presented here is widely used for the determination of the hydroxyl content of intermediates and finished products such as polyols, PU resins, paint resins, lubricants, and so on.

### 2.1.4 Nanoparticles with different functional groups

In order to find out if there are functional groups which provide a better interaction with silica than hydroxyl groups, and which result in improved vulcanizate properties, Lanxess supplied a series of Nanoprene<sup>®</sup> grades with different functional monomers. The designation of the Nanoprene<sup>®</sup> grades with the different functional monomers, the chemical structure of the functional monomers, and the respective CAS-numbers are summarized in Table 1.

Table 1. Range of Nanoprene<sup>®</sup> grades with different functional monomers

Nanoprene <sup>®</sup> grade	Rubber	Functional monomer	CAS No.	Structure
OBR 1504 D	BR	Glycidyl methacrylate (GDMA)	106-91-2	
OBR 1504 F	BR	2-Vinylpyridine (2-VP)	100-69-6	
OBR 1504 G	BR	4-Vinylpyridine (4-VP)	100-43-6	
OBR 1504 H	BR	N-[3-(Dimethylamino)propyl] methacrylamide (DMAPMA)	5205-93-6	
OBR 1504 I	BR	2-(Dimethylamino)ethyl methacrylate (DMAEMA)	2867-47-2	
OBR 1504 K	BR	2-(tert-Butylamino)ethyl methacrylate (BAEMA)	3775-90-4	
OBR 1504 L	BR	Acrylic acid (AA)	79-10-7	
OBR 1504 M	BR	Methacrylic acid (MAA)	79-41-4	
OBR 1504 N	BR	2-Vinylpyridine (2-VP)	100-69-6	
BM75OH*	BR	2-Hydroxyethyl methacrylate (HEMA)	868-77-9	

\* Commercial grade with hydroxyl groups.

The Nanoprene<sup>®</sup> grades shown in Table 1 are all BR-based. They were synthesized by the direct emulsion polymerization route. The functional monomers were chosen in order to achieve good interactions with the silanol groups of silica. The amount of functional monomers which was charged in the polymerization reactor was kept constant on a weight basis (7.5 parts by weight per 100 parts by weight of monomer). As the functional monomers

were added on a weight basis the respective molar contents of the functional monomers are not constant. The hydroxylated Nanoprene® which is commercially available is included in this list. The majority of experiments were performed with this grade performed. This grade is also used as a reference with which the grades with other functional groups are compared.

## 2.2 Properties and characterization of fumed and precipitated silica

Amorphous synthetic silicas are produced by two different processes referred to as fumed silica and precipitated silica<sup>[51]</sup>. Fumed silica, also known as pyrogenic silica, is made by a dry process. The manufacturing process for fumed silica is the vapor phase hydrolysis of silicon tetrachloride in a hydrogen oxygen flame at a temperature of about 1800 °C. Contrary to fumed silica, the precipitated silica is produced by a wet process in which an aqueous solution of sodium silicate is acidified. By the acidification precipitation of silica is achieved. After the precipitation it is subsequently separated by filtration, washed, dried and milled. The properties of fumed and precipitated silica are compared in Table 2.

Table 2. Properties of fumed silica and precipitated silica<sup>[52]</sup>

Property	Fumed silica	Precipitated silica
CAS #	69012-64-2	7699-41-4
SiO <sub>2</sub> [%]	96.0-99.9	97.5-99.4
CaO [%]	trace	0.5
Na <sub>2</sub> O [%]	trace	0-1.5
Loss on ignition [%]	1.0-2.5	3-18
Surface area [m <sup>2</sup> /g]	15-400	45-700
pH, aq. suspension	3.5-8	4-9
Density [g/cm <sup>3</sup> ]	2.2	2.0-2.1
Hardness [Mohs]	6.5	1.0
Dielectric constant [10 <sup>4</sup> Hz]	1.9-2.8	1.9-2.8

It is worth noting that the weight loss on ignition is higher for precipitated silica than for fumed silica, indicating that the silica manufactured by the wet process has a fully hydroxylated surface and also contains water, whereas fumed silica, produced by a dry process at high temperature, although water vapor is one of the reactants, does not. Further, the compacted volume of precipitated silica is lower than that of fumed silica since the former silica consists of 3-dimensional aggregates, whereas the later silica consists of chain-shaped aggregates<sup>[53]</sup>.

Another important feature of silica is the specific surface area defined as the total surface area of a material per unit of mass. Two methods are generally used for determining the specific surface area of silica. The first is Brunauer-Emmett-Teller (BET) method that measures the entire surface area including the mesopores and micropores by using the adsorption of chemically inert gases, such as nitrogen, argon or krypton<sup>[54]</sup>. The BET method is graphically depicted in Figure 4. This method has a potential to overestimate the surface area due to the penetration of the gases into the pores. Conventional silicas have a BET surface area which ranges from 50 to 350 m<sup>2</sup>/g and more preferably from 100 to 300 m<sup>2</sup>/g<sup>[55]</sup>.

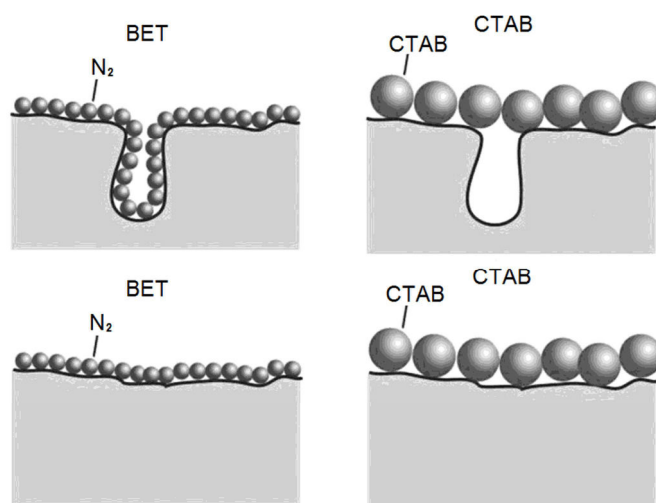


Figure 4. Schematic presentation of the BET and CTAB method used for the characterization of silica<sup>[56]</sup>

Another method for the determination of specific surface areas is the adsorption of the cationic surfactant cetyltrimethylammonium bromide (CTAB). As of today the CTAB method is the most commonly used method for the determination of the specific surface area of silica and the particle size. This method is also used for the shape control of silica particles in the production process. The adsorption of CTAB is schematically shown in Figure 4. As the CTAB molecules have a larger specific adsorption area than the gases used in the BET method they cannot penetrate into the micro pores. Therefore the CTAB method allows for the measurement of the external surface area which is more closely related to the area available for the interaction with rubber. The physical properties of the filled compounds strongly correlate with the CTAB surface area. The CTAB values of silica may vary in the range of 100 to 200 m<sup>2</sup>/g<sup>[57]</sup>.

The surface of precipitated silica is covered with a layer of siloxane groups and acidic silanol groups. The silanol groups are usually referred to as isolated, geminal or vicinal (Figure 5).



These functional groups are randomly distributed over the silica surface. The silanol groups interact with each other resulting in strong agglomerates through hydrogen bonds. Due to the hydrophilic character of silica, the silanol groups also form hydrogen bonds with absorbed moisture. The qualitative and quantitative determination of silanol groups on the silica surface can be performed by using  $^{29}\text{Si}$  solid state NMR spectra<sup>[58-60]</sup> or Fourier Transform Infrared Spectroscopy (FTIR)<sup>[61-64]</sup>.

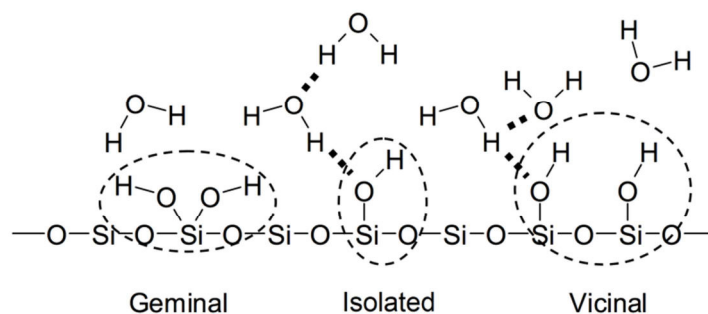


Figure 5. Types of hydroxyl groups on the silica surface<sup>[6]</sup>

As the surface of precipitated silica is covered with a large number of silanol and siloxane groups, the surface energy of silica which depends on dipole-dipole interactions, van der Waals forces, hydrogen bonding and electrostatic interactions is relatively high compared to that of carbon black. Thus, it is difficult to mix silica with nonpolar hydrocarbon rubbers because of the large number of polar groups on the silica surface. In rubber compounds the filler-rubber interaction is important for the final properties. The compatibility between silica and different rubbers has been reported and can be ranked in the following order: NBR > SBR > NR > BR > high vinyl BR > EP(D)M > IIR, in which NBR has the highest compatibility with silica and IIR has the lowest compatibility<sup>[65]</sup>.

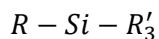
## 2.3 Silanization

Beside the hydrophobization reaction using poly(ethylene glycol) the silanization is now a widely used treatment of the hydrophilic silica surface with a reactive silane (coupling agent) in order to render it more hydrophobic. Through the use of coupling agents, it is possible to promote silica dispersion and to improve in the filler/polymer interaction, which leads to tire tread materials with lower rolling resistance and higher wet traction.

### 2.3.1 Silane coupling agents

As the compatibility between hydrophobic rubber and hydrophilic silica is poor, a reduction of the polarity differences is required. This can be achieved by the use of silane coupling agents

which offer the potential to overcome the agglomeration of silica in rubber compounds. The silane coupling agent is capable of reacting with the silica surface or with both the silica surface and the polymer. Therefore silane coupling agents are widely used in silica loaded rubber compounds. A general chemical structure of silane coupling agents is given below:



where R and R' are organic functional groups attached to silicium, like alkoxy for R' and H, alkyl, SH, or sulfidic bridges for R. The R group can be chosen according to the reactivity of the polymer matrix used, whereas the R' group reacts directly with the silanol groups on the silica surface<sup>[66]</sup>.

One of the most commercial significant coupling agents is bis[3-(triethoxysilyl)-propyl] tetrasulfide (TESPT, Si 69<sup>®</sup>), a bifunctional polysulfidic organosilane. It has been described more extensively in the literature than other silane coupling agents. The use of Si 69<sup>®</sup> improves the reinforcing properties and offers the following advantages<sup>[67]</sup>:

- Reduction of hysteresis in silica filled compounds
- Increase of tensile strength and 300 % modulus
- Improvement of DIN abrasion resistance
- Increase of reinforcing effect of clays and whiting
- Reversion resistor in equilibrium sulfur cure systems

However, due to the splitting of the polysulfide bridges which are present in Si 69<sup>®</sup> reactive sulfur moieties are released which start to react with the polymer matrix at high temperatures even when no vulcanizing agent is present. As a rule of thumb, the reactivity of the polysulfides increases with an increasing length of the sulfur chains. Therefore, a mixing temperature of less than 155 °C should be maintained for Si 69<sup>®</sup> in order to suppress the risk of undesirable scorching.

In order to overcome the scorch problems which are observed with Si 69<sup>®</sup> in the late 1990s Evonik introduced a second generation of silanes with shorter sulfur bridges. The trade names of these second generation silanes are Si 266<sup>®</sup> and Si 75<sup>®</sup>. Compared to the tetrasulfidic organosilane Si 69<sup>®</sup>, the disulfidic silane Si 75<sup>®</sup> (bis[triethoxysilylpropyl] disulphide, TESPd) offers a higher thermal stability, a greater scorch safety, an improved shear stability and therefore allows higher mixing temperatures<sup>[68]</sup>. In the present thesis the disulfidic silane Si 75<sup>®</sup> was used exclusively.

### 2.3.2 Mechanism and kinetics of silanization reaction

The modification of hydrophilic silica surfaces through reactions with organosilanes is used in a manifold of technological fields. The reaction between silica and silane contains two-process-steps. The primary step is the reaction of the first alkoxy group of the silane with a silanol group on the silica surface. This reaction is followed by a secondary reaction, the condensation between pairs of vicinal silane groups which are already bound to the silica surface. A general reaction model of the two steps is presented Figure 6.

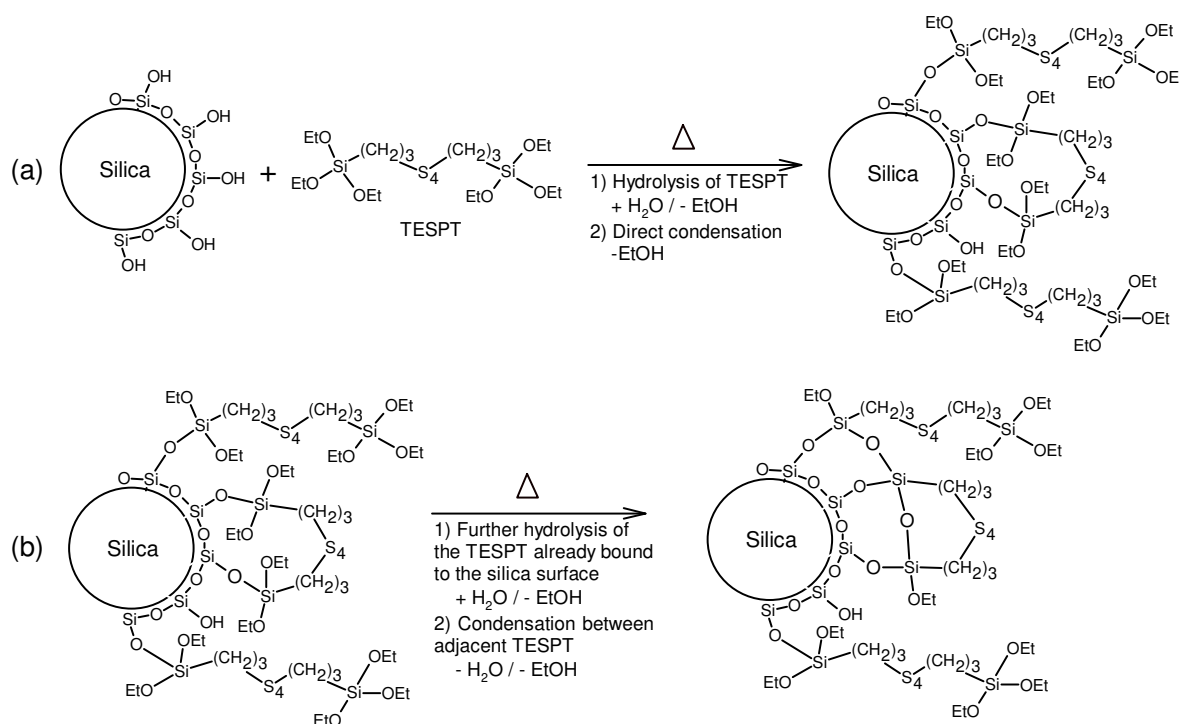
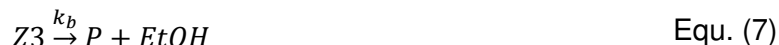


Figure 6. Silanization of silica by TESPT: (a) primary reaction (b) secondary reaction<sup>[58]</sup>

The kinetic parameters of the primary and the secondary reactions can be obtained by a determination of the amounts of released ethanol at different temperatures. In the low temperature range, such as 30 to 60 °C, the primary reaction statistically converts 1 mole of TESPT into 2 moles of ethanol without any secondary reaction proceeding. As a consequence the rate of the primary reaction can be calculated by the following equation:

$$-\frac{d[TESPT]}{dt} = k_a[TESPT] = \frac{1}{2} \frac{d[EtOH]}{dt} \quad \text{Equ. (3)}$$

After the calculation of the rate constant  $k_a$ , it is possible to further calculate the rate of the secondary reaction. Both the primary and the secondary reactions take place at high temperatures, typically in the temperature range of 100 to 200 °C, based on the following model reactions:



in which  $k_b$  is the rate constant of the secondary reaction;  $Z1$ ,  $Z2$ ,  $Z3$  are the intermediate products; and  $P$  is the final product of the silanization between TESPT and silica. The model reactions are predicated on the assumption that the rate constants of all secondary reaction steps are equal. The rate constant  $k_b$  for the secondary reaction is obtained by the following equation:

$$\frac{d[EtOH]}{dt} = 2k_a[TESPT] + k_b[Z1] + k_b[Z2] + k_b[Z3] \quad \text{Equ. (8)}$$

The temperature dependence of the silanization of silica can be described by an Arrhenius equation<sup>[69]</sup>,  $\ln K = \ln A - E_a/RT$ , in which  $E_a$  represents the activation energy and  $R$  is the gas constant. The activation energies are 47 kJ/mol and 28 kJ/mol for the primary reaction and the secondary reaction, respectively<sup>[58]</sup>.

### 2.3.3 Factors affecting silanization reaction

The interaction between silica and silane can indeed vary from physisorption to covalent bonding depending on specific parameters and reaction conditions such as temperature<sup>[70]</sup>, silane type and concentration<sup>[71]</sup>, moisture<sup>[72]</sup>, pH value<sup>[73]</sup> and so on.

In the case of dehydrated silica, the silanization occurs only at high temperatures (> 100 °C) through the direct condensation of alkoxy silanes with the silanol groups on the silica surface and the formation of the respective alcohols<sup>[74]</sup>. Without a prehydrolysis process the silanes do not react with a dehydrated silica surface at low temperatures. However, in the case of a hydrated system, water plays an important role in facilitating the prehydrolysis of the silane, and the mechanism of silanization is more complex. It is now well established that the hydrolysis of silanes consists of several steps. For example, the hydrolysis of TESPT initially proceeds through the conversion of an ethoxy group into a silanol group (Figure 7a). The silanol group of hydrolyzed TESPT can then undergo a condensation reaction with a silanol group on the silica surface, leading to grafted silane species (Figure 7b). The hydrolyzed silane can further react with hydrolyzed or nonhydrolyzed silane via nucleophilic substitution with the release of ethanol (Figure 7c) or water (Figure 7d), respectively. In contrast to the

direct condensation of silane and silanol groups of silica under fully anhydrous conditions, the grafting reaction of hydrolyzed silanol groups with silica starts at much lower temperatures ( $< 70\text{ }^{\circ}\text{C}$ ).

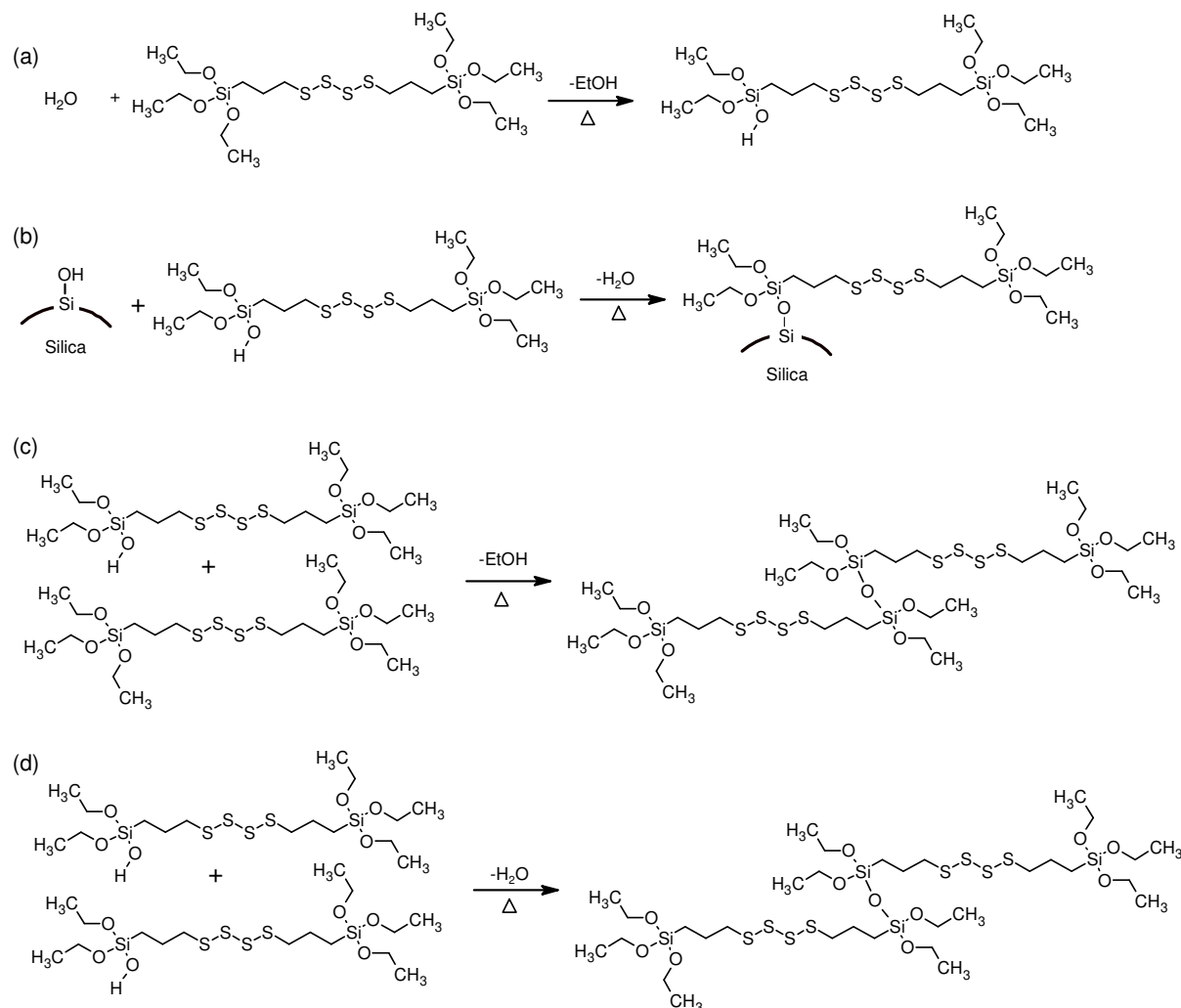


Figure 7. Hydrolysis of ethoxy groups of TESPT and subsequent reactions<sup>[75]</sup>

The rate of silanization is also determined by the chemical structure of the alkoxy group of the silane<sup>[76]</sup>. The rates decrease in the following order: methoxy group  $>$  ethoxy group  $>$  propoxy group and so on. With a longer alkoxy group, such as a propoxy group, the rate becomes too slow for the in situ reaction in an internal mixer. Although the methoxy group reacts rapidly enough, for toxicological reasons, it is unsuited at least for the in situ process because it evolves methanol. As a consequence, silanes with ethoxy groups are widely used in the rubber industry. Also the chemical structure of the alkylidene spacer between the silicon and the sulfur atoms influences the reaction rate. Silanes with longer and higher branched alkylidene spacers show lower rates of silanization<sup>[77]</sup>.

In addition, the pH is important since acidic or alkaline conditions affect the relative rate of silane hydrolysis and condensation. Both alkaline and acidic conditions have a catalytic effect (e.g. amines or acid<sup>[78, 79]</sup>) in the hydrolysis reaction of the silane and thus enhance the efficiency of silanization.

## 2.4 Filler reinforcement of elastomers

In general, vulcanized rubbers (elastomers) which do not contain fillers are too soft for the practical use. This means that the reinforcement of rubber by the incorporation of various solid substances which are uniformly distributed in the elastomer matrix is necessary. Therefore filling or reinforcement of rubbers to achieve improvements in mechanical and physical properties for a given practical application is widely used in the industries since decades. These improvements can be attributed to the inclusion of a solid dispersed phase, resulting in an internal stress that is higher than the external stress applied to the composite. The addition of fillers to rubber compounds not only has a high impact on the static properties but also on the dynamic behaviour of the elastomers. The dynamic modulus  $G^*$  shows a strong strain dependency at low strains according to Payne<sup>[80]</sup>. This stress softening at small deformation is ascribed to the breakdown of the filler-filler network. Besides the strain dependent contribution of the filler network, the filler-rubber interaction, the hydrodynamic effect and the crosslink density of the matrix show an independency on strain<sup>[81]</sup>. The different contributions to the complex modulus of a typical filled compound and their dependency on strain, the so-called “Payne effect”, are depicted in Figure 8.

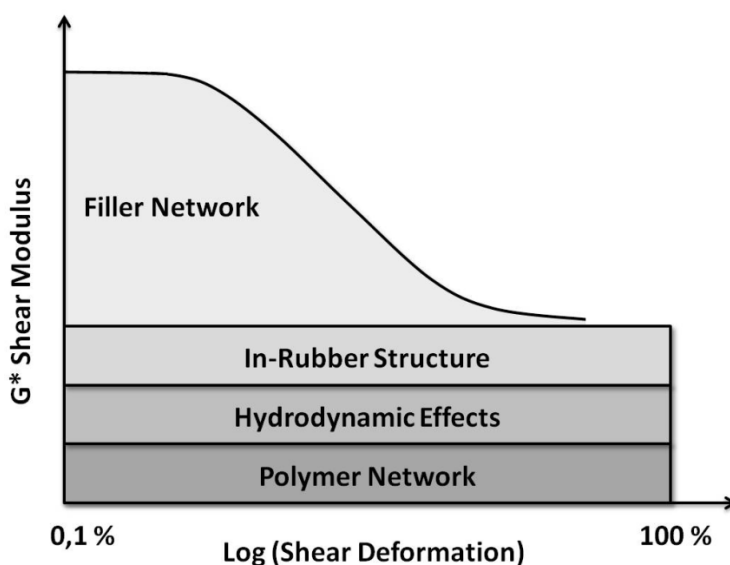


Figure 8. Parameters contributing to the shear modulus of a filled compound<sup>[82, 83]</sup>

### 2.4.1 Contribution of the polymer network

The polymer network contribution depends on the nature of the polymer and the crosslink density of the matrix which is unaffected by deformation. Flory<sup>[84, 85]</sup> has developed a theory about rubber elasticity. According to this theory the shear modulus  $G$  is proportional to the absolute temperature and the polymer network density:

$$G = \nu \times k \times T \quad \text{Equ. (9)}$$

where  $\nu$  is the number of effective chains bounded by cross-linkages in the network,  $k$  is the Boltzmann constant, and  $T$  is the absolute temperature.

In an ideal, perfect network it is assumed that every polymer chain is connected at each chain end to another, and that each crosslink is the terminal point of four chains. Under these conditions the number of chains is exactly twice the number of junction points. Since the original molecules are of finite length, there will be two polymer chain ends for each original molecule which are attached to the network at one end only<sup>[86]</sup>. Thus, the number of effective chains which are attached to the network can be given as follows<sup>[84]</sup>:

$$\nu = \nu_0 \left(1 - 2 \frac{M_c}{M_n}\right) \quad \text{Equ. (10)}$$

here  $\nu_0$  refers to the total number of cross-linkages,  $M_n$  refers to the average number molecular weight of the primary rubber molecules before crosslinking,  $M_c$  is the average molecular weight of a network chain.

### 2.4.2 Hydrodynamic effects

The hydrodynamic effect in this model arises from the presence of rigid particles which also results in one of the strain-independent contributions to the modulus. The incorporation of fillers into elastomer matrices leads to an increase in the viscosity of viscous fluids or an increase in the modulus of the polymer matrix. This phenomenon is well known as the hydrodynamic effect in a filled rubber compound, which mainly depends on two factors, i.e. the volume fraction and the shape factor of the filler particles<sup>[87]</sup>. The modulus change can be described by the Guth-Gold equation in the case of spherical particles in rubber<sup>[88]</sup>:

$$G = G_0 \times (1 + 2.5\phi + 14.1\phi^2) \quad \text{Equ. (11)}$$

In this equation  $G_0$  refers to the modulus of the gum rubber and  $\phi$  refers to the filler volume fraction. However, this equation is inadequate for reinforcing fillers since it is based on some assumptions, i.e. spherical particles, well wetted particles, well dispersed particles, low

strain, negligible particle-particle interaction, and no influence of the characteristics of the polymer.

In practice, it is difficult to satisfy all the conditions because most fillers depart considerably from the spherical shape, and the mobility of the polymer matrix is not uniform due to different polymer-filler interactions. Moreover, filler-filler interaction enables the filler particles to agglomerate, which influences the uniformity and continuity of the rubber matrix. As a consequence, Guth<sup>[89]</sup> introduced a shape factor ( $f$ ) and proposed the following equation for asymmetrically shaped particles:

$$G = G_0 \times (1 + 0.67f\phi + 1.62f^2\phi^2) \quad \text{Equ. (12)}$$

The shape factor  $f$  is described as the ratio between the longest dimension of the particle to the shortest. Equ. (12) is derived on the assumption that the particles are wetted, and that there is no chemical interaction between the particles<sup>[90]</sup>.

As the filler is the rigid phase and cannot be deformed, the external strain amplitude of the polymer matrix is lower than the intrinsic strain yielding a strain-independent contribution to the modulus.

### 2.4.3 Polymer-filler interaction

Another strain independent contribution is attributed to the in-rubber structure, which can be understood as the ability of a filler to immobilize rubber in its structure, even under high deformations<sup>[91]</sup>. The polymer-filler interaction involves the physical adsorption and the chemisorption or a mixture of both. The adsorbed rubber, the so-called bound rubber, in an unvulcanized compound cannot be extracted by good solvents. Bound rubber is the amount of polymer that is bound to the filler before vulcanization and cannot be extracted. There are two typical bound rubber models, i.e. the occluded rubber model and the shell rubber model<sup>[92]</sup> (see Figure 9).

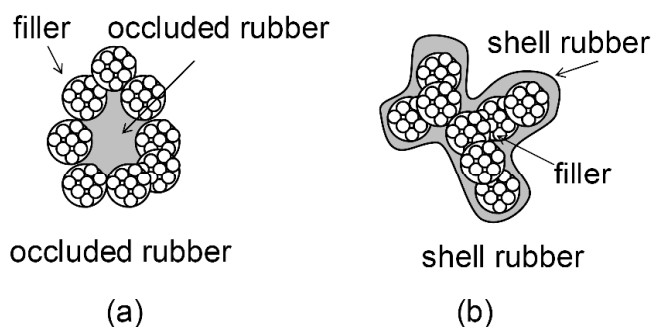


Figure 9. Schematic models for occluded rubber and shell rubber<sup>[6]</sup>



The portion of the rubber which is trapped in the cavities of the filler aggregates is named occluded rubber<sup>[93, 94]</sup>. The occluded rubber is shielded from deformation and therefore increases the effective filler volume. Another result of polymer-filler interaction is the formation of the rubber shell. The rubber shell in compounds and vulcanizates is an immobilized rubber layer surrounding the filler surface resulting from the restriction of the molecular motion of the rubber in the vicinity of filler. The rubber shell is related to the change of segmental mobility rather than the mobility of rubber molecules.

The immobilized rubber chains do not contribute to the elastic behaviour of the rubber matrix, but act as rigid filler particles, and hence increase the effective filler loading and lead to an increase of the strain-independent modulus<sup>[95]</sup>.

#### 2.4.4 Filler-filler interaction

According to Payne the modulus of filled rubber samples is the highest at small amplitudes and gradually decreases to lower values with increasing strain amplitudes. The magnitude of the difference between the moduli at low and high strains ( $\Delta G^*$ ) is defined as the Payne effect<sup>[80]</sup>. The Payne effect plays an important role in the understanding of the reinforcement mechanism of filled rubber compounds. The increasing deformation leads to a successive breakdown of the filler aggregates into a secondary network until, at high strain, the network is completely destroyed as shown in Figure 10.

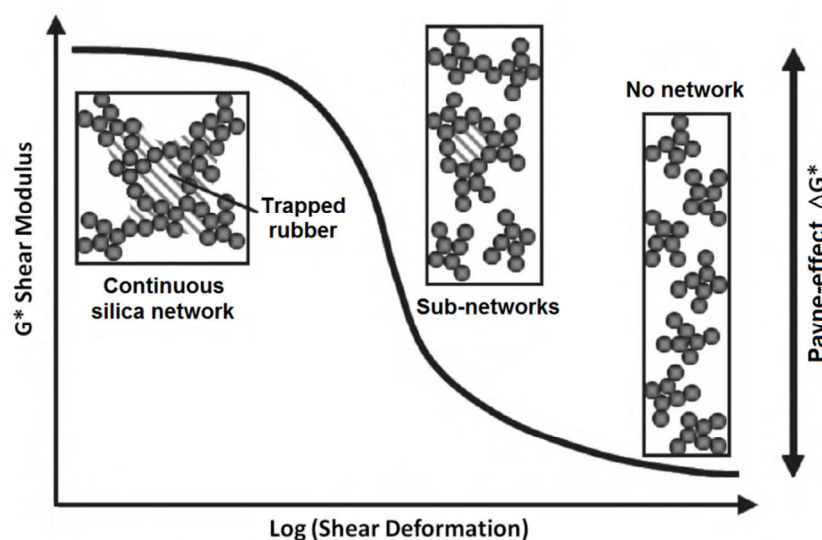


Figure 10. Strain-dependent breakdown of the filler network<sup>[96]</sup>

It is proposed that the trapped rubber is allowed to rejoin the polymer matrix after the breakdown of the continuous filler network, and results in a decrease of the effective filler

volume<sup>[83]</sup>. The decreased effective filler volume fraction results in a reduction of the modulus even at high temperatures.

Although there is no doubt that the Payne effect is caused by the breakdown of the filler network and that a secondary network exists, there are many publications on the influence of the Payne-effect. From these publications it is well known that the amplitude of the Payne effect increases with the filler loading<sup>[97]</sup> and decreases with the increase of temperature<sup>[98]</sup>. It has also been found that increases in surface area and filler structure increase the storage modulus<sup>[99]</sup>. The Payne-effect of silica filled rubber compounds is also influenced by the structure of the silane and its amount.

#### 2.4.5 Filler flocculation in a filled compound

As there is a large polarity difference between silica and tire tread polymers, silica flocculation occurs during the heating up of an unvulcanized compound and during the early stages of vulcanization before the rubber network is formed<sup>[100]</sup>. The reagglomeration of dispersed filler particles or the reformation of a filler network at elevated temperatures, the so called filler flocculation, has an important influence on the dynamic mechanical properties of the filled compounds. The filler aggregation in a network structure results in a nonlinear amplitude behaviour of the polymer compound (Payne effect) and an increased energy dissipation under dynamic conditions.

The filler flocculation can be explained by a filler diffusion at high temperatures. It is well established that the particle diffusion coefficient ( $D$ ) for a colloid system can be expressed as:

$$D = kT \frac{1}{6\pi\eta a} \quad \text{Equ. (13)}$$

in which  $k$  represents the Boltzmann constant,  $T$  represents the absolute temperature,  $\eta$  represents the viscosity of the polymer matrix, and  $a$  represents the radius of the filler particle. The tire tread compounds are normally vulcanized in the temperature range of 140 to 170 °C. During the vulcanization process the increase of temperature results in the decrease of the polymer viscosity and thus the filler diffusion coefficient increases. This means that the filler movement in a rubber matrix greatly enhances and the probability of filler-filler interactions increases. The filler movement can also take place during the processing steps of mixing, milling, and extrusion etc. The motion of filler particles which is caused by either process can be expected to cause filler-filler linkages and as a consequence the formation of a filler network-like structure.

Lin et al.<sup>[101]</sup> studied the flocculation suppression of silica filled compounds using different silane coupling agents and emulsifiers. Experimentally the measurements were performed in a moving die rheometer (MDR) at 100 °C, 0.5 % strain and at a frequency of 1 Hz by observing the storage modulus of the rubber compound in the absence of curatives. As shown in Figure 11, the storage moduli increase due to filler flocculation, and the unmodified silica compound shows a much stronger filler flocculation due to the high polarity of silica in a nonpolar rubber matrix (NR/SBR). The silica flocculation can be reduced by a silane coupling agent, and triethoxy(octyl)silane (OCTEO) is more effective to reduce silica flocculation during thermal annealing than sorbitan monooleate (SMO).

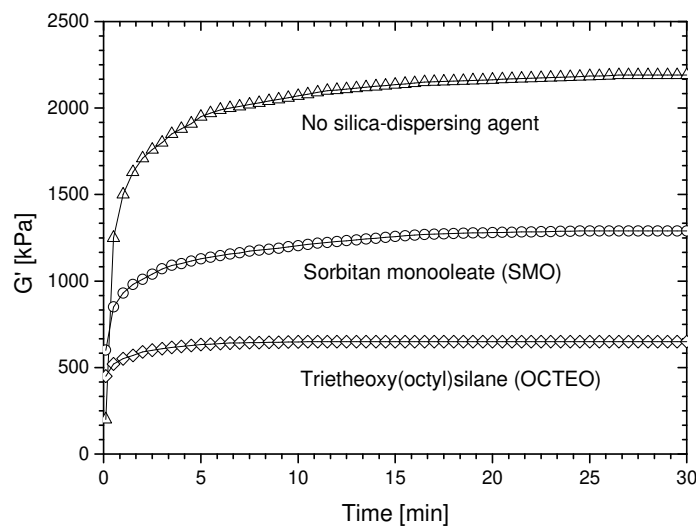


Figure 11. Filler flocculation in silica filled stocks<sup>[101]</sup>

Stöckelhuber et al.<sup>[102]</sup> reported the filler flocculation in carbon black and silica filled compounds after annealing at 160 °C. Without surface modification various silica types showed the highest flocculation tendency in S-SBR. After the addition of silane coupling agents the flocculation was reduced as the compatibility between silica and SBR was improved. By contrast, carbon black exhibited the lowest filler flocculation.

The kinetics of the filler flocculation can be described by a simple kinetic parameter through the reaction rate constant  $k_A$  which is extracted from plots of the normalized modulus ( $G$ ) versus annealing time ( $t$ ), as follows:

$$-\frac{dG}{dt} = k_A G^n \quad \text{Equ. (14)}$$

and

$$G = \frac{G'_t - G'_\infty}{G'_0 - G'_\infty} \quad \text{Equ. (15)}$$

where  $G$  is the normalized modulus,  $k_A$  is the reaction rate constant and  $n$  is the process order,  $G'_0$  is the initial value of the low strain modulus,  $G'_\infty$  is the value of the low-strain storage modulus after infinite annealing time, and  $G'_t$  is the storage modulus measured at an annealing time after the flocculation process begins. The value of the normalized modulus ( $G$ ) indicates the degree of filler dispersion, and Equ. (14) describes how fast a filled system reaches the equilibrium of filler flocculation.

## 2.5 Crosslinked polymer networks

### 2.5.1 Vulcanization process

Rubber must be vulcanized to obtain useful elastomeric and more durable properties. More than 160 years ago, a technology was developed to change the viscous raw rubber to an elastic material<sup>[103]</sup>. This technology, the so-called vulcanization, is a chemical process to improve the rubber elasticity and the strength by heating it in the presence of sulfur or other equivalent curatives, which results in the formation of a three-dimensional crosslinked molecular network. There is a series of vulcanization systems which are used for the vulcanization of rubber: sulfur, peroxides, metal oxides, diisocyanates, hydrosilylation, radiation curing, and so on. The vulcanization system is strongly related to the type of rubber and its chemical structure. Accelerated sulfur vulcanization is the most widely used cure method for polydienes, and sulfenamides being the most widely used accelerators for the vulcanization with sulfur.

The vulcanization process is one of the key factors in determining the properties of rubber products. It involves the conversion of long polymer chains into a network through the formation of crosslinks as illustrated schematically in Figure 12.

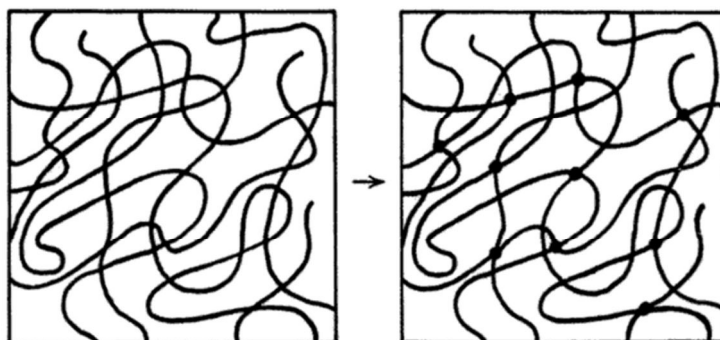


Figure 12. Schematic representation of crosslinking e.g. by the vulcanization rubber<sup>[104]</sup>

An essentially non-Newtonian fluid material is irreversibly transformed into a fully elastic rubbery product during crosslinking. As more crosslinks are formed, the polymer network becomes tighter and the forces necessary to accomplish a given deformation or compression increase.

Characteristics related to the vulcanization process are the time elapsing before crosslinking starts, the rate of crosslink formation, and the final extent of crosslinking. There must be sufficient scorch resistance to permit flowing, shaping, and forming in the mold. Then, it is important to speed up the rate of crosslink formation and to avoid over cure to obtain the optimum performance. These vulcanization characteristics can be relatively easily determined by the increase of the torque as a function of time. The measurements are commonly performed in an oscillating disc rheometer (ODR), moving die rheometer (MDR) or rubber process analyzer (RPA). In one version of the torsional (dynamic) rheometers the rubber compound is enclosed within a heated chamber required to maintain a low amplitude of oscillation at a given temperature. It is implicitly assumed that the torque, or shear modulus, is proportional to the evolving concentration of rubber crosslinks<sup>[105]</sup>.

It is often desirable to increase the vulcanization rate in order to enhance throughput and reduce energy consumption in curing operations. Even a modest increase in the rate of vulcanization can result in greatly increased productivity and substantial cost savings in the production of rubber articles. Initially, vulcanization was accomplished by heating elemental sulfur without accelerator. Sulfur vulcanization can only be applied to rubbers with unsaturated backbone or double bonds in side groups. Only in the presence of accelerators, zinc oxide and stearic acid sulfur vulcanization is fast and the consumption of sulfur for the formation of crosslinks is effective. The organic chemical accelerators were not used until 1906, when Oenslager<sup>[106]</sup> discovered an accelerating effect of aniline on the rate of sulfur vulcanization. In addition, the increase of aniline greatly improved the final vulcanizate properties. Aniline, however, is too toxic for the use in rubber products. Various derivatives of amines were soon introduced which were less toxic and possessed increased acceleration activity. The further developments of the accelerators are composed of one or two sulfur atoms between a pair of organic end groups, structurally containing the common functionality,  $-N=C-S-$ .

The mechanism of accelerated sulfur vulcanization is fairly complex. A typical example of the vulcanization mechanism with sulfur and the accelerator MBT (2-mercaptobenzothiazole) is shown in Figure 13.

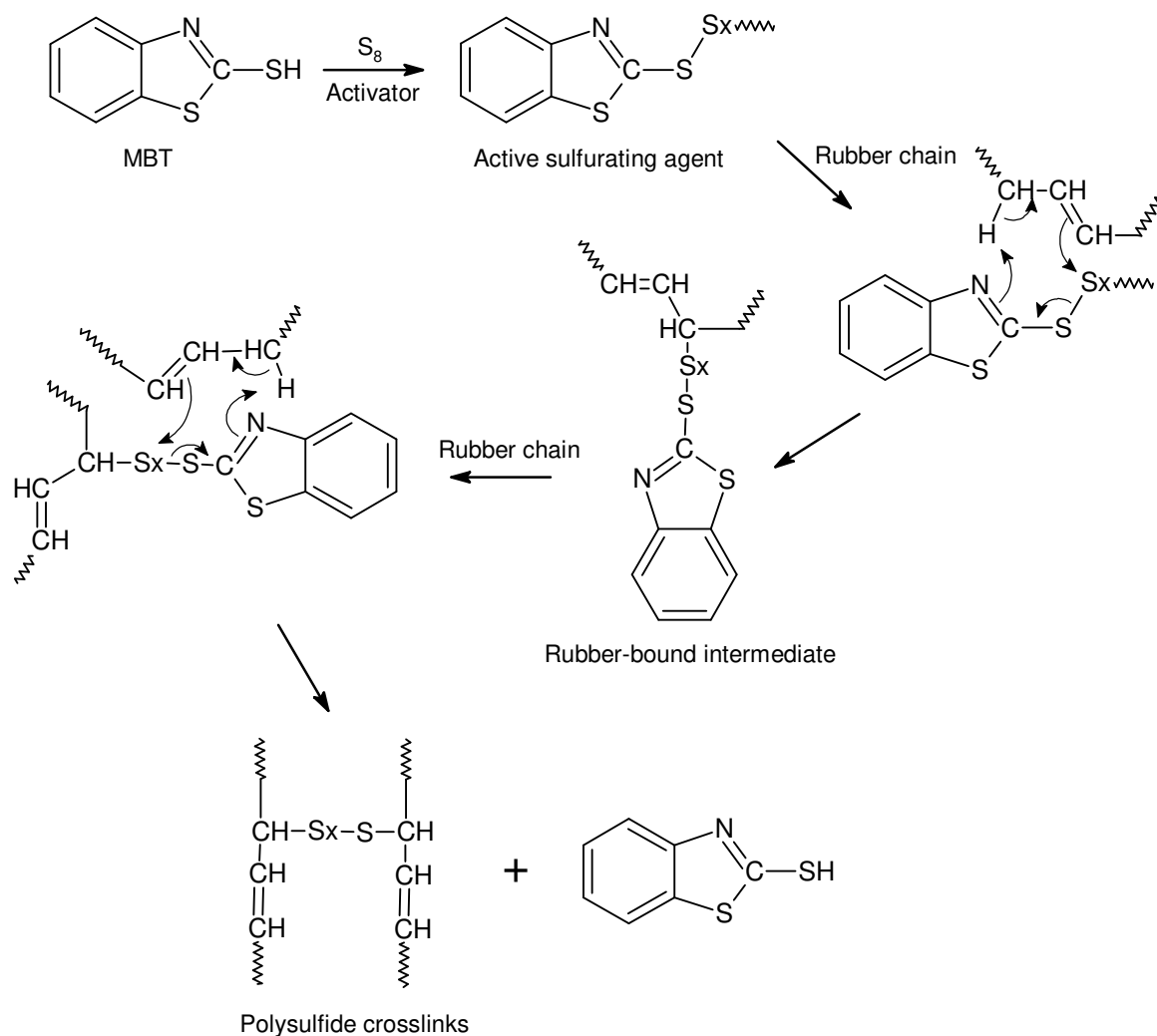


Figure 13. Mechanism of the accelerated sulfur vulcanization of rubber<sup>[67, 107, 108]</sup>

The reaction occurs by a synchronous or ionic mechanism and leads to the formation of sulfur bridges between the rubber macromolecules ( $-C-S_x-C-$ ). As a first step in sulfur vulcanization, an active sulfurating agent is formed by the interaction of the accelerator molecule with sulfur in the presence of an activator e.g. zinc oxide which plays an important role in the formation of such active species. Crosslinks are not formed until all the accelerator is quantitatively consumed<sup>[109]</sup>. By this delayed action the scorch time is increased<sup>[110]</sup>. When the original accelerator molecules are consumed the polysulfidic accelerators react with the unsaturated rubber chains resulting in the formation of rubber-bound intermediates. The rubber-bound intermediates then form polysulfidic crosslinks, and release the accelerator<sup>[111]</sup>.

Depending on the ratio of sulfur/sulfenamide the vulcanization with sulfur is usually classified as conventional (CV), semi-efficient (SEV), and efficient (EV). The levels of sulfur and accelerator in CV, SEV and EV systems are shown in Table 3.

Table 3. CV, SEV and EV vulcanization systems<sup>[112]</sup>

Type	Sulfur [phr]	Accelerator [phr]	Accelerator/sulfur ratio
CV	2.0-3.5	1.2-0.4	0.1-0.6
SEV	1.0-1.7	2.4-1.2	0.7-2.5
EV	0.4-0.8	5.0-2.0	2.5-12

The CV systems are those where a high level of sulfur and a correspondingly low level of accelerators are employed. The CV systems provide better flex and dynamic properties but worse heat and reversion resistance because of a high number of polysulfidic bridges. In the EV systems the sulfur dosage is low and correspondingly the accelerator level is high. The consequence is crosslinks with more mono- or disulfide structure. The thermal and reversion resistance of the EV systems are improved over those of the CV systems. For an optimum balance of properties the SEC systems with an intermediate level of sulfur and accelerator are used. It has to be emphasized that in the sulfur cure systems there is always zinc oxide and stearic acid present as activators. The cure systems based upon sulfur and accelerators are much more complex in mechanism than the other vulcanization methods and produce a high variety of crosslinks together with other chain modifications.

The vulcanization results in an increase of the crosslink density which has a significant impact on the properties of the resulting vulcanizate or elastomer. The following physical properties of rubber are improved by the vulcanization:

- tensile strength
- elasticity
- hardness
- tear strength
- abrasion resistance
- resistance to solvents

The density of crosslinks has to be well controlled in order to prevent overcure and the formation of brittle rubber. Some of the mechanical properties deteriorate when the crosslink density increases over a critical value as illustrated in Figure 14.

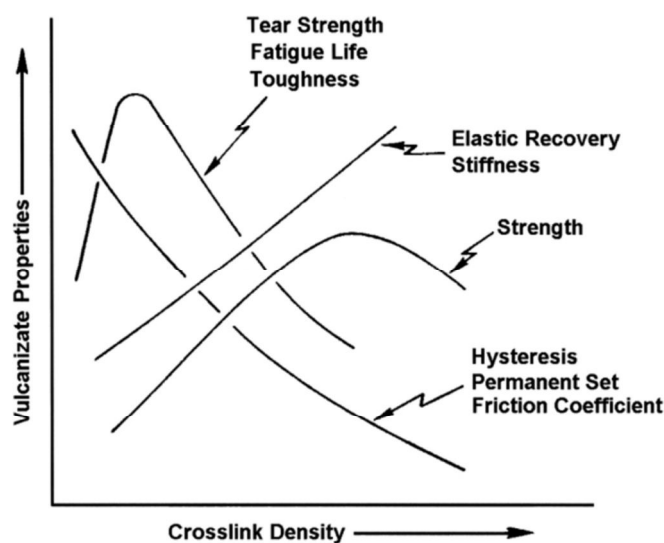


Figure 14. Impact of crosslink density on mechanical properties<sup>[113]</sup>

Therefore, there is an optimal crosslink density for the rubber compound, which can be optimized by selecting the right dosages of sulfur, accelerator, curatives and vulcanization conditions, in particular vulcanization time and temperature.

### 2.5.2 Effect of silane on the crosslink density

As discussed in Chap. 2.3 silane coupling agents especially the bifunctional polysulfidic organosilane Si 69<sup>®</sup> are widely used for the production of silica loaded tire tread compounds. The coupling reaction of the bifunctional polysulfidic organosilane can be divided into two separate reactions. On the one hand, using Si 69<sup>®</sup> as an example, the triethoxysilyl group reacts with the silanol groups on the silica surface during mixing. On the other hand, under vulcanization conditions the tetrasulfane chain reacts with the rubber and both the silica-silane-rubber and rubber-rubber networks are formed.

The reaction of the Si 69<sup>®</sup> polysulfane group in tire tread compounds and the mechanistic model for the accelerated insertion of sulfur into the tetrasulfane chain of Si 69<sup>®</sup> has been reported by Görli<sup>[114]</sup> as shown in Figure 15. The mechanism is in accordance with the 2,2'-Dithiobenzothiazole (MBTS) accelerated vulcanization mechanism, however, the difference is that in the Si 69<sup>®</sup> system MBTS delivers the sulfur chains between the rubber matrix and the sulfide groups of silane.



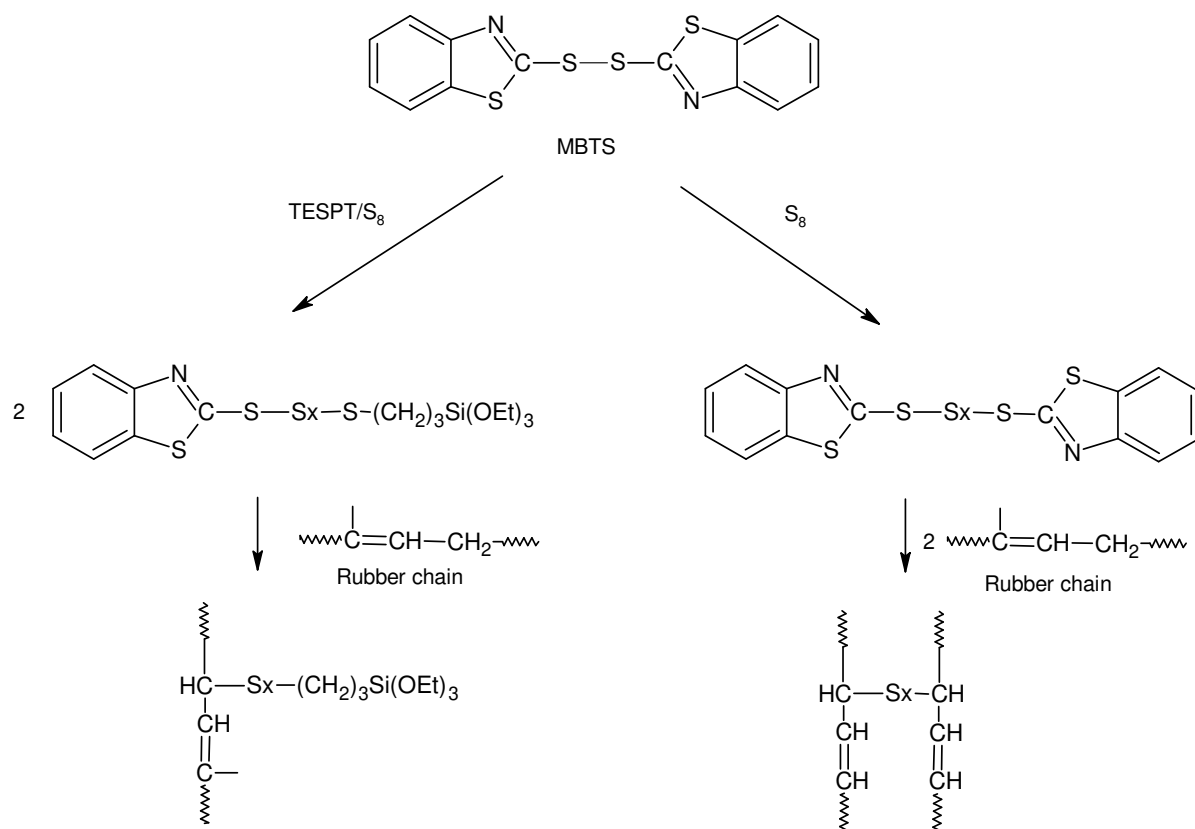


Figure 15. Comparison of the possible reaction models in sulfur/accelerator vulcanization systems with and without TESPT<sup>[14]</sup>

It was reported by Luginsland et al.<sup>[15]</sup> that TESPT actually comprises a mixture of compounds with sulfur chain lengths between  $S_2$  to  $S_{10}$  with an average polysulfane chain length of 3.8, whereas the average sulfur chain length of TESP is 2.1 – 2.2. In order to simulate the reactions of the bifunctional silane in a rubber matrix experiments were carried out in which rubber was replaced by squalene. Under these conditions the average length of the sulfur chain  $S_x$  and the polysulfane chain length distribution could be detected by high performance liquid chromatography (HPLC). The sulfanes from  $S_2$  to  $S_{10}$  could be quantified by different absorption intensities obtained from the HPLC measurements. The length of the sulfur chains was influenced by the reaction conditions such as temperature, the presence of sulfur and accelerator, etc.

It is well established that both TESP and TESPT act increasingly as sulfur acceptors rather than as sulfur donors during the vulcanization process. The addition of sulfur and accelerators is needed in order to achieve an efficient vulcanization. Only in the cases in which no free sulfur or a relatively low amount of sulfur are added to a compound, TESPT which contains sufficiently long polysulfane chains is able to couple silica and rubber by a thermally induced mechanism during mixing at excessive temperatures. In this case TESPT

acts like a sulfur donor. The thermally induced pre-crosslinking during mixing leads to a risk of increased compound viscosity and unwanted pre-scorch of the compound. In contrast to TESPT, without the addition of free sulfur and accelerators the thermostable disulfane silane (TESPD) will not cause the formation of rubber-silane-silica bonds<sup>[116]</sup>.

In silica containing compounds the presence of sulfur and accelerator creates two types of networks in parallel: the rubber crosslinking (polymer-polymer network) and the silica-rubber coupling. Both types of networks form simultaneously and compete until sulfur and accelerator are totally consumed. In Figure 16 the influence of the amount of added sulfur on rubber crosslinking and on silica rubber coupling as well as on the total crosslink density are shown at a constant level of TESPD.

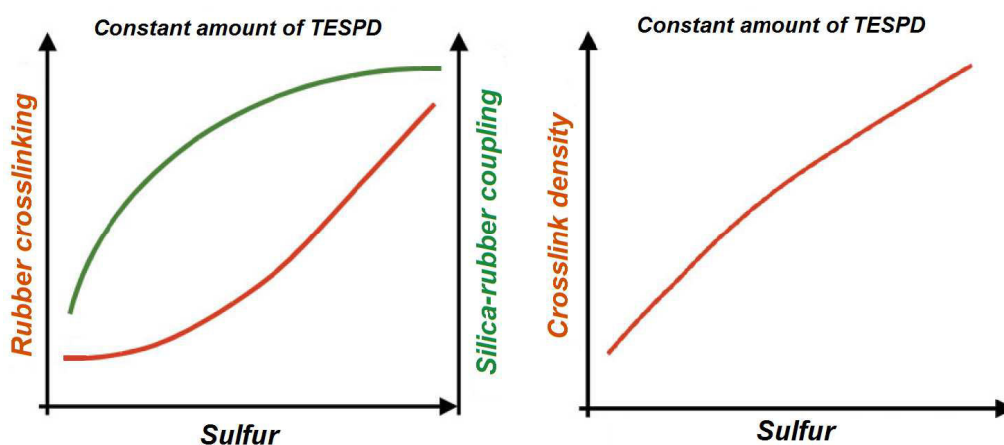


Figure 16. Influence of the quantity of added sulfur on the rubber crosslinking, the silica-rubber network (left) and the resulting crosslink densities (right), at a constant amount of bis[triethoxysilylpropyl]disulfide<sup>[117]</sup>

As shown in Figure 16 increasing dosages of sulfur result in an increase of rubber crosslinking, an increase of silica-rubber coupling and an overall increase of the crosslink density. Regarding the silica rubber coupling there is a threshold which is limited by the amount of TESPD present in the compound.

If the level of sulfur is kept constant the influence of increasing amounts of silane (TESPD) on rubber crosslinking, on silica rubber coupling, and on the total crosslink density are shown in Figure 17.

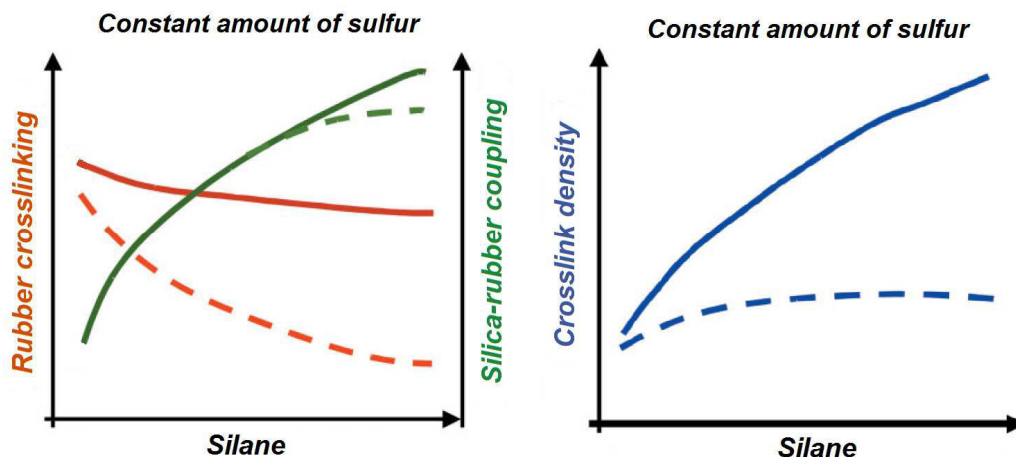


Figure 17. Relationships of the amount of TESPT (full line) and TESPd (dashed line) to the rubber crosslinking, the silica-polymer network (left), and the resulting crosslink densities (right), at a constant amount of sulfur<sup>[117]</sup>

An increase of the TESPd dosing leads to a higher level of silica-silane-rubber coupling. In this case the level of silica-rubber coupling is not limited by the amount of sulfur present in the compound. This result indicates that at low silane levels TESPT acts as a sulfur donor. The rubber-rubber network decreases with increasing dosages of both silanes (TESPT and TESPd), but the decrease with TESPd is more significant than with TESPT. Therefore, adjustments in the levels of the silane and sulfur level are important issues in the optimization of the compound composition towards the performance optimization of rubber compounds.

### 2.5.3 Determination of crosslink densities

It is well established that linear or uncrosslinked polymers are capable of being dissolved in a suitable solvent to form polymer solutions. Vulcanized rubbers, however, are able to absorb a portion of suitable solvent and subsequently swell, but do not dissolve<sup>[118]</sup>. A slightly swollen vulcanizate exhibits elastic rather than viscous properties. The extent of swelling depends on the chemical structure of the polymer, the crosslink density, the solvent, and the temperature. On the one hand, the free energy of mixing, which has to be negative, causes the diffusion of the solvent into the polymer. An increase of the temperature will result in an increase of the entropy of mixing. On the other hand, as the polymer network is expanded by swelling of the solvent, the chains connecting multifunctional network junction points generate an elastic retractive force in opposition to the deformation by swelling, which results in a decrease in chain configurational entropy. The equilibrium of the volumetric swelling will be attained when the opposing entropies balance each other.

When an isotropic polymer sample is immersed in a pure solvent the free energy change of mixing ( $\Delta F$ ) consists of two parts, the ordinary free energy of mixing ( $\Delta F_M$ ) and the elastic free energy ( $\Delta F_{el}$ ) which is associated with the expansion of the polymer network. For a spontaneous mixing process in an isolated swollen system the free energy change ( $\Delta F$ ) can be defined as:

$$\Delta F = \Delta F_M + \Delta F_{el} < 0 \quad \text{Equ. (16)}$$

When a state of equilibration swelling is reached, the change of free energy becomes:

$$\Delta F = \Delta F_M + \Delta F_{el} = 0 \quad \text{Equ. (17)}$$

From Flory-Huggins solution theory<sup>[119]</sup> the free energy change for mixing a polymer with a solvent can be expressed by:

$$\Delta F_M = kT[n_1 \ln v_1 + n_2 \ln v_2 + \chi n_1 v_2] \quad \text{Equ. (18)}$$

where  $n_1$  and  $n_2$  are the mole numbers of solvent and polymer,  $v_1$  and  $v_2$  are volume fractions of solvent and polymer,  $\chi$  is the polymer solvent interaction parameter,  $k$  is the Boltzmann constant, and  $T$  is the absolute temperature.

The chemical potential of the solvent ( $\Delta\mu_1^M$ ) in the mixture relative to the pure component, is obtained by differentiating Equ. (18) with respect to the mole number of the solvent ( $n_1$ ) in the polymer network:

$$\Delta\mu_1^M = N \left( \frac{\partial \Delta F_M}{\partial n_1} \right)_{T,P,n_2} = RT [\ln(1 - v_2) + (1 - \frac{1}{x})v_2 + \chi v_2^2] \quad \text{Equ. (19)}$$

The multiplication of the result by Avogadro's number  $N$  is to obtain the chemical potential per mole. The symbol  $x$  used here represents the number of the polymer segments, which is proportional to the degree of polymerization. For a crosslinked polymer the degree of polymerization is infinite ( $\frac{1}{x} \rightarrow 0$ ).

By analogy with the deformation of rubber, assuming that the deformation process during swelling occurs without an appreciable change in internal energy of the polymer network structure, the elastic free energy  $\Delta F_{el}$  is associated with the entropy change according to the statistical theory of rubber elasticity<sup>[120, 121]</sup>:

$$\Delta F_{el} = \frac{kT v_e}{2} (3\alpha_s^2 - 3 - \ln \alpha_s^3) \quad \text{Equ. (20)}$$

in which  $v_e$  is the effective number of the polymer chains in the network,  $\alpha_s$  is the linear deformation factor by the condition of an isotropic dilatation. It is noted that  $\alpha_s^3 = V/V_0$  in which  $V$  is the volume of the swollen network and  $V_0$  represents the volume of the unswollen polymer. Incorporating the molar volume of the solvent  $\varphi_1$  to evaluate the solvent contribution to the volume yields the following expression:

$$\alpha_s^3 = \frac{1}{v_2} = \frac{V_0 + n_1\varphi_1/N}{V_0} \quad \text{Equ. (21)}$$

Thus, the chemical potential of the elastic reaction ( $\Delta\mu_1^{el}$ ) due to the network extension can be obtained by differentiating Equ. (20) with respect to the mole number of the solvent ( $n_1$ ) in the polymer network:

$$\Delta\mu_1^{el} = N \left( \frac{\partial \Delta F_{el}}{\partial \alpha_s} \right)_{T,P} \cdot \left( \frac{\partial \alpha_s}{\partial n_1} \right)_{T,P} = \varphi_1 \left( \frac{v_e}{V_0} \right) (v_2^{1/3} - 0.5v_2) \quad \text{Equ. (22)}$$

When the swelling reached a state of equilibration, the change of the chemical potentials becomes zero.

$$\Delta\mu_1 = \Delta\mu_1^M + \Delta\mu_1^{el} = 0 \quad \text{Equ. (23)}$$

$$\ln(1 - v_2) + v_2 + \chi v_2^2 + \varphi_1 \left( \frac{v_e}{V_0} \right) (v_2^{1/3} - 0.5v_2) = 0 \quad \text{Equ. (24)}$$

Finally, the crosslink density  $\nu$  is obtained from equilibrium swelling data which is well known as the Flory-Rehner equation<sup>[122]</sup>:

$$\nu = \frac{-[\ln(1 - v_2) + v_2 + \chi v_2^2]}{\varphi_1 (v_2^{1/3} - 0.5v_2)} \quad \text{Equ. (25)}$$

The volume fraction of swollen polymer  $v_2$  can be calculated from the following equation:

$$v_2 = \frac{1}{1 + Q} \quad \text{Equ. (26)}$$

here  $Q$  is the equilibrium swelling ratio, which is given by

$$Q = \left( \frac{W_1 - W_2}{W_2} \right) \cdot \left( \frac{\rho_p}{\rho_s} \right) \quad \text{Equ. (27)}$$

where  $W_1$  is the weight of swollen polymer,  $W_2$  is the weight of unswollen polymer,  $\rho_p$  is the density of polymer, and  $\rho_s$  is the density of the solvent.

The solvent sorption method is a simple and economic technique to characterize polymer networks. At the simplest level of analysis, the steady swelling ratio can be used for quality control and serve as an indexing tool for vulcanizates with different degrees of crosslinking. At a higher level of analysis, the crosslink density of the rubber matrix can be calculated by using the Flory-Rehner equation.

#### 2.5.4 Swelling of filler-reinforced vulcanizates

The interaction of fillers with the rubber matrix can be also studied by means of swelling experiments in suitable solvents. In the presence of fillers, the swelling is influenced not only by the crosslink density, but also by the filler volume fraction, the filler-polymer interaction, as well by the filler dispersion. Overall the filler-polymer contact surface is an important factor. The higher the filler-polymer interaction the higher is the additional reduction in swelling.

The Kraus model has been used for the investigation of the restricted swelling of filler reinforced vulcanizates. It allows for a distinction between particles which are either completely unbonded, or permanently and completely bonded to the polymer. On the basis of the Kraus-plots equation<sup>[123]</sup>, the ratio of the volume fraction of unfilled rubber ( $Vr_0$ ) is plotted over the volume fraction of the filled rubber ( $Vr_f$ ). The slope of the straight line is a measure of the degree of restriction due to the interaction between the polymer and the filler.

$$\frac{Vr_0}{Vr_f} = 1 - m \left[ \frac{\phi}{1 - \phi} \right] \quad \text{Equ. (28)}$$

where  $\phi$  is the filler volume fraction in the vulcanizate, and

$$m = 3C(1 - Vr_0^{1/3}) + Vr_0 - 1 \quad \text{Equ. (29)}$$

The parameter  $C$  in Equ. (29) is named Kraus parameter which is the characteristic constant for the filler-polymer interaction. It is given by the following equation:

$$C = \frac{m - Vr_0 + 1}{3(1 - Vr_0^{1/3})} \quad \text{Equ. (30)}$$

The Kraus parameter  $C$  is dependent on the types of filler, but independent on the used solvent, the filler volume fraction and  $Vr_0$ .

The ratio of  $Vr_0/Vr_f$  decreases with the increase of filler loading, and it varies linearly with  $\phi/(1 - \phi)$ . The parameter  $m$  obtained from the slope of the plot according to Equ. (28) indicates how much swelling is restricted for a given volume fraction of filler. By analogy with the Flory-Rehner theory for the unfilled polymer system,  $Vr_0$  is a measure of polymer-solvent

interaction. If the filler swells as much as the rubber matrix, then the ratio  $Vr_0/Vr_f$  will be equal to unity and independent of the filler volume. However, most of the fillers do not swell and if the movements of polymer chains are restricted because of polymer segments being attached onto the surface of filler particles, then  $Vr_0/Vr_f$  will decrease as the filler fraction increases. Conversely, in a total lack of polymer-filler adhesion, this ratio increases with the increase of filler loading. The reason is that in this case the swollen sample forms a vacuole around each filler particle which will fill with solvent, and this volume of solvent is not taken into account<sup>[124]</sup>. As a consequence, a low value of the filler specific Kraus parameter is taken as evidence of lack of polymer-filler adhesion.

The volume fractions  $Vr_0$  and  $Vr_f$  can be calculated from the equilibrium swelling data based on the following equations<sup>[125]</sup>:

$$Vr_0 = \frac{W_d/\rho_p}{W_d/\rho_p + (W_s - W_d)/\rho_s} \quad \text{Equ. (31)}$$

$$Vr_f = \frac{(W_d - W_f)/\rho_p}{(W_d - W_f)/\rho_p + (W_s - W_d)/\rho_s} \quad \text{Equ. (32)}$$

in which  $W_d$  represents the weight of the sample after swelling and drying,  $W_f$  represents the weight of the non-extractable filler in the sample,  $W_s$  is the weight of the swollen sample, and  $\rho_p$  and  $\rho_s$  are the densities of the polymer and the solvent.

## 2.6 Dynamic mechanical properties of vulcanizate

### 2.6.1 Energy loss during dynamic load

A powerful tool for the investigation of polymer dynamics as well as for the investigation of polymer-filler interactions is dynamic mechanical analysis (DMA). This technique allows measuring the response of viscoelastic properties to a cyclic or sinusoidal deformation as a function of the temperature, frequency or strain amplitude, giving valuable information about the elastic and damping behaviour of elastomers as used for example for the tire tread. Properties like wet skid performance and rolling resistance can be predicted<sup>[126]</sup>.

When a viscoelastic material is subjected to periodically varying stress, strain will vary sinusoidally and lag behind the stress. Thus the strain ( $\epsilon$ ) and stress ( $\sigma$ ) can be described as:

$$\epsilon = \epsilon_0 \sin(\omega t) \quad \text{Equ. (33)}$$

$$\sigma = \sigma_0 \sin(\omega t + \delta) \quad \text{Equ. (34)}$$

in which  $\varepsilon_0$  and  $\sigma_0$  are the maximum strain and maximum stress,  $\omega$  is the radian frequency,  $t$  is the time, and  $\delta$  is the delayed phase angle which indicates the phase difference between the dynamic stress and the dynamic strain as graphically depicted in Figure 18 (a). A large phase angle represents high viscosity and low elasticity. Conversely, a smaller phase angle indicates a higher elasticity as seen in Figure 18 (b).

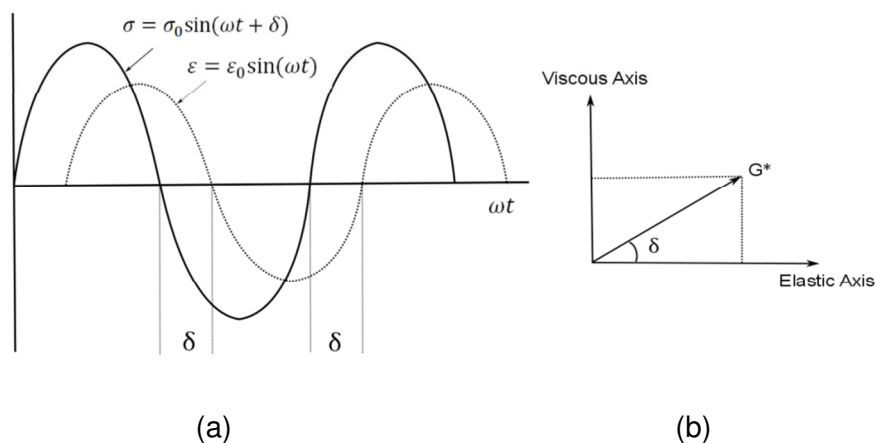


Figure 18. Definition of the phase angle<sup>[127]</sup>

In the uncured state a high elasticity of the rubber could mean that the mixed stock underwent premature vulcanization (scorching). As a result problems in processing such as excessive die swell in extrusions, nerviness, molding problems, dimensional stability, and so on will be observed<sup>[128]</sup>.

The stress can be subdivided further into two contributions, i.e. in phase with strain and 90° out of phase.

$$\sigma = \sigma_0 \sin \omega t \cos \delta + \sigma_0 \cos \omega t \sin \delta \quad \text{Equ. (35)}$$

As polymers display properties of both elastic solids and liquids specific relationships of the dynamic stress-strain behaviour can be expressed by the storage modulus  $G'$  (or elastic modulus), which is the component in phase, and the loss modulus  $G''$  (or viscous modulus), which is out of phase with the oscillatory strain.

$$\sigma = \sigma_0 G' \cos \delta + \sigma_0 G'' \sin \delta \quad \text{Equ. (36)}$$

with

$$G' = (\sigma_0 / \varepsilon_0) \cos \delta \quad \text{Equ. (37)}$$

and



$$G'' = (\sigma_0/\varepsilon_0)\sin\delta \quad \text{Equ. (38)}$$

When the shear modulus is written in the complex form, the complex modulus  $G^*$  is obtained by the real and imaginary part.

$$G^* = \sigma_0/\varepsilon_0 = G' + iG'' \quad \text{Equ. (39)}$$

The storage modulus ( $G'$ ) corresponds to the material's elastic deformation, and the loss modulus ( $G''$ ) corresponds to the material's plastic deformation. The mechanical loss factor is expressed as:

$$\tan \delta = G''/G' \quad \text{Equ. (40)}$$

which indicates the occurrence of molecular mobility and segmental transitions such as the glass transition temperature ( $T_g$ ).

## 2.6.2 Rolling resistance and wet skid performance

Vulcanized rubber (elastomer) is a viscoelastic material, having both elastic and viscous characteristics. When elastomers are deformed they lose part of energy as heat and cannot recover completely due to the viscous properties. Hysteresis loss therefore occurs during dynamic deformation. It has been demonstrated that the hysteresis loss is related to the dynamic properties of an actual vehicle's tire and is generally expressed using  $G'$  and  $G''$ <sup>[129,130]</sup>.

In practice, conventional tread compound development involves the efforts to improve rolling resistance and wet grip performance without deteriorating abrasion resistance. The energy lost when a tire is moving is described as rolling resistance and is proportional to the fuel consumption and CO<sub>2</sub> emission. The rolling resistance can be reduced by decreasing the loss modulus and  $\tan \delta$  of the tread rubber<sup>[131]</sup>. The wet grip capacity is an important safety aspect of a tire. Tires with excellent grip in the wet which are determined by the hysteresis loss of the tread rubber and the adhesion friction force between tires and asperities have shorter braking distances. When a braking force is applied on a wet road, the water film reduces the adhesion friction force, and thus an increase in the hysteresis loss is necessary for the safety aspect<sup>[132]</sup>. As rolling resistance and wet grip performance are contradictory parameters, it is difficult to simultaneously enhance both parameters.

As a consequence, the rolling resistance and wet traction of a tire can be predicted by the frequency dependencies of the storage modulus  $G'$  and the loss modulus  $G''$  of the tire tread compound, as shown in Figure 19.

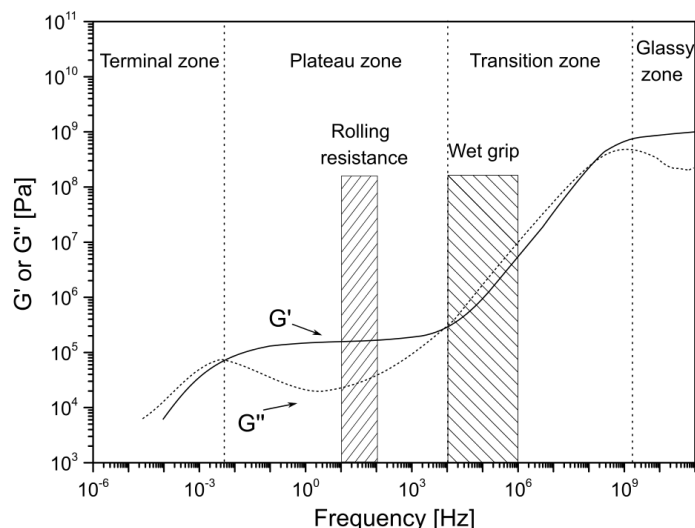


Figure 19. Dependencies of the storage modulus  $G'$  and the loss modulus  $G''$  on frequency of a typical tire tread compound<sup>[133]</sup>

The frequency of deformation depends on the speed of the vehicle and on the asperities of the road surface. As the rolling resistance is generated by the deformation of the tire which occurs once per revolution, the frequency encountered by the speed is between  $10^1$  and  $10^2$  Hz. By contrast, the braking force corresponds to a deformation input frequency of  $10^4$  –  $10^6$  Hz by assuming the space between the asperities is approximately 0.1 to 0.01 mm. It is generally accepted that the wet traction is linked with the dynamic losses in the glass transition region of the polymer<sup>[134]</sup>.

### 2.6.3 Temperature dependence of moduli and $\tan \delta$

With the increase of temperature an amorphous polymer goes from the glassy state to the rubbery state. The temperature at which this transition happens is defined as the glass transition temperature ( $T_g$ ). In the tire industry, very often,  $T_g$  is used as an indicator for the wet grip performance<sup>[135-137]</sup>. As a rule of thumb, it is assumed that the higher  $T_g$  the higher is the wet skid resistance. In most of the cases, the  $T_g$  of rubbers such as polybutadiene and poly(styrene-co-butadiene) are below ambient temperature. At ambient temperatures, the hysteresis is higher for elastomers with a higher  $T_g$ . This can be explained by the Williams-Landel-Ferry (WLF) principle<sup>[138]</sup>. According to the WLF principle the linear viscoelastic behaviour at different temperatures and frequencies can be superimposed into one smooth master curve by a horizontal or vertical shift factor. For instance, the high-frequency data correspond to low temperatures whereas the low frequency data correspond to high temperatures. Therefore, the measurement is performed in the temperature range from about  $-100$  °C to about  $+120$  °C at a constant frequency of around 10 Hz. At 10 Hz the wet

grip with a deformation input frequency of  $10^4 - 10^6$  Hz corresponds to the temperature range from about 0 °C to about 20 °C. As a consequence a rubber with a high  $\tan \delta$  at around 0 °C will enable a reduction of the braking distance on a wet road.

The  $T_g$  of a tire tread compound is an important property as it is an important indicator not only for the wet grip of a tire, but also for the rolling resistance, the low temperature performance, and the abrasion resistance. The temperature dependencies of the storage modulus  $G'$ , the loss modulus  $G''$  and  $\tan \delta$  of a typical SBR compound are shown in Figure 20.

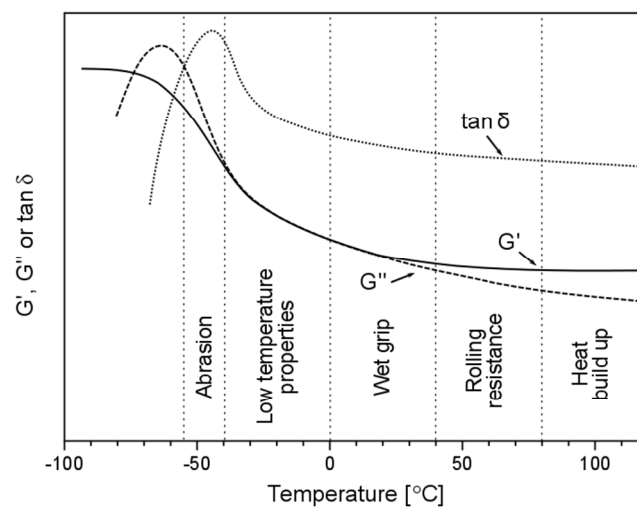


Figure 20. Temperature dependences on the storage modulus  $G'$ , loss modulus  $G''$  and phase angle  $\tan \delta$  of a typical SBR compound<sup>[139]</sup>

Also the typical temperature ranges for important tire tread properties are given in this figure. At low temperatures around the glass transition temperature, the rubber is in the glassy state and has a high hardness. In actual practice, elastomers with a relatively high  $T_g$  of about -40 °C provide a high wet grip and a high rolling resistance, and also a reduced wear resistance whereas a tire tread with a lower  $T_g$  (about -90 °C) will provide a low rolling resistance, a good winter performance, and an improved wear resistance but a reduced wet traction<sup>[140]</sup>. In the temperature region of around 60 °C, a low  $\tan \delta$  and a low loss modulus  $G''$  are indicators for a low rolling resistance. With a further increase of the temperature, the tire compound reaches the limits of driving safety. In this temperature region the moduli and  $\tan \delta$  correlate with the heat build-up of the tire tread.

Therefore, the temperature dependence of the dynamic properties provides important indicators for the practical performance of tire treads.

### 3 Results and discussion

The target of this thesis is focused on a better understanding of the reinforcing mechanism of functionalized nano-sized particles (Nanoprene®) in silica loaded rubber compounds. The first point to be addressed is an investigation of the silanization reaction of the functionalized nanoparticles with a special emphasis on the silanization of the hydroxyl modified nanoparticles and of silica. In this context an analytical method is established which allows for the qualitative monitoring of the silanization reaction and also for the quantification of the silanization rate. In the next step a compound study is performed in which the impact of the silanization reaction on the mechanical and dynamic mechanical properties is considered in detail. Subsequently, the influence of water is investigated for silanized and for unsilanized silica-loaded vulcanizates. Finally the study on the influence of water is extended on vulcanizates which are not filled with silica but with either carbon black, or with hydroxylated nanoparticles. In this study an unfilled compound is included.

#### 3.1 Silanization of the functionalized nanoparticles

##### 3.1.1 Features of Nanoprene® grades with different functional monomers

As pointed out the standard Nanoprene® BM75OH grade is hydroxylated. In order to find out if other functional groups result in better properties, a series of nanoparticles with different functional groups were investigated. In these products the hydroxyl containing monomer (hydroxyethyl methacrylate) was substituted with other functional monomers. According to the supplier (Lanxess) the same “direct” polymerization procedure was applied for the synthesis of the different grades (details on the polymerization were described in Chap. 2.1.2). From this background and as a result of analytical evidence it is to be expected that the different functionalized nano-sized particles have the same morphology. In order to account for the different functional groups Figure 1 in which the structure of the standard hydroxylated grade is given, has to be redrawn as shown in Figure 21.

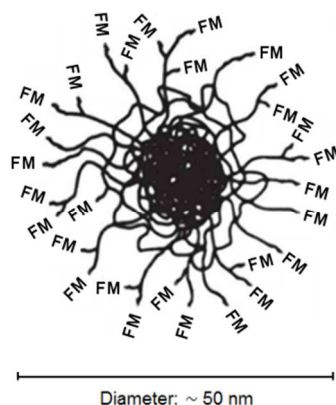


Figure 21. Structure of nano-sized rubber particles with different functional groups (FM)

The Nanoprene® grades, which were obtained from Lanxess, were initially characterized by ATR-FTIR spectroscopy. The results are comprised in Figure 22.

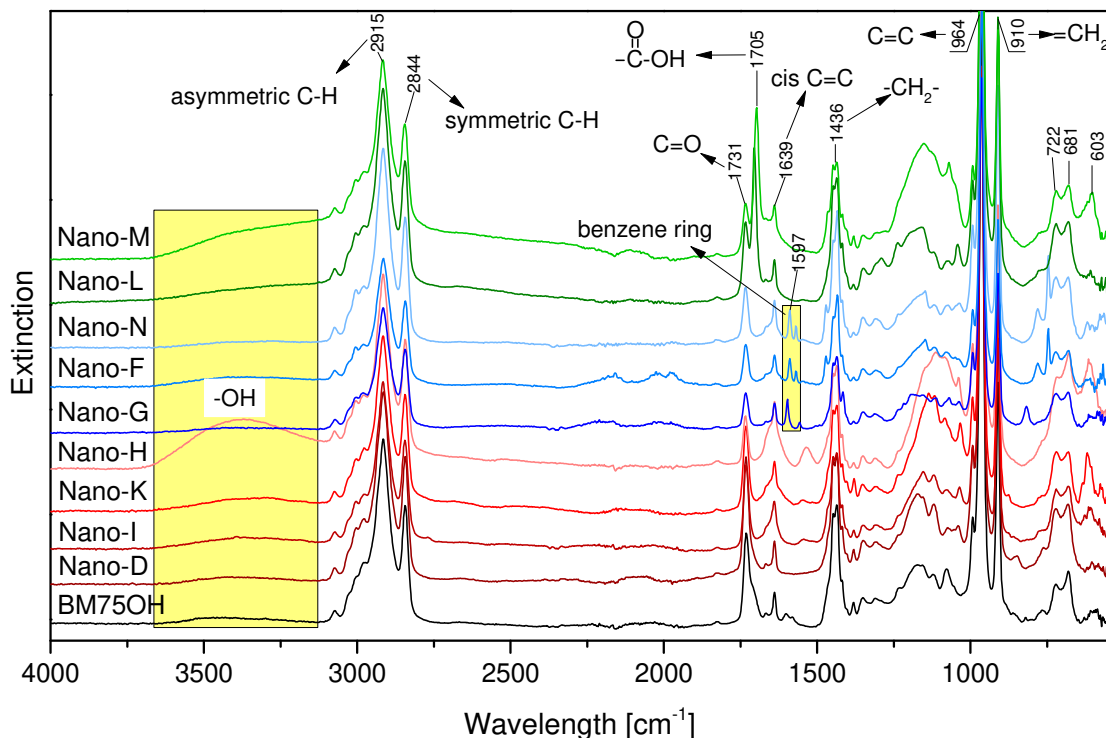


Figure 22. Comparison of the ATR-FTIR spectra of the Nanoprene® grades

In the spectrum the characteristic bonds of the asymmetric C–H oscillation ( $2915\text{ cm}^{-1}$ ), the symmetric C–H oscillation ( $2844\text{ cm}^{-1}$ ), the cis C=C group stretching vibration ( $1639\text{ cm}^{-1}$ ), the asymmetric  $-\text{CH}_2-$  bending vibration ( $1436\text{ cm}^{-1}$ ), the C=C group out-of-plane bending ( $964\text{ cm}^{-1}$ ), the  $=\text{CH}_2$  group vibration ( $910\text{ cm}^{-1}$ ), and the  $-(\text{CH}_2)_n-$  group ( $n > 4$ ) at  $722\text{ cm}^{-1}$  represent the characteristic infrared absorptions of 1,4-polybutadiene rubber with a small proportion of vinyl moieties. This result means that the bulk monomer of the investigated Nanoprene® grades is BR. Furthermore, all Nanoprene® grades present a characteristic bond at  $1731\text{ cm}^{-1}$  which indicates the stretching vibration of the C=O group. Nanoprene® M and L with the functional monomers of acid show an additional absorption at  $1705\text{ cm}^{-1}$  for the carboxyl group. The spectra of Nanoprene® N, F and G exhibit the aromatic ring at  $1597\text{ cm}^{-1}$  in correspondence to their functional monomers (vinylpyridine).

The functional monomers were varied in the synthesis of the different Nanoprene® grades according to Table 4.

Table 4. Characteristic features of Nanoprene®

Nanoprene® grades	FM*	Content of FM [wt.%]	Molecular Weight of FM [g/mol]	Molar content of FM [mol/kg Pol]	Diameter [nm]	T <sub>g</sub> [°C]
OBR 1504 D	GDMA	7.5	142.2	0.53	51	-76.4
OBR 1504 F	2-VP	7.5	105.1	0.71	57	-73.9
OBR 1504 G	4-VP	7.5	105.1	0.71	49	-73.8
OBR 1504 H	DMAPMA	7.5	170.3	0.44	86	-79.1
OBR 1504 I	DMAEMA	7.5	157.2	0.48	61	-77.0
OBR 1504 K	BAEMA	7.5	185.3	0.40	51	-76.7
OBR 1504 L	AA	7.5	72.1	1.04	53	-74.6
OBR 1504 M	MAA	7.5	86.1	0.87	43	-78.2
OBR 1504 N	2-VP	7.5	105.1	0.71	48	-75.3
BM 75OH	HEMA	7.5	130.1	0.58	51	-76.0

\* FM = functional monomer.

As described in Table 4, the same mass fraction of functional monomer (7.5 wt.% based on 100 wt.% of the total loading of monomers) was used in the emulsion recipe. Assuming that the monomer conversion was 100 % in each polymerization, the molar content of the functional monomers can be calculated. Due to the differences in the molecular weight of the functional monomers, the molar content of the functional groups on the nanoparticle surface is different. As the functional monomer of acrylic acid in Nanoprene® L has the lowest molecular weight (72.1 g/mol), the molar content of the carboxyl groups is the highest. The other extreme is Nanoprene® K which contains the functional monomer 2-(tert-butylamino)ethyl methacrylate (BAEMA) with the highest molecular weight (185.3 g/mol). As a result the molar content of the functional monomer is only 0.4 mol/kg polymer.

In Table 4 also the T<sub>g</sub> of the different Nanoprene® grades which were determined by Differential Scanning Calorimetry (DSC) are given. As all Nanoprene® grades are based on polybutadiene, the differences in T<sub>g</sub> are mainly due to structural differences of the functional groups. It can be speculated that the higher T<sub>g</sub> of the Nanoprene® grades F, G and N is the result of the larger volume of the pyridin side group which hinders bond rotation more effectively than side groups with a smaller volume. Furthermore, the flexible spacers in the methacrylate containing Nanoprene® grades H, I and K could compensate the T<sub>g</sub> increases of the methacrylate entity and of the voluminous disubstituted amino-groups. Therefore the

$T_g$  of these Nanoprene<sup>®</sup> grades is close to the  $T_g$  of polybutadiene which is obtained by emulsion polymerization (-80 °C to -81 °C).

### 3.1.2 Test method development using headspace gas chromatography

It is speculated from the literature<sup>[141]</sup> that the silanization of the hydroxyl modified standard Nanoprene<sup>®</sup> grade is possible, but the silanization reaction has not yet been confirmed. Also, the relative silanization rates of hydroxyl groups versus silanol groups which are present in silica are not yet known. In order to elucidate these questions the silanization is first to be studied in model reactions in which the evolution of ethanol is monitored by headspace gas chromatography.

Headspace gas chromatography (HSGC) is a sampling technique in GC used for the analysis of volatile organic compounds with medium to high vapour pressure in less volatile samples<sup>[142]</sup>. It is generally applied to the analysis of vapours in contact with the sample from which they come<sup>[143]</sup>. For example, sample matrices like blood, polymer, and cosmetics contain high molecular weight, nonvolatile material that can remain in the GC system. Without the use of headspace sampler the compounds of interest from this unwanted nonvolatile material need to be extracted and concentrated. Static headspace analysis avoids extensive sample preparation by direct sampling of the volatiles from the vial in which the sample is placed. This technology is relatively simple and time saving.

In this work, the purpose of analysis is to determine the concentration of the released ethanol in the silanization of the different Nanoprene<sup>®</sup> grades and silica. For the quantitative determination of the ethanol release a method was established which uses an internal standard in order to overcome any potential problems particularly associated with the injection technique<sup>[144]</sup>. Isopropanol was chosen as the internal standard<sup>[145, 146]</sup>. The determination of the response factor between ethanol and isopropanol and the validation of the HSGC method which was used in this thesis are described in the experimental section.

### 3.1.3 Silanization of silica and Nanoprene<sup>®</sup>

The silanization of the different Nanoprene<sup>®</sup> grades and of silica was studied in order to gain a better understanding of the reinforcing mechanisms of the hybrid filler system. The questions to be answered are about the chemical structure of the silica/Nanoprene<sup>®</sup>-filler hybrid systems. Some of these questions are: How can a positive effect of Nanoprene<sup>®</sup> on the improvement of silica dispersion be explained? Does the silane generate bonds between

the Nanoprene® surface and the rubber matrix? Are there agglomerates between unsilanized Nanoprene® and the parts of silica which are not silanized?

The silanization reactions of Nanoprene® and silica were neither performed with TESPT nor with TESPd but with the model silane triethoxy(octyl)silane (OCTEO). OCTEO was chosen in order to avoid side reactions such as the release of reactive sulfur moieties. Prior to the use of OCTEO the thermal stability of OCTEO was determined by the storage in dodecane at 120/140/160 °C up to 300 min. During storage the amount of evolved ethanol was determined by HSGC. It was found that OCTEO is stable at 120 °C and 140 °C, but the thermal degradation of OCTEO starts at 160 °C at reaction times from 60 min.

### 3.1.4 Kinetics of silanization reaction

Theoretically, the hydroxyl groups of Nanoprene® BM75OH can react with silane by condensation. Figure 23 shows the capillary gas chromatography charts of volatiles obtained after reaction of Nanoprene® BM75OH with OCTEO for 20 and 300 min at 120 °C, respectively.

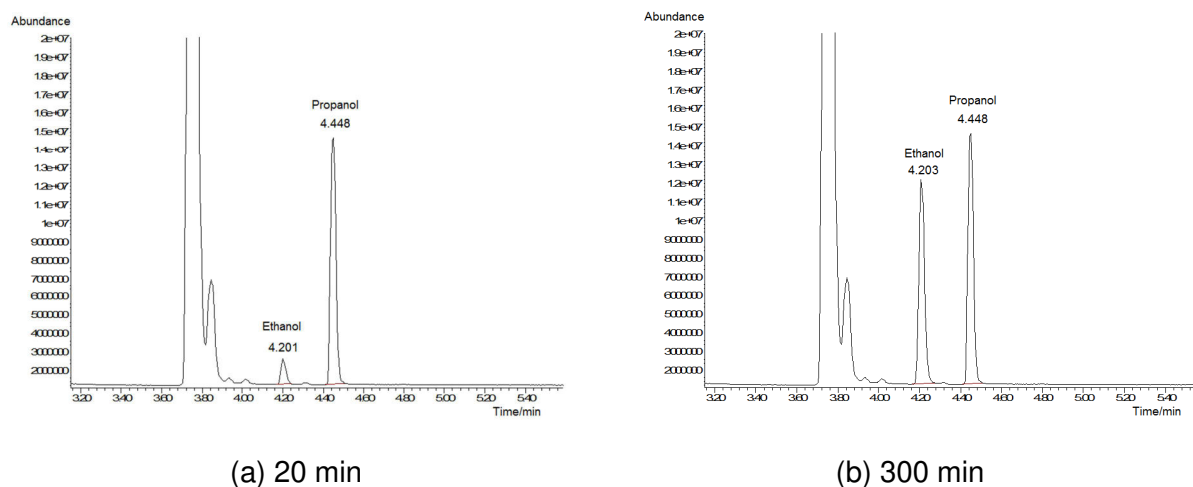


Figure 23. Chromatograms of Nanoprene® BM75OH reacted with OCTEO at 120 °C

A comparison of both chromatograms shows an increment of the response appearing at a retention time of 4.20 min which is related to the emitted ethanol. The response of the internal standard (isopropanol) which appears at a higher retention time (4.45 min) shows identical elution intensity at the reaction time of 20 min and 300 min due to the same concentration applied in the vial. The huge peak before 3.8 min is assigned to air which is present in the gas phase of the vial. The significant difference in the ethanol responses confirms that ethanol is released in the reaction of Nanoprene® BM75OH with OCTEO.



Furthermore, the content of ethanol increases with reaction time. From these observations it is evident that there is indeed a silanization of Nanoprene® BM75OH.

Similar experiments were carried out with the other Nanoprene® grades as well as with the reference silica. The quantitative data on the amount of the released ethanol can be found in annexes.

The conversion rate of the functional groups of silica and Nanoprene® grades during the silanization can be calculated by the following equation:

$$\text{Conversion rate (\%)} = \frac{C_{(\text{Ethanol})}}{C_{(\text{Functional groups})}} \times 100 \% \quad \text{Equ. (41)}$$

where  $C_{(\text{Ethanol})}$  is the concentration of the released ethanol as detected in the GC measurement, and  $C_{(\text{Functional groups})}$  is the molar amount of silanol groups of silica or of the functional groups of different Nanoprene® grades. The number of silanol groups on the silica surface (isolated silanol) was obtained from literature which was published by Blume et al.<sup>[62]</sup>. The molar content of functional groups of Nanoprene® is identical with the molar content of functional monomers which are given in Table 4.

Figure 24 shows the dependence of the conversion of functional groups on the reaction time at 120 °C.

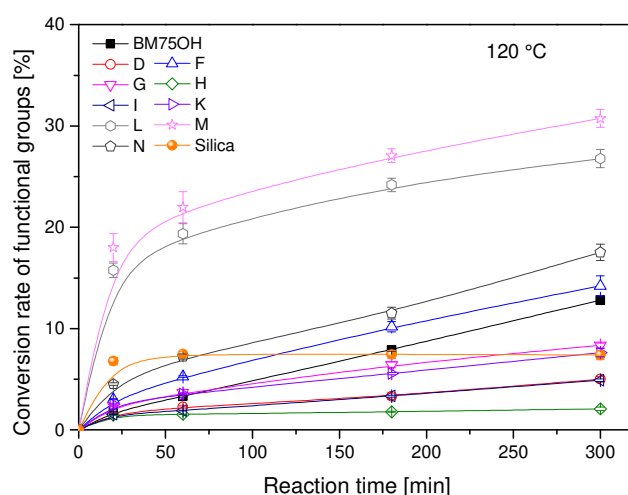


Figure 24. Conversion/time-dependence of the silanization reactions of the Nanoprene® grades with different functional groups at 120 °C

The results show that the production of ethanol is detected during the reactions with silica and with all Nanoprene® grades. This demonstrates that all types of Nanoprenes react with

silane. The reaction with silica is completed between 20 and 60 min, as indicated by the constant conversion after 60 min, whereas the reactions with the different Nanoprene® grades are much slower and are not finished even after 300 min. Further, the conversion rates are different for the different Nanoprene® grades.

In order to gain a deeper insight into the conversion of silica and Nanoprene®, the molecular size of triethoxy(octyl)silane was estimated by molecular modelling which was calculated by Hyperchem 7.0 software as seen in Figure 25.

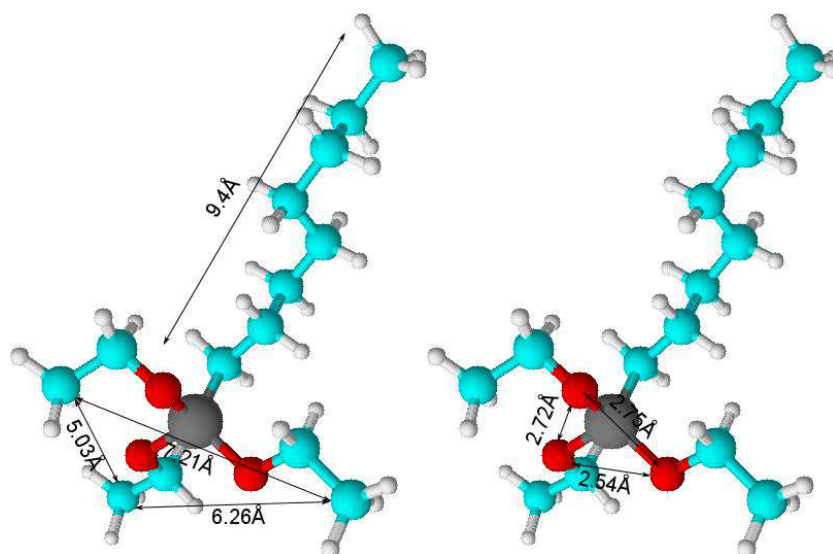


Figure 25. Molecular modelling of triethoxy(octyl)silane (Si in gray, O in red, C in blue and H in white)

The degree of surface coverage with OCTEO of silica, respectively Nanoprene® can be calculated by means of the following equation:

$$\text{Degree of coverage (\%)} = \frac{\text{Projected surface area}_{(\text{OCTEO})}}{\text{Projected surface area}_{(\text{Filler})}} \times 100 \% \quad \text{Equ. (42)}$$

in which the “Projected surface area<sub>(OCTEO)</sub>” corresponds to the total projected surface area of OCTEO (0.27 nm<sup>2</sup>), and the “Projected surface area<sub>(Filler)</sub>” corresponds to the surface area of the silica or Nanoprene®. As isomolar concentrations of the OCTEO were used the surface coverage is inversely proportional to the surface area of silica and Nanoprene®. The surface area of silica is based on the CTAB surface area, whereas the surface area of the different Nanoprene® grades is calculated from the average diameters and the polymer density (0.94 g/cm<sup>3</sup>). The degree of surface coverage for the different Nanoprene® grades, as shown in Table 5, is between 35.4 % (Nanoprene® N) to 63.4 % (Nanoprene® H). For

silica the degree of surface coverage is significantly lower (29.4 %). This finding can be rationalized on the basis that silica has the highest specific surface area.

Table 5. Evaluation of the silanization reaction in silica and Nanoprene®

Samples	FM <sup>a</sup> [mol/kg]	OCTEO <sup>b</sup> [mol/kg filler]	Density [g/cm <sup>3</sup> ]	Surface area [m <sup>2</sup> /g]	Degree of coverage [%]
Silica (VN3)	2.62	0.29	-	160	29.4
OBR 1504 D	0.53	0.29	0.94	125	37.6
OBR 1504 F	0.71	0.29	0.94	112	42.0
OBR 1504 G	0.71	0.29	0.94	130	36.1
OBR 1504 H	0.44	0.29	0.94	74	63.4
OBR 1504 I	0.48	0.29	0.94	105	44.9
OBR 1504 K	0.40	0.29	0.94	125	37.6
OBR 1504 L	1.04	0.29	0.94	120	39.0
OBR 1504 M	0.87	0.29	0.94	148	31.7
OBR 1504 N	0.71	0.29	0.94	133	35.4
BM75OH	0.58	0.29	0.94	125	37.6

<sup>a</sup>. Molar number of functional groups on 1 kg silica or Nanoprene® surface.

<sup>b</sup>. Molar number of OCTEO by gram of filler applied in the reaction system.

The differing degrees of surface coverage could be one of the factors which are relevant for the final conversion of the silanization. As can be seen in Figure 24, the final conversion of silica is only around 7 %, firstly because the silane molecules are oriented in the space when chemically bonded to the silica surface, and secondly the silanization reaction depends on the coverage ratio of silane that is about 30 % used on the silica surface. However, the conversion rates of the Nanoprene® grades gradually increase with reaction time. The difference in conversion rates can be explained by a difference in the reactivities of the functional groups and the accessibilities of these groups in the agglomerated filler particles. As carboxyl groups have a much higher acidity than the hydroxyl groups the higher silanization rate for Nanoprene® L and M is not really surprising. In the experimental set-up of the silanization experiments silica and Nanoprene® were dispersed in dodecane by shaking. As a result of lower viscosities in this procedure the shear energies are much lower than during the preparation of the rubber compounds in an internal mixer. Therefore the dispersion state of the fillers was definitely poorer in the silanization experiments than in the rubber compounds.

Similar experiments were carried out at a reaction temperature of 140 °C. With respect to the silanization at 120 °C, the same trends regarding the conversion rates could be observed at 140 °C (Figure 26).

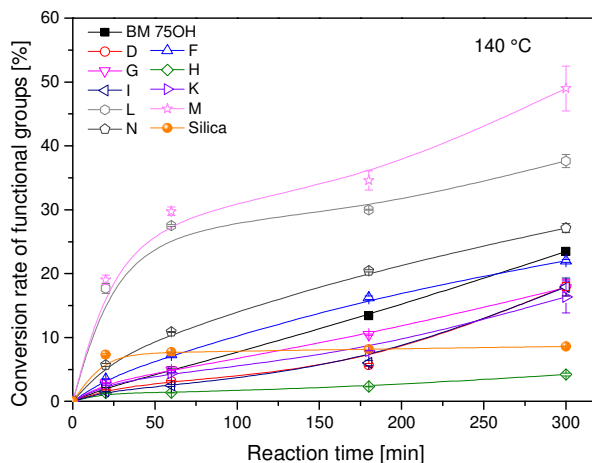


Figure 26. Conversion/time-dependence of the silanization reactions of the Nanoprene® grades with different functional groups at 140 °C

But at the same reaction times significantly higher conversions were found for the Nanoprene® grades. In parallel, the reaction with silica is almost completed at around 20 min, which is faster than the reactions with Nanoprene®. The silanization of silica reaches a final conversion of approximately 7 – 8 % which is not increased when the temperature is increased from 120 °C to 140 °C. This result is confirmed by a further increase of the temperature to 160 °C as depicted in Figure 27.

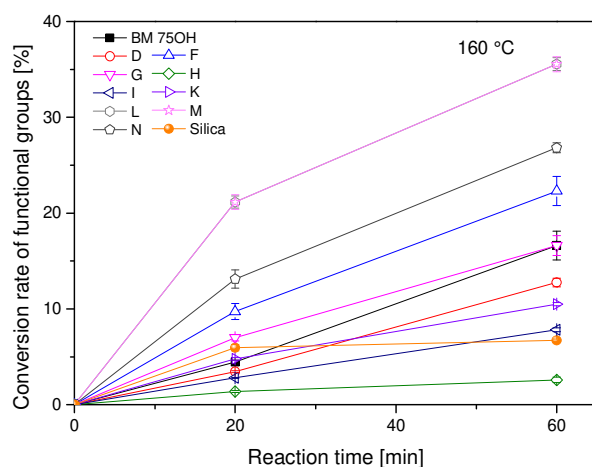


Figure 27. Conversion/time-dependence of the silanization reactions of the Nanoprene® grades with different functional groups at 160 °C

At 160 °C the silanization reactions were only studied up to 60 min in order to avoid degradation phenomena from OCTEO which decomposes at 160 °C/> 60 min. The conversion rates of the Nanoprene® grades increase with the increase of the reaction temperature from 140 °C to 160 °C.

Without any doubt, the different Nanoprene® grades do undergo silanization. In Figure 28 the mean values of the conversions at 20 min are plotted over the reaction temperature. This clearly confirms the previous assignment of the conversion rates. The ranking regarding the rates of the initial reaction is the following: Nanoprene® L  $\geq$  M > N > F > G > BM75OH > K > D > I > H. From the kinetic data the reaction rates of the carboxylated Nanoprene® grades (L and M) are as high as for silanol groups of silica. The high silanization rate of Nanoprene® L and M can be assigned to the high acidity of the carboxyl groups. In the case of the other Nanoprene® grades the silanization reactions are considerably lower than for silica. This means that in a competitive situation in which silica and the different Nanoprenes (except L and M) are simultaneously silanized the silane will be more rapidly consumed by the silanol groups than by the other functional moieties including hydroxyl groups or the N moieties.

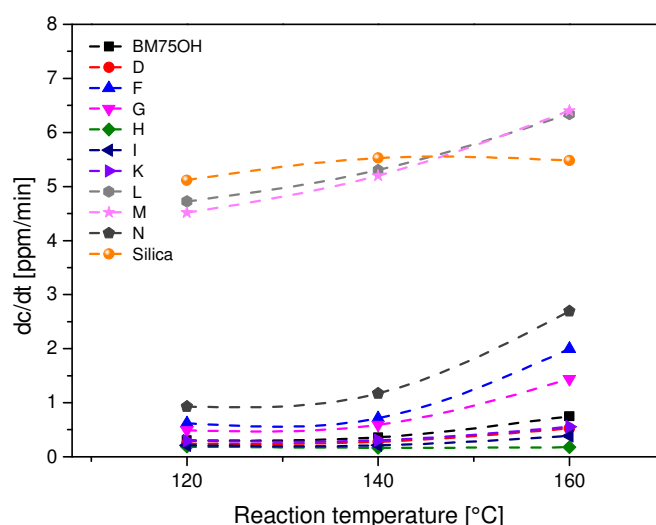


Figure 28. Dependence of the conversion at 20 min on temperature

The relationship between the molar content of functional monomers and the initial conversions at 20 min/120 °C is illustrated in Figure 29. This figure shows that the chemical structure and the molar content of the functional monomers influence the kinetic behaviour when all molecules react with the same amount of silane. As the functional monomer was used 7.5 wt.% for each Nanoprene®, the higher molecular weight of the functional monomer

means a lower molar content. For Nanoprene® L and M with the lowest molecular weight of functional monomers (acrylic acid and methacrylic acid) show the highest reaction rate of the silanization. In this respect, the relative abundance of carboxyl groups in the chain ends has much higher acidity and polarity than the other functional groups resulting in a much higher silanization rate with the ethoxy groups. Nanoprene® grades N, F, G with the same molar content of functional monomers, but Nanoprene® N and F show a higher start reaction rate because the vicinal pyridine groups have a higher reactivity than para-position. Nanoprene® K with the lowest molar content of functional monomers has a medial rate of silanization probably because of the relative higher reactivity of the –NH– moiety.

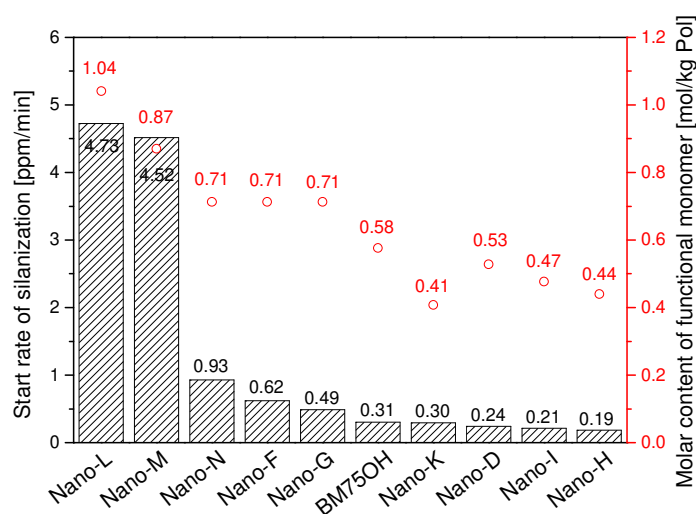


Figure 29. Plot of the silanization rate at 20 min/120 °C versus the molar content of the functional monomers

### 3.2 Reinforcing mechanisms of hydroxyl modified nanoparticle in silica hybrid systems

For an elucidation of the reinforcing mechanisms of the different Nanoprene® grades in silica loaded vulcanizates, compound studies were performed in addition to the investigations on the model silanization reaction with OCTEO. The compound studies were performed on 5 compounds with the hydroxylated Nanoprene® grade (Nanoprene® BM75OH) as shown in Table 6. The first of these compounds contained no filler. The second compound contained silica and was not silanized. The third compound contained silica and was also silanized. It can be considered as reference silica compound which is widely used in the tire industry. The fourth compound contained silica and Nanoprene® BM75OH and was not silanized. In comparison with the fourth compound the fifth compound was silanized. It has to be mentioned that the amount of vulcanization agents was kept constant throughout the study and that concerning the influence on the vulcanization no adjustments were made when Si 75® was used.

Table 6. Compound study on the influences of silica, Nanoprene® and silanization\*

Compound No.	1	2	3	4	5
Buna® VSL 4526-2 HM	96	96	96	96	96
Buna® CB 25	30	30	30	30	30
Ultrasil® VN3 GR		80	80	80	80
Mixing step 1 & 2 Nanoprene® BM75OH				15	15
Si 75®			6.4		6.4
Vivatec® 500	10	10	10	10	10
Zinc oxide	3	3	3	3	3
Stearic acid	2	2	2	2	2
Vulkanox® 4020	2	2	2	2	2
Mixing step 3 Antilux® 500	1	1	1	1	1
Vulkacit® CZ	1.6	1.6	1.6	1.6	1.6
Vulkacit® D	1.5	1.5	1.5	1.5	1.5
Sulfur	2	2	2	2	2

\* All weights are in phr (parts in weight per 100 g rubber).

In the first step the compounds were studied in the unvulcanized state regarding filler flocculation and the subsequent break-down of the filler network. In the second step the

vulcanizates were characterized by stress-strain measurements and by dynamic mechanical analysis. Also TEM micrographs of representative vulcanizates were recorded, and equilibrium swelling experiments were made in order to determine the swelling ratios and to investigate filler/matrix interactions. By incorporation of the relative silanization rates of hydroxyl and silanol groups (in Chap. 3.1.3) the explanations of reinforcing mechanism of the hydroxylated Nanoprene® grade in silica loaded rubber compounds can be finally attempted.

### 3.2.1 Filler flocculation and break-down of filler network structure

In order to study the filler flocculation uncured samples which were taken after the mixing steps one and two were tested. Filler flocculation was monitored by the increase of the storage modulus ( $G'$ ) at 1 % strain for 60 min at 160 °C. Subsequently the breakdown of the filler structure was monitored by the decrease of  $G'$  on increasing the shear-strain from 1 % to 400 % at 160 °C. The performance of the 5 compounds which were taken after the first mixing step is given in Figure 30.

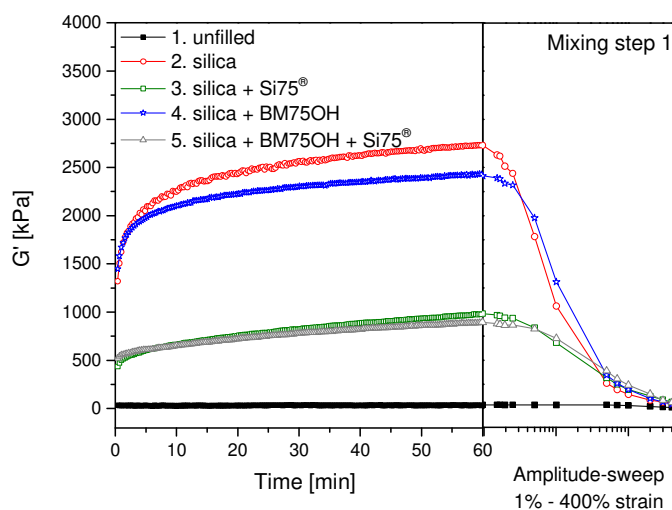


Figure 30. Filler flocculation of unvulcanized compounds at 160 °C after mixing step one and subsequent dependence of  $G'$  on strain

For the unfilled compound 1 no increase in  $G'$  is observed even after 60 min. There is also no decrease in  $G'$  upon increasing the shear amplitude for this compound. The highest increase in  $G'$  and the most pronounced filler break-down are found for the unsilanized compounds 2 and 4. It is worth mentioning that the unsilanized compound 4 which contains Nanoprene® BM75OH performs remarkably better than the silica loaded compound 2. This clearly demonstrates the improvement of silica dispersion by Nanoprene® BM75OH. For the silanized compounds 3 and 5 filler flocculation and the subsequent break down of the filler-



network is much less pronounced than for the unsilanized compounds 2 and 4. Again, compound 5 which contains Nanoprene® BM75OH performs better than compound 3 even though the positive effect of Nanoprene® BM75OH is smaller than in compound 4 over compound 2. Furthermore, it is to be considered that if Nanoprene® is used as a polymeric additive, a dilution effect for the silica is a second reason for the decrease of the Payne effect.

The performance of the 5 compounds which were taken after mixing step two is given in Figure 31. The qualitative dependency of the 5 compounds regarding the increase of  $G'$  over time and the subsequent breakdown of  $G'$  on increasing the shear amplitude is the same as in the previous Figure 30. The only difference is that in Figure 31 the  $G'$  values are considerably lower than in Figure 30. This difference demonstrates the necessity of mixing step two which considerably improves filler dispersion and reduces the scope of filler flocculation.

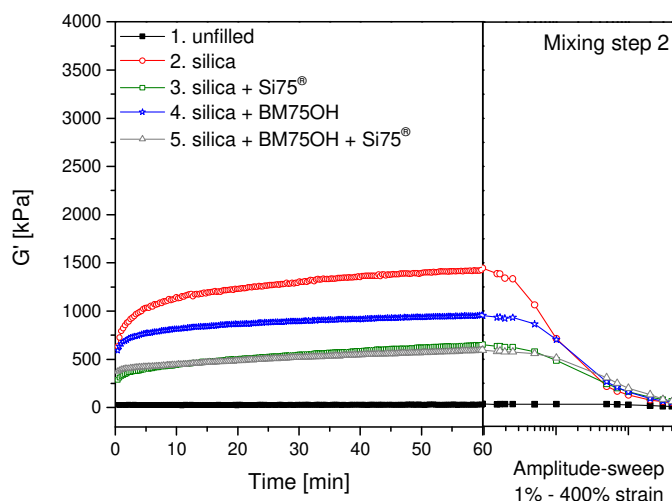


Figure 31. Filler flocculation of unvulcanized compounds at 160 °C after mixing step two and subsequent dependence of  $G'$  on strain

In spite of the better filler dispersion after mixing step two the beneficial influence of Nanoprene® BM75OH can be seen from a comparison of the unsilanized compounds 2 and 4 as well as from a comparison of the silanized compounds 3 and 5. The difference between the Nanoprene® free samples (compounds 2 and 3) and the respective Nanoprene® BM75OH containing compounds 4 and 5 is bigger for the silane-free compounds than for the silanized compounds. Despite this small difference, the beneficial influence of Nanoprene® BM75OH on the quality of filler dispersion is quite evident.

### 3.2.2 Tensile testing

The static mechanical behaviour of the vulcanized rubber compounds was analyzed with a tensile tester. The stress-strain curves of the 5 vulcanizates are shown in Figure 32.

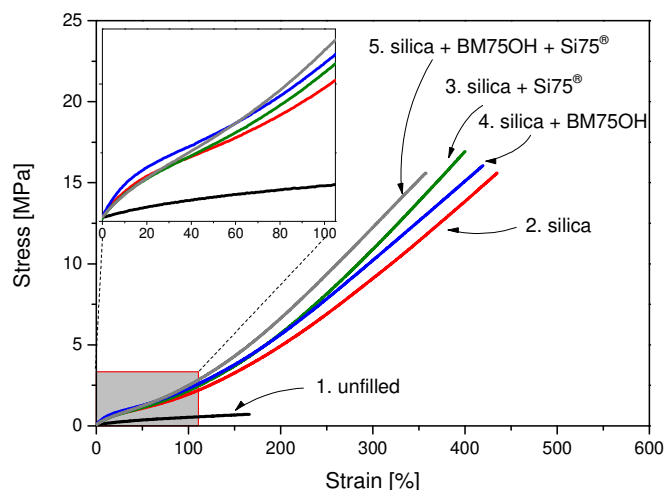


Figure 32. Stress-strain curves of the indicated vulcanizates at 23 °C

At high elongations > 100 % the silanized compound which contains both silica and Nanoprene® BM75OH (compound 5) exhibited the highest moduli. Lower moduli were obtained for the silane-coupled silica mixture (compound 3), followed by the unsilanized compound 4 which contains silica and Nanoprene® BM75OH. Significantly lower moduli were found for the unsilanized silica loaded vulcanizate (compound 2), and very low moduli were found for the unfilled compound 1. The moduli at 100 % and 300 % elongation are related to the crosslink density and the strength of polymer-filler interactions<sup>[97, 147]</sup>. As the contribution of the filler network to the moduli is most pronounced at low elongations < 10 % the ratios of moduli at high and low elongations ( $M_{100}/M_{10}$  and  $M_{300}/M_{10}$ ) give an indication of the quality of filler dispersion. As can be seen from Table 7 the ranking of the values is in the following order:  $5 > 3 > 4 \sim 2 > 1$ . The ratios of moduli for the silanized hybrid filler system are clearly the highest (compound 5). Lower values were obtained for the silanized silica reference compound 3. It is also shown that the values for compounds 4 and 2 are fairly close. This means that the quality of filler dispersion by silanization (compound 3) is superior to the modification only by use of Nanoprene® BM75OH (compound 4). The results from stress-strain measurements fall in line with the results from the flocculation experiments: the filled compounds which display the lowest flocculation tendencies show the highest level of reinforcements.

Table 7. Tensile strength, elongation at break, tensile modulus, and the ratio of  $M_{100}/M_{10}$  and  $M_{300}/M_{10}$ 

Compound No.	1	2	3	4	5
Tensile strength [MPa]	0.7±0.1	15.6±0.9	16.9±0.5	16.0±0.6	15.6±0.7
Elongation at break [%]	166±34	435±15	400±7	420±12	358±12
Modulus @ 10% elongation [MPa]	0.14±0.00	0.44±0.00	0.40±0.00	0.54±0.00	0.39±0.00
Modulus @ 20% elongation [MPa]	0.21±0.00	0.66±0.00	0.62±0.00	0.79±0.00	0.63±0.01
Modulus @ 50% elongation [MPa]	0.35±0.00	1.08±0.01	1.12±0.01	1.26±0.01	1.22±0.04
Modulus @ 100% elongation [MPa]	0.52±0.01	1.94±0.03	2.16±0.01	2.31±0.02	2.50±0.09
Modulus @ 300% elongation [MPa]	-	9.09±0.21	10.9±0.12	10.2±0.10	12.2±0.25
$M_{100}/M_{10}$	3.71	4.41	5.40	4.28	6.41
$M_{300}/M_{10}$	-	20.66	27.25	18.89	31.28

### 3.2.3 Dynamic mechanical properties

Dynamic mechanical properties are of primary importance in rubber industry and comprise the measurement of elastic modulus, loss modulus, rate of heat generation and material microstructure. The temperature dependency of the indicated vulcanizates was investigated by DMA measurement.

In Figure 33 the temperature dependencies of the storage ( $G'$ ) and loss ( $G''$ ) moduli of the 5 vulcanizates from Table 6 are given. Over the temperature range from -70 °C to +80 °C the storage ( $G'$ ) and loss moduli ( $G''$ ) of the filled vulcanizates (compounds 2, 3, 4, and 5) are significantly higher than those of the unfilled gum stock (compound 1). This finding can be attributed to the reinforcement by filler<sup>[148]</sup>. In the temperature range from -20 °C to +80 °C the ranking of  $G'$  of the compounds has the following order: 2 > 4 > 3 > 5 >> 1. As  $G'$  was determined at a strain amplitude of 0.5 % it is not surprising that the order is similar to the one found in the stress/strain measurements at elongations < 10 %. As in tensile testing the filler network is preserved at low elongations < 10 %, respectively at low strain amplitudes in dynamic experiments, the filler network will show under these experimental conditions. In the temperature range -20 °C to +80 °C the ranking of  $G''$  values is 2 > 4 > 3 > 5 >> 1. As the loss modulus  $G''$  is mainly caused by the friction between filler particles it is no surprise that

exactly the same ranking is found as for the ratios of  $M_{100}/M_{10}$  and as for the ranking of filler flocculation after the first and after the second mixing step.

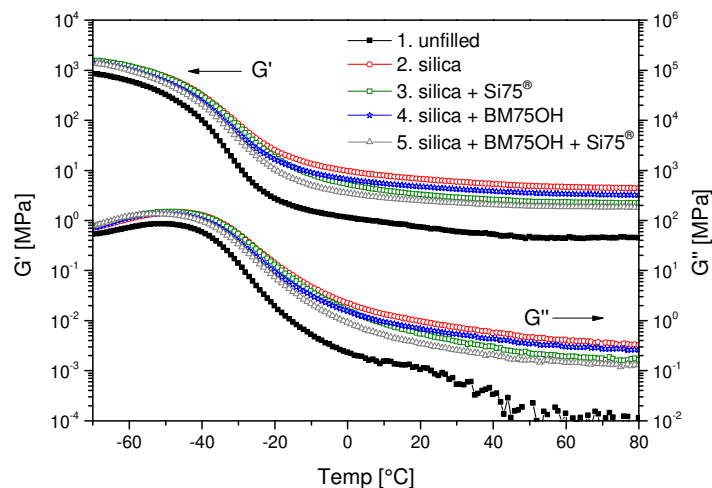


Figure 33. Dependences of the storage moduli  $G'$  and the loss moduli  $G''$  on temperature

As in the temperature region from  $-70\text{ }^{\circ}\text{C}$  to  $-20\text{ }^{\circ}\text{C}$  there is some overlap of the dependencies of  $G'$  and  $G''$  on temperature the ratio  $G''/G'$  ( $\tan \delta$ ) cannot be predicted in a straightforward manner. The dependencies of  $\tan \delta$  on temperature are given for the 5 vulcanizates in Figure 34.

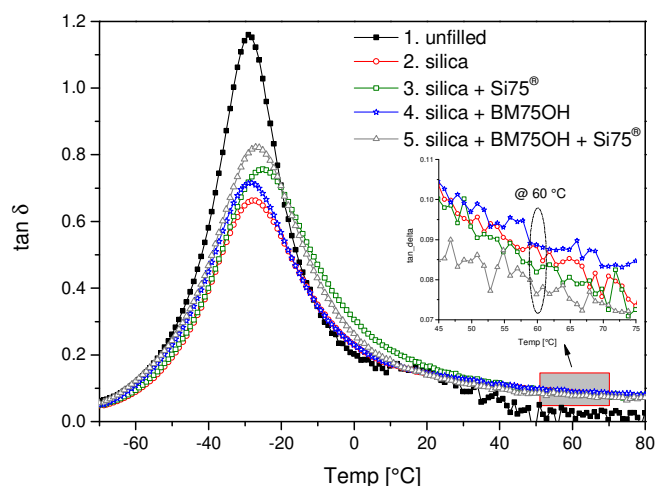


Figure 34. Temperature dependence of  $\tan \delta$  for the indicated vulcanizates

Regarding the maximum peak heights the ranking of the 5 vulcanizates is:  $1 > 5 > 3 > 4 > 2$ . Regarding the temperature range from  $-10\text{ }^{\circ}\text{C}$  to  $+20\text{ }^{\circ}\text{C}$  the ranking of the vulcanizates is: 3

$5 > 4 = 2 > 1$  and in the temperature range  $> 30\text{ }^\circ\text{C}$  the ranking of  $\tan \delta$  is  $4 > 2 > 3 > 5 >> 1$ . As a high  $\tan \delta$  in the temperature range from  $-10\text{ }^\circ\text{C}$  to  $+10\text{ }^\circ\text{C}$  and a low  $\tan \delta$  at temperatures  $> 30\text{ }^\circ\text{C}$  are taken as predictors for a good wet skid performance respectively a low rolling resistance<sup>[149]</sup>. Vulcanizate 3 performs best in wet skid resistance (with vulcanizate 5 being the second) and the unfilled compound 1 performs best in rolling resistance. Amongst the filled vulcanizates vulcanizate 5 performs best in rolling resistance. From the temperature sweep experiments, it is concluded that Nanoprene® BM75OH reduces the fraction of agglomerated silica formally in the compound and improve the rolling resistance.

The effects of the strain amplitude on the storage modulus  $G'$  for the indicated composites are shown in Figure 35.

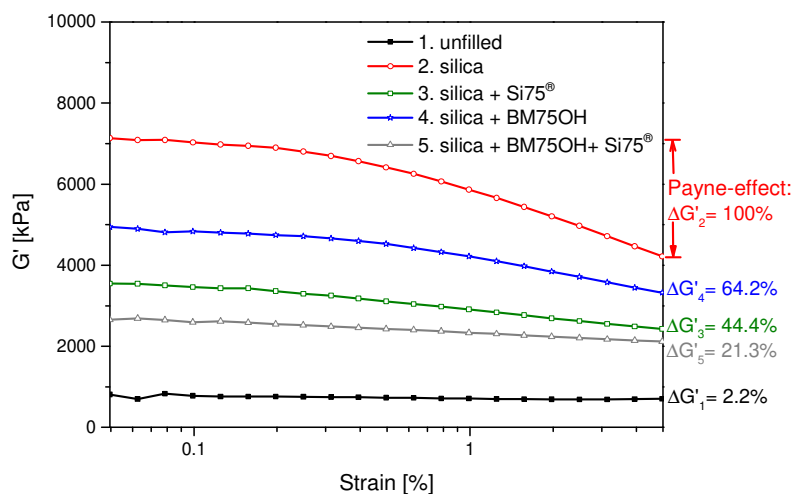


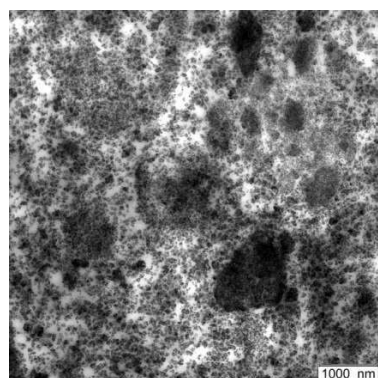
Figure 35. Dependencies of storage moduli  $G'$  on strain amplitude (Payne effect)

For all vulcanizates, the storage modulus is the highest at small amplitudes (referred to as  $G'_0$ ). With increasing strain amplitudes it gradually decreases to lower values (referred to as  $G'_\infty$ )<sup>[80]</sup>. The Payne effect ( $G'_0 - G'_\infty$ ) of vulcanizate 2 which is the highest among the investigated vulcanizates is assumed to be 100 % ( $\Delta G'_2$ ). It decreases with the addition of silane to 44.4 % ( $\Delta G'_3$ ), but also with the addition of Nanoprene® BM75OH 64.2 % ( $\Delta G'_4$ ). The Payne effect is the lowest for the unfilled vulcanizate 1 ( $\Delta G'_1 = 2.2\%$ ). Regarding the Payne effect of the filled vulcanizates compound 5 ( $\Delta G'_5$ ) which is only 21.3 % performs the best. As the Payne effect is attributed to the break down of the filler network<sup>[150]</sup>, the low Payne effect of compound 5 shows that rubber/filler interaction is particularly strong in this compound. It is also apparent that Nanoprene® BM75OH and silanization display a synergistic effect on silica dispersion since  $\Delta G'_5$  (21.3 %) is lower than the value of  $\Delta G'_3 \times$

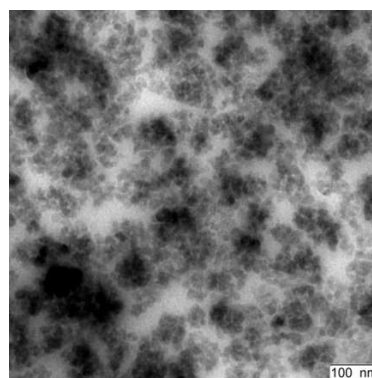
$\Delta G'_4$  (28.5 %), provided that the dilution effect for Nanoprene® as a polymeric additive is not the determining effect.

### 3.2.4 Characterization of vulcanizates by transmission electron microscopy (TEM)

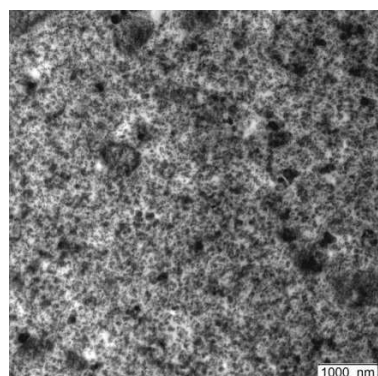
The effect of Nanoprene® BM75OH on the dispersion of silica was studied by TEM on microtomes which were taken from the vulcanizates 2, 3 and 5. The respective micrographs are given in two magnifications (Figure 36).



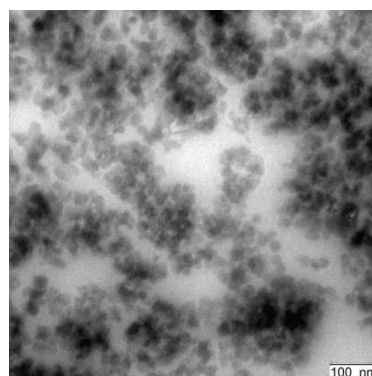
(a) Unmodified silica compound



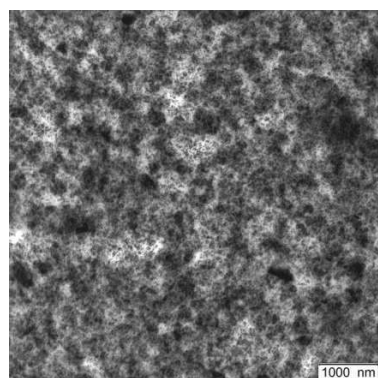
(b) Unmodified silica compound



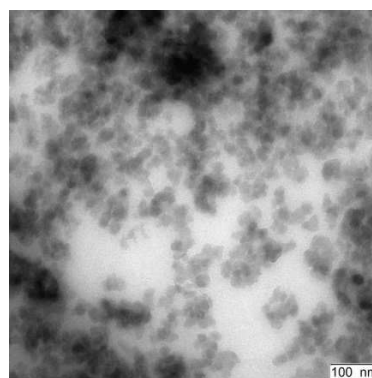
(c) Silica + Si 75®



(d) Silica + Si 75®



(e) Silica + BM75OH + Si 75®



(f) Silica + BM75OH + Si 75®

Figure 36. Transmission electron micrographs of three mixtures with two magnifications

Figure 36 (a) and (b) give the micrographs (in two magnifications) which were obtained from the unsilanized silica compound 2. The two micrographs show silica agglomerates and reveal that without silanization silica dispersion is very poor. Figure 36 (c) and (d) show micrographs from vulcanizate 3. A comparison of these micrographs shows that silica dispersion is much better in vulcanizate 3 than in vulcanizate 2. The only difference between these vulcanizates is silanization. Electron micrographs from vulcanizate 5 are given in Figure 36 (e) and (f). A comparison of these two figures with Figure 36 (c) and (e) shows no apparent difference regarding silica dispersion. This means that silica dispersion in vulcanizates 3 and 5 is comparably good. The more qualitative results gained by TEM are in good agreement with the observations from the flocculation experiments of the unvulcanized compounds as well with the results from the stress/strain and dynamic mechanical tests which were performed on the vulcanizates.

### 3.2.5 Equilibration swelling experiments

Additional information on the modification effects of Nanoprene® BM75OH containing compounds can be obtained from swelling experiments in which the equilibrium degree of swelling is determined. For a given solvent, a higher degree of equilibrium swelling indicates a lower degree of crosslinking. It is to be mentioned that contrary to Nanoprene® BM75OH, silica as a filler cannot swell. On the basis of the equilibrium swelling data the swelling ratio of the filled vulcanizates were calculated by means of Equ. (27).

The swelling ratios which were determined for the 5 compounds are listed in Table 8. As can be seen from this table the swelling ratios are higher for the compounds without Si 75® (compounds 1, 2 and 4) than for those which contain Si 75® (compounds 3 and 5). The highest swelling ratio ( $5.33 \pm 0.22$ ) is determined for compound 1. At the same time this value is representative for the chemical crosslink density (XLD) generated by the sulfur curing package without any filler effects. By the addition of silica the swelling ratio is reduced to  $4.19 \pm 0.02$  (compound 2). As silica interacts strongly with the rubber matrix the swelling experiments show an increase of the overall crosslink density in compound 2 over compound 1. For sure, the overall crosslink density is the sum of covalently bonded chemical crosslinks and strong physical interactions, which also add a portion of apparent crosslink density. The addition of Nanoprene® BM75OH further decreases the swelling ratio to  $4.04 \pm 0.04$  (compound 4) which is surprising as the polymer gel itself does swell in toluene. This is an indication for further improved filler dispersion and a stronger filler-polymer interaction. In the presence of Si 75®, which may support co-crosslinking of silica with the rubber matrix and at least to a very small degree the co-crosslinking of Nanoprene® BM75OH with the rubber

matrix, the measured swelling ratio is further reduced. A comparison of compound 5 with compound 3 shows that compound 5 has a lower degree of swelling. As compound 5 contains silica + Nanoprene® BM75OH + silane and compound 3 only contains silica + silane the lower degree of swelling of compound 5 must be caused by the presence of Nanoprene® BM75OH.

Table 8. Swelling ratio and thermodynamic parameters of swelling

Compound No.	$Q$ [-]	$\Delta G$ [J/mol]	$\Delta S$ [J/mol/K] $\times 10^{-2}$
1 Unfilled	$5.33 \pm 0.22$	$-9.74 \pm 0.86$	$3.32 \pm 0.30$
2 Silica	$4.19 \pm 0.02$	$-15.87 \pm 0.16$	$5.42 \pm 0.06$
3 Silica + Si75®	$3.82 \pm 0.01$	$-19.10 \pm 0.08$	$6.52 \pm 0.03$
4 Silica + BM75OH	$4.04 \pm 0.04$	$-17.06 \pm 0.41$	$5.82 \pm 0.14$
5 Silica + BM75OH+Si75®	$3.73 \pm 0.01$	$-20.01 \pm 0.15$	$6.83 \pm 0.05$

Evidently, Si 75® induces permanent chemical crosslinks and/or strong physical adsorption effects which are either located within the rubber matrix or between silica and the rubber matrix. As it was shown that Nanoprene® BM75OH is hardly silanized (see Chap. 3.1.3) the reason for the overall lower swelling degree of compound 5 is very likely not caused by chemical bonds between the Nanoprene® surface and the rubber matrix. For this finding no simple and straight forward explanation can be given. But since Nanoprene® BM75OH particles bring their own chemical network, there has to be a certain XLD figure attributed to this additive. On the other hand it was clearly demonstrated that Nanoprene® BM75OH supports the dispersion of silica and the stronger polymer-filler interaction. Therefore the silanization of silica seems to be increased by the presence of Nanoprene® BM75OH. In this way Nanoprene® BM75OH provides an increase in the polymer-filler interaction. By this mechanism Nanoprene® BM75OH is the indirect root cause for additional chemical crosslinks.

The swelling ratio of the compound which only contains Nanoprene® BM75OH is also lower than that of the unmodified silica compound. This effect is probably due to a reduction of the pockets around the silica agglomerates in which the solvent accumulates and not due to additional chemical bonds between Nanoprene® and silica. As the degree of crosslinking or the degree of physical adsorption increases, the available free volume between the adjacent molecules decreases and more rubber chains are constrained or immobilized<sup>[151]</sup>. In a proper range, an increase in the immobilization of the polymer chains could improve the final



properties in particular the wet skid performance. From this perspective the compound with the highest amount of immobilized chains, which contains silica, Nanoprene® BM75OH, and silane (compound 5), will exhibit the best performance profile regarding rolling and wet skid resistance in addition to the best reinforcement behaviour.

According to the Kraus-plots theory (see Chap. 2.5.4), the degree of swelling of filled vulcanizates should linearly depend on the loading of a vulcanizate with filler. The slope ( $m$ ) of the Kraus plots reflects the quality of the adhesion of the filler to the rubber matrix. The lack of adhesion will result in a low value of the Kraus parameter  $C$  under the same swelling condition. The influence of filler-loading on the equilibrium degree of swelling is illustrated in Figure 37.

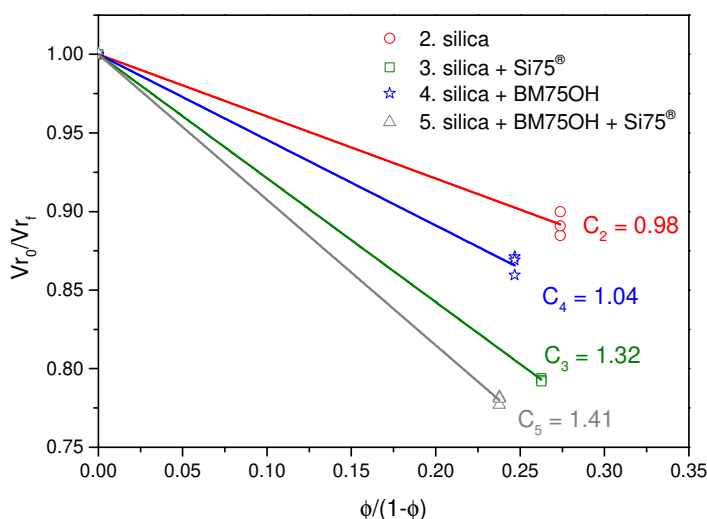


Figure 37. Kraus plot and Kraus parameters of the filled compounds

As can be seen from Figure 37 the lowest Kraus parameter  $C$  is determined for compound 2 which contains neither silane nor Nanoprene® BM75OH ( $C_2 = 0.98$ ). At the same time the parameter  $C$  provides clear indication for a good wetting of the silica surface with the rubber matrix as otherwise  $C$  would be close to 0 or even negative. By the addition of Nanoprene® BM75OH or silane the Kraus parameters are increased to  $C_4 = 1.04$  (compound 4) and  $C_3 = 1.32$  (compound 3), respectively. The addition of both silane and Nanoprene® BM75OH further increases the Kraus parameter to  $C_5 = 1.41$  (compound 5). This means that silane as well as Nanoprene® BM75OH increases the adhesion between the silica filler and the rubber matrix, which can be attributed to the higher rubber-filler interaction.

The approach of thermodynamics is also of great importance for understanding the rubber-filler interaction in the nanocomposites. Thus, thermodynamic effects were also analyzed during the swelling process. The crosslink density, the solvent used and the testing temperature also influence the swelling results. The swollen rubber in the presence of a solvent will significantly modify the elastic Gibbs free energy ( $\Delta G$ ) and the conformational entropy ( $\Delta S$ ). The relationship is quantitatively expressed by the Flory-Huggins equation<sup>[119,152]</sup>:

$$\Delta G = RT[\ln(1 - v_2) + v_2 + \chi v_2^2] \quad \text{Equ. (43)}$$

where  $R$  is the gas constant,  $T$  is the swelling temperature in K,  $\chi$  is the polymer solvent interaction parameter, and  $v_2$  is the volume fraction of swollen polymer, which can be calculated from Equ. (26).  $\Delta S$  can be obtained from the equation  $\Delta S = -\Delta G/T$  according to the statistical theory of rubber elasticity, which assumes no change in internal energy of the network in a constant condition of pressure and temperature. Both thermodynamic parameters of  $\Delta S$  and  $\Delta G$  are given in Table 8. A lower  $\Delta G$  indicates a better compatibility between filler and rubber<sup>[153]</sup>. The value of  $\Delta G$  becomes more negative with the addition of silane or Nanoprene® BM75OH in the blend. It should also be noted that addition of silane or Nanoprene® BM75OH increases the  $\Delta S$  value. It is considered that  $\Delta S$  in an isolated system increases during all spontaneous chemical and physical processes from the principle of the increase of entropy<sup>[154]</sup>. Thus, the compound of silica-silane-Nanoprene® BM75OH shows better chemical stability and homogeneity after diffusion processes than the other compounds.

### 3.2.6 Reinforcement mechanism of silica and Nanoprene® BM75OH

As discussed in Chap. 3.1.3 Nanoprene® BM75OH does undergo silanization which was confirmed by means of gas chromatography. In comparison with the silanization of silica the reaction of Nanoprene® BM75OH occurs at a significantly lower rate. In a competitive situation, however, in which silica and Nanoprene® BM75OH are simultaneously silanized the silane will be more rapidly consumed by the silica than by the hydroxyl groups of Nanoprene® BM75OH. From this perspective the coupling by persistent chemical bonds between Nanoprene® BM75OH and the surrounding rubber matrix will be much lower than for silica. A rough estimate gives a ratio of 5/95. From this line of reasoning there must be other mechanisms than chemical bonds between Nanoprene® BM75OH and the rubber matrix alone which account for the reinforcing effect of Nanoprene® BM75OH. One possibility is hydrogen bonding between hydroxyl groups and unsilanized silanol groups during the mixing procedure (Figure 38).

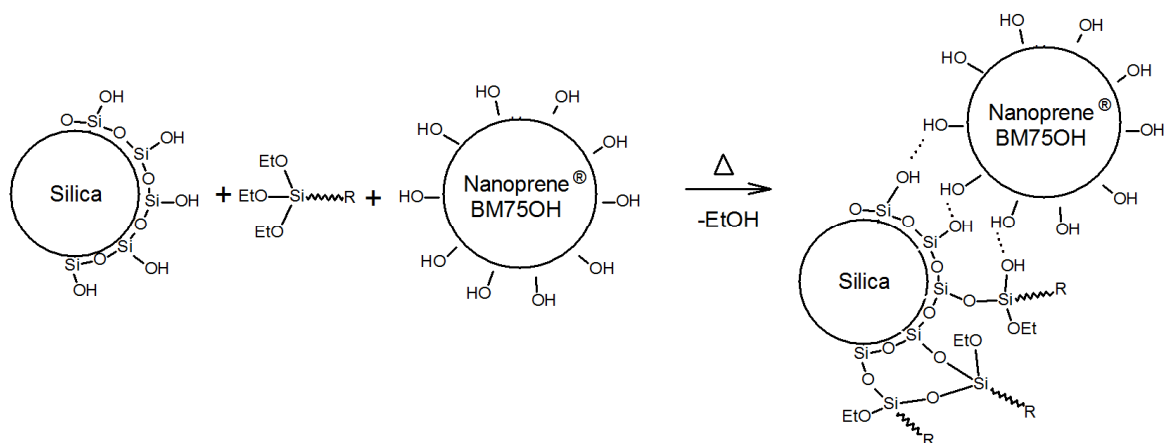


Figure 38. Schematic representation of the silanized filler hybrid system based on silica and Nanoprene<sup>®</sup>

If this is the case there will be mixed agglomerates of silica and Nanoprene<sup>®</sup> BM75OH. These agglomerates will coexist with agglomerates of pure silica and those of pure Nanoprene<sup>®</sup> BM75OH particles.

### 3.3 Influence of different functionalized nanoparticles on silica hybrid systems

The reinforcing mechanism of the hydroxyl modified Nanoprene<sup>®</sup> grade BM75OH is referred to in Chap. 3.2. In this chapter the performance of Nanoprene<sup>®</sup> grades with different types of functional groups are compared in order to detect the best functional group. For the comparison of properties a compound study was performed in which Nanoprene<sup>®</sup> BM75OH was replaced by grades with different functional groups. For the study the following grades were selected (functional monomers in brackets): Nanoprene<sup>®</sup> L (acrylic acid), F (2-vinylpyridine), G (4-vinylpyridine), BM75OH (hydroxyethyl methacrylate), D (glycidyl methacrylate), I (2-dimethylamino ethyl methacrylate).

The basic formulation of the compound study is shown in Table 9. The compound called “Nano-free” is the reference as it only contains silica and no Nanoprene<sup>®</sup>. The other compounds contain the different Nanoprene<sup>®</sup>-grades (15 phr) in addition to silica. All compounds were silanized by the use of a constant amount of the silane coupling agent (Si 75<sup>®</sup>).

Table 9. Formulation for the rubber compounds

	Compound	Nano-free	Nano
Mixing step 1 & 2	Buna <sup>®</sup> VSL 4526-2 HM	96	96
	Buna <sup>®</sup> CB 25	30	30
	Ultrasil <sup>®</sup> VN3 GR	80	80
	Nanoprene <sup>®</sup> *	-	15
	Si 75 <sup>®</sup>	6.4	6.4
	Vivatec <sup>®</sup> 500	10	10
	Zinc oxide	3	3
Mixing step 3	Stearic acid	2	2
	Vulkanox <sup>®</sup> 4020	2	2
	Antilux <sup>®</sup> 500	1	1
	Vulkacit <sup>®</sup> CZ	1.6	1.6
	Vulkacit <sup>®</sup> D	1.5	1.5
	Sulfur	2	2

\* Nanoprene<sup>®</sup> L (Acrylic acid), F (2-Vinylpyridine), G (4-Vinylpyridine), BM75OH (Hydroxyethyl methacrylate), D (Glycidyl methacrylate), I (2-Dimethylamino ethyl methacrylate).

On the one hand, the compounds were investigated in the unvulcanized state regarding rheometrical properties, scorch, Mooney viscosity and Mooney relaxation. On the other hand, the vulcanizates were characterized by strain-stress measurements, dynamic mechanical analysis, hardness, rebound resilience, compression set and abrasion resistance. As a result of the study, the best functionalized Nanoprene® grade is to be detected.

### 3.3.1 Influence of different functionalized nanoparticles on silica flocculation

The influence of different Nanoprene® grades on the silica flocculation was investigated by measuring the storage modulus ( $G'$ ) at low strain amplitude during the temperature treatment. The breakdown of the filler structure was subsequently monitored by the dependence of  $G'$  on gradually increasing the shear strain up to 400 %. The performance of the Nanoprene® modified compounds which were taken after the first mixing step and the reference compound without Nanoprene® is given in Figure 39.

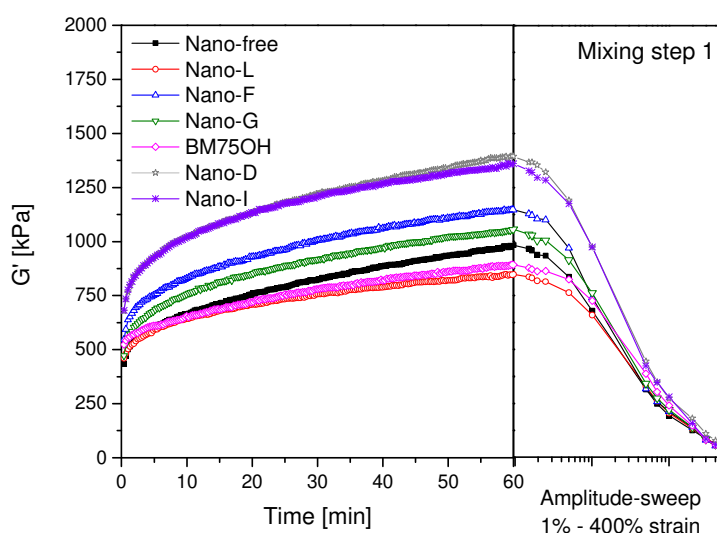


Figure 39. Filler flocculation behaviour at 160 °C of unvulcanized compounds after the first mixing step and subsequent dependence of  $G'$  on strain

Although all the indicated compounds were silanized in the first mixing step, silica flocculation still takes place during the heating process involved in mixing and vulcanization. For the reference compound without Nanoprene® silica flocculation as well as the result of the subsequent break down of the filler network are most pronounced in comparison with the other compounds modified by Nanoprene®. This means that the different functional monomers influence the silica flocculation quite differently. As can be seen the compound with Nanoprene® L, which was polymerized with the functional monomer of acrylic acid,

exhibits the lowest increase in  $G'$  and the least pronounced filler break-down. That is due to the high polarity of the carboxyl groups on the particle surface of Nanoprene<sup>®</sup> L, which can reduce the polarity differences between silica and polymer. Besides the Nanoprene<sup>®</sup> L compound, the Nanoprene<sup>®</sup> BM75OH compound, which contains the functional groups of hydroxyl also performs better than the reference Nanoprene<sup>®</sup> free compound. The reason has been discussed in Chap. 3.2.1. For the compounds Nanoprene<sup>®</sup> F (2-vinylpyridine) and G (4-vinylpyridine) filler flocculation and the subsequent break down of the filler-network is deteriorated comparing with the reference compound. Again, the compounds, which contains Nanoprene<sup>®</sup> D (glycidyl methacrylate) and I (2-dimethylamino ethyl methacrylate), show the worst filler flocculation. If the Nanoprene<sup>®</sup> grades contain no hydrophilic functional groups, for the more hydrophobic functional groups there is a higher tendency for silica flocculation. The results clearly demonstrate the improvement of silica flocculation and dispersion by Nanoprene<sup>®</sup> L and Nanoprene<sup>®</sup> BM75OH.

The performance of the Nanoprene<sup>®</sup> modified compounds taken after the second mixing step is given in Figure 40.

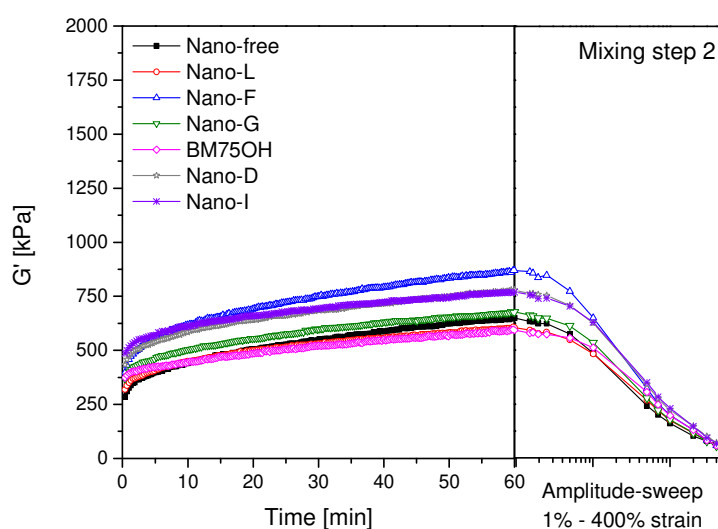


Figure 40. Filler flocculation behaviour at 160 °C of unvulcanized compounds after the second mixing step and subsequent dependence of  $G'$  on strain

As can be seen in Figure 40 the  $G'$  values are considerably lower than the values after the first mixing step. It has already demonstrated in Chap. 3.2.1 that the second mixing step plays an important role in the silica dispersion. Still the beneficial influence of Nanoprene<sup>®</sup> L and Nanoprene<sup>®</sup> BM75OH can be seen from a comparison of the reference Nanoprene<sup>®</sup> free

compound. The difference of the filler flocculation between the Nanoprene<sup>®</sup> free sample and the respective Nanoprene<sup>®</sup> containing compounds get smaller after the second mixing procedure. Despite this small difference, the beneficial influences of Nanoprene<sup>®</sup> L and Nanoprene<sup>®</sup> BM75OH on the quality of silica dispersion are quite apparent.

### 3.3.2 Properties of unvulcanized compounds

After mixing step two the vulcanizing package of comprising constant amount of sulfur and accelerator was added to the mixtures in the third mixing step. Mooney viscosity of the rubber mixtures was determined at 100 °C and subsequently Mooney relaxation was determined in the same apparatus. The cure characteristics were measured by the increase of the torque values as a function of time at 160 °C according to a standard procedure with a moving die rheometer (MDR). The rheometrical properties, scorch, Mooney viscosity, and Mooney relaxation are shown in Table 10. The rheometer curves are given in the annexes.

Table 10. Effects of Nanoprene<sup>®</sup> grades with different functional groups on rheometrical properties, scorch, Mooney viscosity and Mooney relaxation

Item	Nano-free	Nano-L	Nano-F	Nano-G	BM75OH	Nano-D	Nano-I
$S_{Min}$ [dNm]	2.1	2.6	2.6	2.3	2.7	2.7	2.7
$S_{Max}$ [dNm]	13.4	11.6	15.4	12.2	12.5	13.8	13.6
$S_{Max} - S_{Min}$ [dNm]	11.4	9.1	12.7	9.9	9.8	11.1	10.9
$t_{10}$ [min]	2.0	2.1	2.0	1.6	2.5	1.8	2.4
$t_{50}$ [min]	3.2	3.4	3.2	2.6	3.6	3.9	4.0
$t_{90}$ [min]	11.4	17.0	12.4	15.4	8.0	21.4	18.3
$t_{s-1}$ [min]	2.0	2.2	1.9	1.6	2.5	1.8	2.3
ML 1+4@100°C [MU]	55.2	60.5	60.7	55.4	59.1	64.3	59.7
Mooney Relaxation, 30 sec. [%]	18.1	19.6	16.8	18.3	20.0	20.2	20.1

As can be seen in this table the different functional monomers have a different effect on the properties of the unvulcanized compounds, e.g. the tendency towards scorching, the vulcanization rates, and the delta torque value ( $S_{Max} - S_{Min}$ ). Regarding the resistance towards scorching Nano-G (2-vinylpyridine) and Nano-D (glycidyl methacrylate) are the most critical products. Regarding the vulcanization time  $t_{90}$ , BM75OH performs particularly well (lowest value). In this respect the performances of Nano-D (glycidyl methacrylate) and Nano-

I (2-dimethylamino ethyl methacrylate) are bad as these two products need the longest time until  $t_{90}$  is reached. Regarding the vulcanization characteristics the performance of BM75OH is the best, as this product shows a high resistance to scorching and also a short  $t_{90}$ -value. After the addition of Nanoprene® in the compound the value of the minimum torque ( $S_{\min}$ ) was raised due to the filler like performance of Nanoprene®. Regarding the delta torque values ( $S_{\max} - S_{\min}$ ), which give an indication for the overall crosslink density, Nano-F which contains 2-vinylpyridine has the best performance. In addition, this product shows a good resistance to scorching and also a short  $t_{90}$ -value.

### 3.3.3 Tensile testing

In the stress/strain diagrams (Figure 41) the most important features are the strains at different elongations. At low elongations up to 10 % the strain values are dominated by the filler network. In this elongation range low values indicate a good filler dispersion. At higher elongations > 100 % the strain values give a reflection of the crosslink density. As a result, the ratio of strains ( $M_{100}/M_{10}$  or  $M_{300}/M_{10}$ ) should exhibit high values as high values indicate a good filler dispersion and a high crosslink density. In this respect Nano-I, Nano-D, BM75OH and Nano-G show a better performance than the silica loaded reference compound.

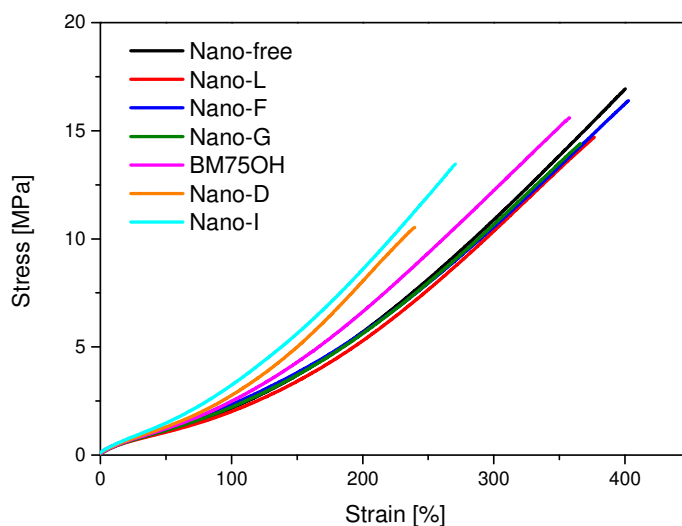


Figure 41. Stress-strain curves of the indicated composites

Another feature for the evaluation is tensile strength. Unfortunately, in most vulcanizates tensile strength reversely depends on the modulus. Therefore vulcanizates which exhibit high tensile strength values and high moduli have the best performance. The reason for a high tensile strength in combination with a high modulus which is usually caused by a high quality



of the network structure, a low concentration of crosslink clusters, a homogenous distribution of the crosslinks over the rubber matrix, and also low concentrations of free chain ends. Regarding the performance evaluation by stress/strain experiments the hydroxylated Nanoprene® grade BM75OH performs better than silica and also better than the nanoparticles with other functionalities.

There is another feature worth mentioning. The ranking of the different Nano-grades regarding the silanization rates is opposite to the ranking regarding  $M_{100}/M_{10}$  (Table 11). For instance, Nanoprene® I exhibits the lowest silanization rate among the investigated Nanoprene® grades but the highest  $M_{100}/M_{10}$  value. These dependencies mean that the quality of silica dispersion improves with a decrease of the silanization rate. From these observations it can be concluded that the unsilanized Nano-grades Nano-I (2-dimethylamino ethyl methacrylate), Nano-D (glycidyl methacrylate), and Nanoprene® BM75OH (hydroxyethyl methacrylate) exhibit a good interaction with silica and that the interaction with silica is reduced by the silanization reaction. From these observations it is evident that the good performance of Nanoprene® BM75OH is due to the low degree of silanization (reactivity of silanization, compare Chap. 3.1.4).

Table 11. Tensile strength, elongation at break, tensile modulus, and the ratio of  $M_{100}/M_{10}$  and  $M_{300}/M_{10}$

Item	Nano-free	Nano-L	Nano-F	Nano-G	BM75OH	Nano-D	Nano-I
Tensile strength [MPa]	16.9±0.5	14.4±0.8	16.4±1.0	14.4±0.8	15.6±0.7	10.5±0.7	13.5±0.8
Elongation at break [%]	400±7	372±17	403±27	366±12	358±12	240±9	271±11
Modulus @ 10% elongation [MPa]	0.40±0.00	0.38±0.00	0.45±0.00	0.37±0.00	0.39±0.00	0.42±0.00	0.46±0.00
Modulus @ 20% elongation [MPa]	0.62±0.00	0.58±0.00	0.67±0.00	0.59±0.01	0.63±0.01	0.66±0.00	0.72±0.00
Modulus @ 50% elongation [MPa]	1.12±0.01	1.06±0.01	1.20±0.02	1.14±0.04	1.22±0.04	1.30±0.02	1.48±0.03
Modulus @ 100% elongation [MPa]	2.16±0.01	2.01±0.03	2.33±0.02	2.21±0.07	2.50±0.09	2.76±0.05	3.23±0.08
Modulus @ 300% elongation [MPa]	10.9±0.12	10.4±0.18	10.6±0.08	10.7±0.20	12.2±0.25	-	-
$M_{100}/M_{10}$	5.4	5.3	5.2	6.0	6.4	6.6	7.0
$M_{300}/M_{10}$	27.3	27.4	23.6	28.9	31.3	-	-

### 3.3.4 Dynamic mechanical properties

By means of DMA measurements the temperature dependencies of the mechanical loss factor ( $\tan \delta$ ) was recorded in Figure 42. The dynamic glass transition temperature ( $T_g$ ) of the nano-free reference compound ( $T_g = -25 \text{ }^\circ\text{C}$ ) and of the nano-modified compounds ( $-25 \text{ }^\circ\text{C}$  to  $-27 \text{ }^\circ\text{C}$ ) almost coincide and the different curves strongly overlap. Only the peak height of the nano-containing vulcanizates is slightly higher than that of the nano-free reference compounds.

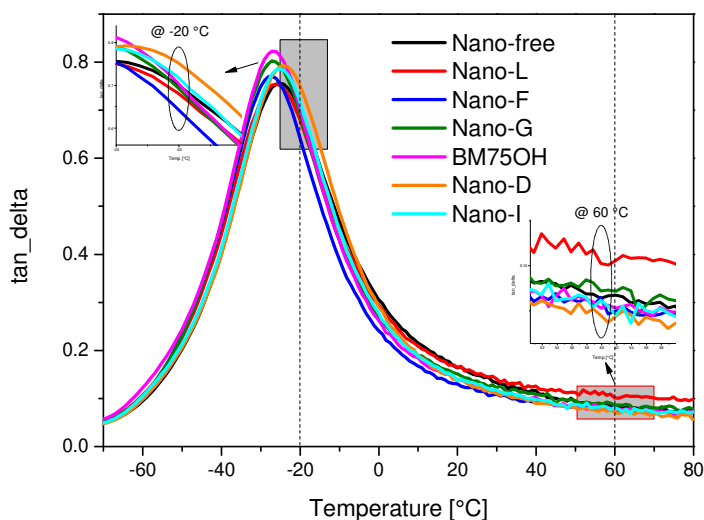


Figure 42. Temperature dependence of  $\tan \delta$  at 10 Hz and 0.5 % strain

The results of  $G'$ ,  $G''$  and  $\tan \delta$  at  $-20 \text{ }^\circ\text{C}$  which could represent the snow and ice grip in tire tread compounds<sup>[155]</sup> are summarized in Table 12. The characteristics of snow or ice traction are highly dependent on the low temperature flexibility of the tire tread compound<sup>[156]</sup>. That means the softer compound with high resilience has higher friction on ice at the temperature around  $-20 \text{ }^\circ\text{C}$ , and for this reason, excellent traction performance on ice and snow can be achieved with low  $G'$ ,  $G''$  and high  $\tan \delta$  values at  $-20 \text{ }^\circ\text{C}$ <sup>[157]</sup>. In the Nanoprene<sup>®</sup> modified compounds exhibited mostly softer characteristics with lower  $G'$  and  $G''$  compared to the Nano-free reference compound. When viewed from the perspective of  $G'$ ,  $G''$  and  $\tan \delta$  values at  $-20 \text{ }^\circ\text{C}$ , for the compounds with Nanoprene<sup>®</sup> BM75OH, Nano-D, and Nano-I an improvement in the snow and ice grip properties can be expected. Furthermore, the rolling resistance can be expressed as the value of low hysteresis at  $60 \text{ }^\circ\text{C}$ . The improved rolling resistance of the BM75OH, Nano-D, and Nano-I compounds with both low  $G''$  and  $\tan \delta$  values at  $60 \text{ }^\circ\text{C}$  was observed.

Table 12. Dynamic mechanical properties

Item	Nano-free	Nano-L	Nano-F	Nano-G	BM75OH	Nano-D	Nano-I
$T_g$ [°C]	-25.2	-26.1	-27.1	-27.1	-27.1	-25.1	-25.1
Height of $\tan \delta$ peak	0.71	0.71	0.72	0.75	0.77	0.75	0.74
$G'$ (-20°C) [MPa]	18.9	15.0	14.0	12.7	10.6	16.0	14.9
$G''$ (-20°C) [MPa]	13.3	10.3	9.03	8.85	7.47	12.0	10.7
$\tan \delta$ (-20°C)	0.703	0.682	0.645	0.695	0.707	0.754	0.720
$G'$ (60°C) [MPa]	2.33	2.05	2.81	2.14	1.89	2.23	2.28
$G''$ (60°C) [MPa]	0.19	0.21	0.23	0.18	0.14	0.16	0.18
$\tan \delta$ (60°C)	0.082	0.101	0.082	0.086	0.076	0.072	0.081
Payne effect* (23°C) [MPa]	1.12±0.03	0.75±0.02	0.72±0.02	0.77±0.02	0.54±0.07	0.65±0.05	0.63±0.03

\* Calculated as  $G'_{(0.05\%)} - G'_{(5\%)}$

The non-linear behaviour of the storage modulus ( $G'$ ) of the indicated vulcanizates according to dynamic strain amplitudes (0.05 – 5.0 %) is shown in Figure 43, and the values of the Payne effect ( $\Delta G'$ ) are listed in Table 12.

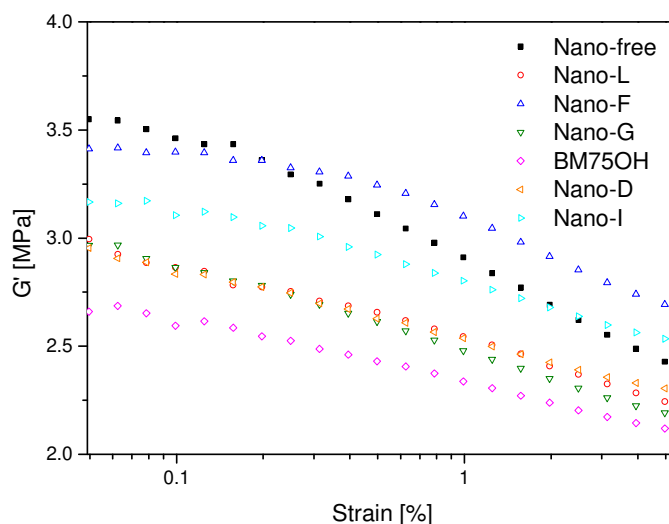


Figure 43. The nonlinear behaviour of the storage modulus ( $G'$ ) according to dynamic strain (0.05 ~ 5.0 %) at 23 °C

As can be clearly seen that the Payne effect is the highest for the Nano-free vulcanizate, and it decreases with the addition of all types of Nanoprene®. Amongst these, the compounds with Nanoprene® BM75OH, Nano-D, and Nano-I perform better. As the Payne effect is ascribed to the filler-filler interaction, the lowering of Payne effect values are indicative of a reduction of filler-filler interaction and an improvement in the dispersion of silica filler. Therefore, from the results of Payne effect it is support that Nanoprene® can improve the silica dispersion.

### 3.3.5 The other mechanical properties

The other physical test values of Shore A hardness, rebound resilience, compression set and DIN abrasion were measured on the vulcanizates and shown in Table 13. The Nanoprene® modified compounds contained different functional monomers have different influences on the physical properties.

Table 13. Shore A Hardness, rebound, compression set, and abrasion

Item	Nano-free	Nano-L	Nano-F	Nano-G	BM75OH	Nano-D	Nano-I
Hardness Shore A (23°C)	54.6±1.2	56.0±0.4	58.7±1.0	54.9±1.1	55.2±0.7	59.0±1.0	60.1±0.8
Hardness Shore A (70°C)	52.8±1.2	52.5±1.5	57.8±1.0	53.4±2.0	53.3±1.8	58.6±1.0	58.5±0.5
Rebound (23°C) [%]	44.7±0.7	45.4±0.8	47.5±0.3	47.9±0.6	49.3±0.3	46.0±0.3	47.3±0.3
Rebound (70°C) [%]	65.4±1.2	62.4±1.6	61.8±0.9	63.9±1.4	67.0±1.0	62.4±0.7	62.0±1.0
Compression set (23°C, 72h) [%]	7.0±0.7	12.6±0.2	7.8±0.4	9.2±0.3	7.2±0.4	5.6±0.3	7.1±0.2
Compression set (70°C, 72h) [%]	25.8±0.7	31.5±0.6	27.0±1.4	27.0±1.0	29.9±0.6	20.0±0.2	19.0±0.6
Abrasion (DIN) [mm <sup>3</sup> ]	96.5±4.6	120.6±9.3	101.2±2.6	93.8±4.7	88.4±3.0	113.2±3.0	89.5±5.5

For very small elongations there is always a correlation between moduli (in Table 11) and Shore A hardness. As a lower Shore A hardness at 23 °C is an indication of a better silica dispersion, in this case, there are no adverse effects exerted by Nano-G and BM75OH on the hardness of the rubber compound. Furthermore, Nanoprene® could increase the rebound resilience at 23 °C, and the compound with Nanoprene® BM75OH exhibited the highest resilience at 70 °C. The compounds with Nano-D and Nano-I could significantly improve the compression set comparing with the Nano-free vulcanizate. Besides these physical

properties, the abrasion resistance is also one of the important parameters for the tire tread compound. It is reported that the abrasion resistance can be improved by increasing the volume fraction of the filler, the filler dispersion, or the filler-rubber interaction<sup>[158,159]</sup>. The compounds containing Nanoprene<sup>®</sup> BM75OH, Nano-I and Nano-G show an excellent abrasion resistances probably due to a good polymer-filler interaction. It is remarkable that the compound Nano-L, which is polymerized with the functional monomer acrylic acid displayed poor physical properties. The high polarity and acidity of the carboxyl groups result in a high silanization rate. In a competitive reaction during which Nano-L and silica compete for silane both, the carboxyl group and the silanol group are silanized to a high extent. It's a result of the silanization. The nanoparticle loses its ability to achieve a good dispersion of silica. This is another proof that for a good dispersion of silica a good interaction between the functional groups on the surface of the Nanoprene<sup>®</sup> particles and the silanol groups is needed.

### 3.4 Influence of water on silica loaded vulcanizates

So far, it was established, that the hydroxylated Nanoprene<sup>®</sup> grade BM75OH undergoes silanization. In comparison with the silanol groups of silica, however, the silanization rate of the hydroxyl groups was significantly lower. As a consequence, when the silane is fully consumed the portion of silanized hydroxyl groups of Nanoprene<sup>®</sup> is much smaller than the portion of silanized silanol groups of silica. On the basis of kinetic data it is speculated that the ratio of silanized silanol groups of silica over silanized hydroxyl groups of Nanoprene<sup>®</sup> is around 95/5. In addition, the mechanical and dynamic mechanical data of the vulcanizate which contains the silanized silica/Nanoprene<sup>®</sup> BM75OH hybrid filler show clear advantages over the reference vulcanizate which only contains silanized silica. From these observations it is concluded that the reinforcing effect of Nanoprene<sup>®</sup> BM75OH is not caused by additional chemical bonds between the surface of a Nanoprene<sup>®</sup> particle and the rubber matrix but by an increase of silica dispersion and a subsequent increase of silica silanization.

If these considerations are correct, a study on the influence of water could yield further information. Additional chemical bonds between the surface of the nano-sized particles and the rubber matrix consist of the following moieties:  $-\text{CH}_2-\text{O}-\text{Si}(\text{OR})_2-(\text{CH}_2)_3-\text{S}_x-\text{rubber}$ . If these moieties are present, there should be a negative effect of water exposure on the performance of the vulcanizates as these moieties are liable to hydrolysis. On the other hand water exposure should not affect the  $\equiv\text{Si}-\text{O}-\text{Si}(\text{OR})_2-(\text{CH}_2)_3-\text{S}_x-\text{rubber}$  bonds which result from the silanization of silica. Regarding silica it is well known that during the silanization process silica is made more hydrophobic. Therefore silica can be better dispersed in the nonpolar rubber matrix. On the other hand, however, even in the silanized state silica still agglomerates. Therefore even in silanized silica there remain enough hydrophilic areas which are the root cause for the agglomeration of silica in a hydrophobic environment. If silica based vulcanizates are exposed to water in particular the hydrophilic areas of silica which are not silanized will adsorb water and the amount of adsorbed water will depend on the degree of silanization in a reciprocal manner.

For a study of the water influence on the vulcanizate properties two compounds were prepared (Table 14). Both compounds contain silica. Contrary to the “silane-activated compound” the “silane-free compound” was not silanized during the preparation of the compound.

Table 14. Composition\* of the silica filled compounds

	Ingredients	Silane-activated compound	Silane-free reference
Mixing step 1 & 2	Buna® VSL 4526-2 HM	96	96
	Buna® CB 25	30	30
	Ultrasil® VN3 GR	80	80
	Si 75®	6.4	-
	Vivatec® 500	10	10
	Zinc oxide	3	3
Mixing step 3	Stearic acid	2	2
	Vulkanox® 4020	2	2
	Antilux® 500	1	1
	Vulkacit® CZ	1.6	1.6
	Vulkacit® D	1.5	1.5
	Sulfur	2	2

\* All weights are in phr (parts in weight per 100 g rubber).

A series of investigations were performed on the two compounds. First, the two vulcanizates were characterized by TEM and by swelling in toluene. Then the weight increase was determined after water storage at different temperatures and different times. Subsequently the influence of water was studied by DMA. In this study the following vulcanizates were included: the original dry samples, the wet samples after water exposure and samples which were dried after water exposure.

Finally, in order to check the reversibility of water swelling the performance of samples was compared regarding chemical changes and physical properties. In detail, the performance of the original dry vulcanizate was compared with a vulcanizate which was dried subsequent to water storage

### 3.4.1 Features of the silane-activated and silane-free reference vulcanizate

As no silane was used for the preparation of the reference vulcanizate, the hydrophilic filler and the hydrophobic polymers were not compatibilized during the compound preparation. Therefore silica distribution is much worse in the reference vulcanizate, as it was shown in Figure 36 (in Chap. 3.2.4). There are also voids between the silica particles and the silica/polymer interface which will cause an increase of the free volume of the silane-free

vulcanizate. These voids can contribute to an increment in permeability<sup>[151]</sup>. This aspect will be discussed in the context of results which were obtained in water storage experiments.

The primary difference between the silane-activated and silane-free vulcanizates is the apparent crosslink density (Figure 44) which was calculated from equilibrium swelling data by means of the Flory-Rehner equation<sup>[122]</sup>. The apparent chemical crosslink densities for the silane-free and the silane-activated vulcanizates before water storage are  $1.27 \times 10^{-4}$  and  $1.51 \times 10^{-4} \text{ mol/cm}^3$ , respectively. The high apparent chemical crosslink density of the silane-activated vulcanizate resulted from matrix crosslinking and silica-rubber coupling (explanation see in Chap. 2.5.2).

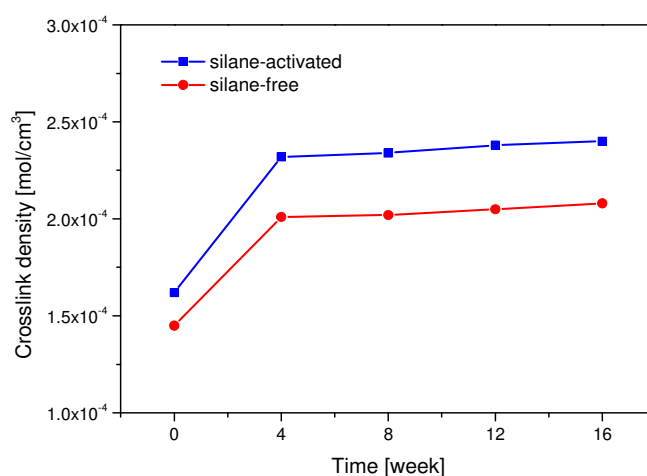


Figure 44. Dependence of the apparent crosslink density on the water storage time at 80 °C for silane-activated silica compound (blue squares) and silane-free reference compound (red circles)

After 16 weeks water storage at 80 °C the apparent crosslink densities are  $2.08 \times 10^{-4} \text{ mol/cm}^3$  for the silane-free vulcanizate and  $2.40 \times 10^{-4} \text{ mol/cm}^3$  for the silane-activated vulcanizate. These increases were either caused by a post-vulcanization during the water storage at 80 °C or by the drying process subsequent to water storage (dried to a constant weight in a vacuum oven at 23 °C). According to the literature, heat and oxygen cause significant increases of the crosslink densities of vulcanizates which are based on unsaturated rubbers e.g. polybutadiene and poly(styrene-co-butadiene). Jitkarnka et al.<sup>[160]</sup> have reported that the crosslink density increases with the thermal aging time, which is primarily caused by both the residual curative and the rearrangement of sulfur crosslinks. Santoso et al.<sup>[161]</sup> have shown that in the case of SBR-matrices, contrary to the vinyl units the styrene units exhibit a stabilizing effect. Therefore, the increase of the apparent crosslink



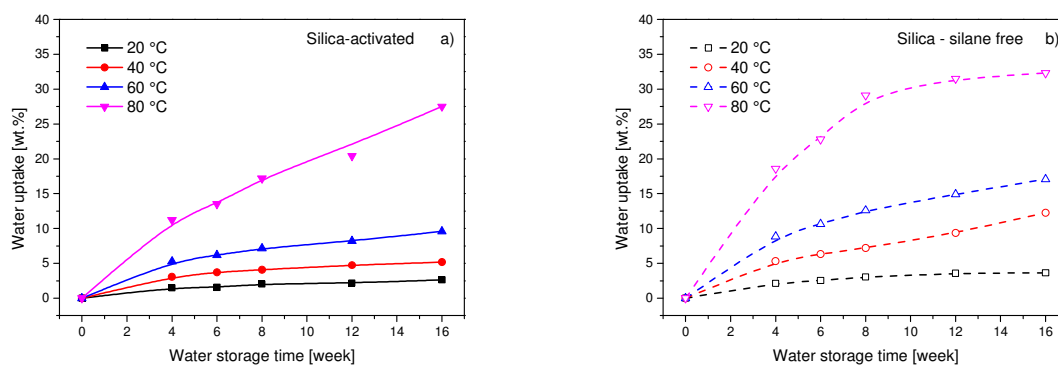
density in the first 4 weeks is primary due to the residual curative of sulfur crosslinks. As aging processes are irreversible they can be easily distinguished from reversible processes which we later describe in this chapter.

### 3.4.2 Influence of water on the weight increase of vulcanizates

The water uptake in the vulcanizate can be calculated using the following equation:

$$\text{Water uptake (\%)} = \frac{W_s - W_0}{W_s} \times 100 \quad \text{Equ. (44)}$$

in which  $W_s$  is the weight of the wet samples after different water storage times and  $W_0$  is the weight of the dry sample before water storage. In Figure 45 (a) and (b) the dependencies of the water uptake is given as a function of water storage time at different storage temperatures. The plot given in Figure 45 (a) refers to the silane-containing vulcanizates whereas the data for the silane-free reference compound are given in Figure 45 (b).



(a) silane-activated silica compound

(b) silane-free reference compound

Figure 45. Dependence of the water uptake on the water storage time for different storage temperatures: 20 °C (black squares), 40 °C (red circles), 60 °C (blue triangles), and 80 °C (pink triangles), (a) silane-activated silica compound (b) silane-free reference compound

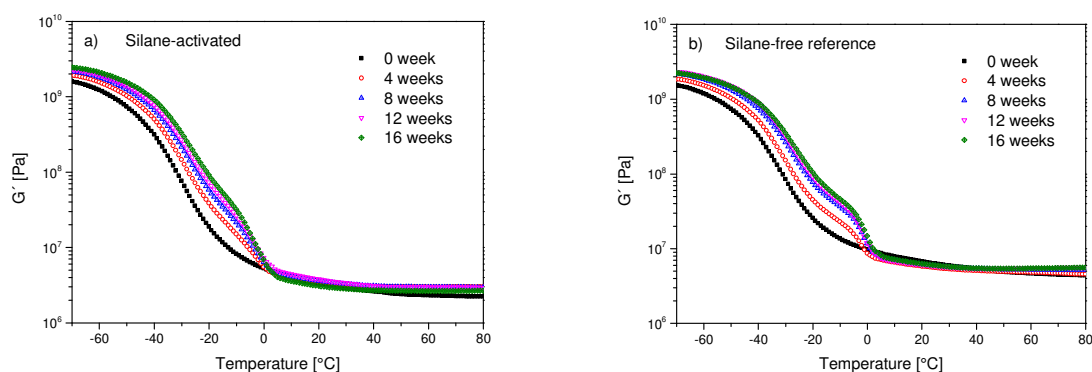
As can be seen from Figure 45 (a) and (b) the weight increase by water is strongly influenced by temperature, storage time, and the presence of silane. The water content after 16 weeks water storage at 80 °C is remarkably high. It is 32.3 wt.% for the silane-free reference compound and 27.5 wt.% for the silane-activated silica compound. A comparison of the Figure 45 (a) and (b) shows that for the same storage times and the same storage temperatures the water uptake of the silane-free reference vulcanizate is always higher than for the silane-activated silica compound. The reasons for this different performance can be

due to: (1) a higher hydrophilicity of the silane-free compound, (2) a higher porosity of the silane-free compound which is the result of a poor filler-polymer interaction and (3) a lower crosslink density of the silane-free compound. Furthermore, the water uptake strongly increases with the water storage temperature. This increase is very likely the result of increasing segmental mobility and the respective increase in free volume of the polymer matrix with increasing temperature.

### 3.4.3 Influence of silane on dynamic mechanical properties after water storage

In order to investigate the influence of water on the dynamic mechanical properties a series of samples was selected which were stored in water at 80 °C for up to 16 weeks. Dynamic mechanical analysis was performed at 10 Hz using a temperature sweep in range of -70 to +80 °C. From the DMA measurements the temperature dependencies of the storage modulus  $G'$ , the loss modulus  $G''$  and  $G''/G'$  ( $\tan \delta$ ) were obtained. These three parameters will be discussed in this order.

Figure 46 (a) shows the temperature sweep of the storage moduli  $G'$  for dry and water containing samples (after different water storage times) for the silane-activated vulcanizate. The respective data for the silane-free reference vulcanizate are depicted in Figure 46 (b).



(a) silane-activated silica compound

(b) silane-free reference compound

Figure 46. Temperature dependence of the storage modulus  $G'$  on water storage time at 80 °C (a) silane-activated silica compound (b) silane-free reference compound

As can be seen from the two figures for temperatures  $< 0$  °C water absorption results in an increase of  $G'$  for the silane-activated and for the silane-free vulcanizates. As water is frozen in this temperature range the water which is adsorbed on the silica surface will result in an increase of the effective filler volume. It is well established that an increase in filler loading will cause an increase in  $G'$ <sup>[162, 163]</sup>, which is found in Figure 46 (a) and (b). In the temperature

range above 0 °C in which water is liquid the effect of water on  $G'$  is rather small. A closer inspection reveals that in the case of the silica-activated vulcanizate water causes a slight increase of  $G'$ .

Figure 47 (a) shows the temperature sweep of the loss moduli  $G''$  for dry and water containing samples (after different water storage times) for the silane-activated vulcanizate. The respective data for the silane-free reference vulcanizate are depicted in Figure 47 (b).

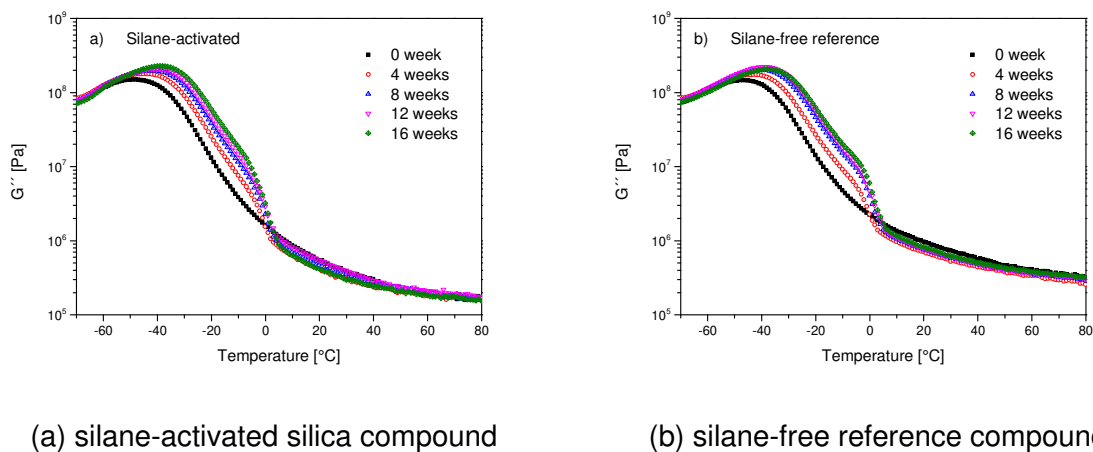


Figure 47. Temperature dependence of the loss modulus  $G''$  on water storage time at 80 °C  
(a) silane-activated silica compound (b) silane-free reference compound

In the low temperature region in which water is frozen we observe an increase of  $G''$ , this can be caused by the apparently increase of filler content by the presence of ice. Also the mobility of the polymer chains which are chemically attached to the silica surface will be reduced by the presence of ice on the silica surface which will also result in an increase of  $G''$ . Both effects, the increase of filler loading and the reduction of chain mobility will cause an increase of energy dissipation<sup>[164]</sup> which is reflected by an increase of  $G''$  at temperatures < 0 °C. In the high temperature region the adsorbed water is liquid in the vulcanizates and  $G''$  is reduced by water.

Figure 48 (a) and (b) show the damping curves of the silane-activated silica compound and of the silane-free reference compound respectively. As can be seen in Figure 48 (a) before water storage the sample shows a single  $\tan \delta$  peak with a maximum at around -25 °C. This peak corresponds to the dynamic glass transition temperature ( $T_g$ ) of the polymer matrix under the indicated testing conditions. By the exposure of the vulcanizates to water a second  $\tan \delta$  peak appears in the temperature range -5 to 0 °C. The height of the second  $\tan \delta$  (water) peak increases with increasing water storage time, whereas the height of the first  $\tan \delta$  peak decreases while the peak maximum ( $T_g$ ) slightly shifts to higher temperatures. It is

quite possible that the incremental increase in  $T_g$  can be attributed to an increase in crosslink density by ageing in hot water.

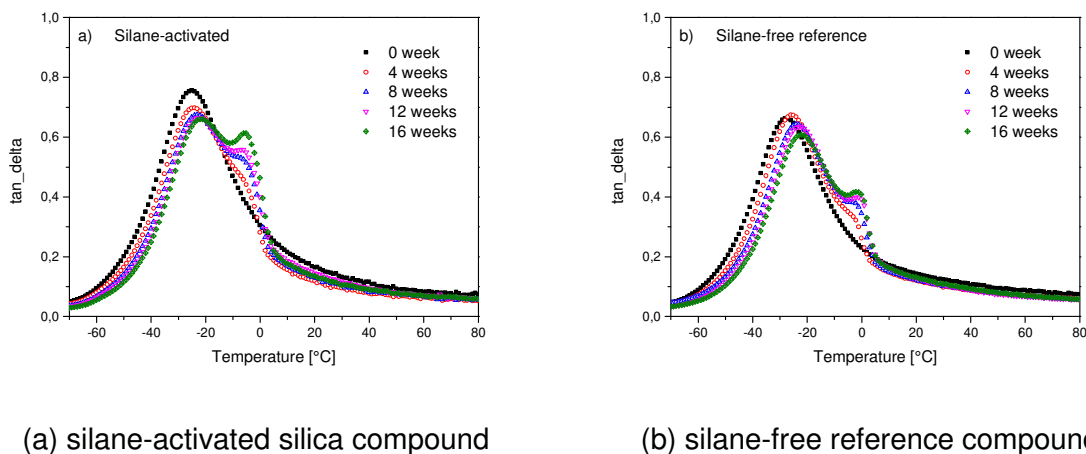


Figure 48. Temperature dependence of  $\tan \delta$  on water storage time at 80 °C (a) silane-activated silica compound (b) silane-free reference compound

The height of the second  $\tan \delta$  peak correlates with the water content of the vulcanizate as shown in Figure 49 (correlation diagram).

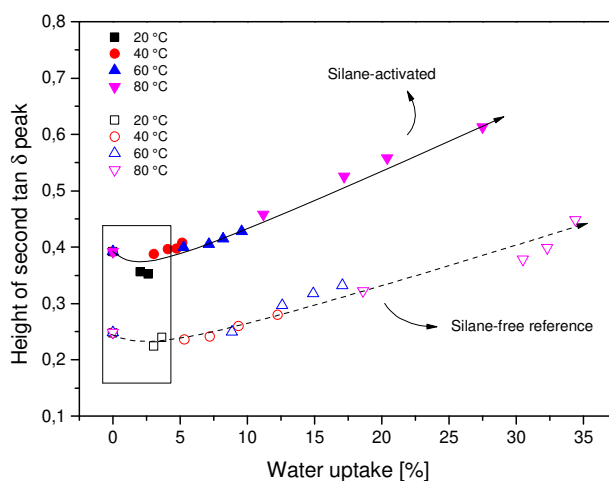


Figure 49. Dependence of the height of the second  $\tan \delta$  peak at -5 to 0 °C on water uptake at different temperatures for the silane-activated silica compound and for the silane-free reference compound

As can be seen from Figure 49 there is an intercept at around 4 wt.% water which means that below this threshold water has no influence on the DMA spectrum. An intercept would mean that small amounts of water could not cause a second peak, because for small

amounts of water there will be no chain extension effect on the polymer chains which are chemically attached on the silica surface. Above this threshold the peak height increases linearly with increasing water content.

The  $\tan \delta$  peak between  $-5$  and  $0$  °C is close to the temperature range in which an increased value indicates an increase of wet skid resistance<sup>[164]</sup>. Hence, water which is absorbed by a tire tread could be advantageous for the performance of a tire on a wet road. In the temperature range  $> 40$  °C  $\tan \delta$  is lower for the wet than for the dry samples. This observation can be explained by a plasticizing effect of liquid water. As  $\tan \delta$  in the temperature range  $> 40$  °C, in particular  $\tan \delta$  at  $60$  °C is usually taken as a predictor for rolling resistance the  $\tan \delta$  reduction by water is a clear indication for the reduction of the rolling resistance of a tire tread<sup>[102]</sup>. Therefore, absorbed water seems to be an advantage for the decrease of the rolling resistance of silica loaded tire treads.

### 3.4.4 Temperature dependence of the rate of water uptake

The temperature dependency of the rate of water swelling can be clearly described by an Arrhenius equation<sup>[69]</sup>,  $k = A \exp(E_a/RT)$ , where  $E_a$  represents the activation energy,  $A$  is the pre-experimental factor,  $R$  is the gas constant,  $T$  is the temperature in K, and  $k$  is the slope of the water uptake taken from the diagrams in which the water uptake is plotted over the water storage time for different water storage temperatures. The Arrhenius plots for the temperature dependencies of the water swelling are shown in Figure 50 for both vulcanizates.

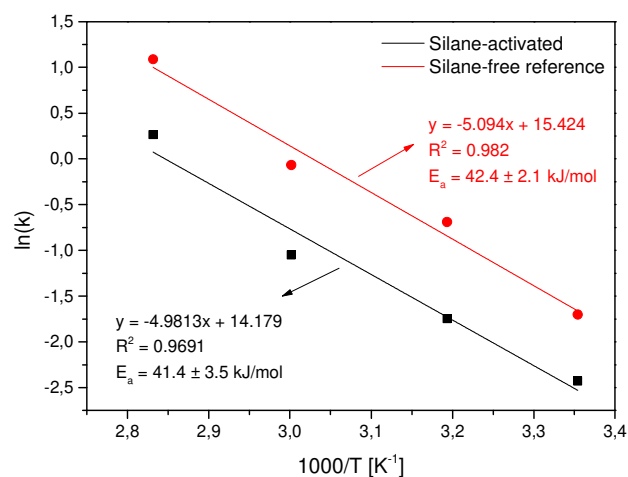


Figure 50. Arrhenius plots for the rates of water uptake for the silane-activated silica compound (black squares) and for the silane-free reference compound (red circles)

The temperature dependencies of the reaction rates can be expressed with good linear fittings with a determination coefficient of  $R^2 = 0.969$  and  $0.982$  respectively for the silane-activated and for the silane-free reference samples at different temperatures. The average values of the calculated activation energies are  $41.4 \pm 3.5$  kJ/mol and  $42.4 \pm 2.1$  kJ/mol for the silane-activated and silane-free samples. That means there is no difference in the activation energies within the standard deviations at temperatures  $\leq 80$  °C. Therefore it can be assumed that there is no difference in the rate-determining reaction of the water uptake for both compounds. The following reaction steps are involved in the water swelling of the vulcanizates: the diffusion of water through the nonpolar rubber matrix and the physisorption of water to the silica surface by the formation of hydrogen-bonds between water and silica. The activation energy which was found in this thesis is consistent with the activation energy for the hydrogen-bonding of water on a silica surface which was reported by Zhuravlev ( $35 - 45$  kJ/mol)<sup>[165]</sup>. From the consistency of the activation energies from this thesis and from the literature it can be concluded that the rate of the determining step in the uptake of water of silica loaded vulcanizates is not the diffusion of water through the nonpolar rubber matrix but the physisorption of water to the silica surface.

### 3.4.5 Reversibility of water swelling/drying on dynamic mechanical properties

In order to check whether the effect of water on the dynamic process is reversible, the hydrated samples (16 weeks, 80 °C) were dried to constant weight in a vacuum oven at room temperature. As can be seen from Figure 51 (a) and (b), for both the silane-activated and silane-free vulcanizates the second  $\tan \delta$  peak between  $-5 - 0$  °C which is caused by water disappears after the removal of water. This indicates the reversibility of the water effect on the damping process. The desorption of physisorbed water can be described by the reaction equation below<sup>[166]</sup>.



The condensation of silanol groups of silica ( $HOSi \equiv$ ) and hydrolyzed silane ( $\sim Si(H)O$ ), which could also lead to water emission, was neglected because of its occurrence at temperatures which are higher than the reaction temperature. Furthermore, according to Figure 51, no shift in the dynamic glass transition temperature ( $T_g = -21.5$  °C) is observed for the vulcanizate which was first stored in water for 16 weeks (red circle) and which was subsequently dried (blue triangle). A similar observation was reported by A. Schwartz et al.<sup>[35]</sup>, who reported that the  $T_g$  of a vulcanizate ( $T_g = -21.4$  °C), which was determined by calorimetry, was not influenced by water. Thus, the segmental relaxation of the polymer matrix in the glassy-rubbery transition region is almost unaffected by solid-water molecules.

However, for the height of the  $T_g$  peaks only a slight increase is observed for the silane-free vulcanizate after the removal of water in contrast to the silane-activated sample for which a significant increase of the peak height is observed after the removal of water. This observation illustrates that in the silane-free sample absorbed water in the solid state performs in the same way as silica particles, which have no interaction with the polymer matrix. From this observation it is to be concluded that frozen water molecules perform like a filler which has an extremely weak interaction with the polymer matrix. This is in contrast to the strong polymer-filler interaction which is created by the silane coupling agent.

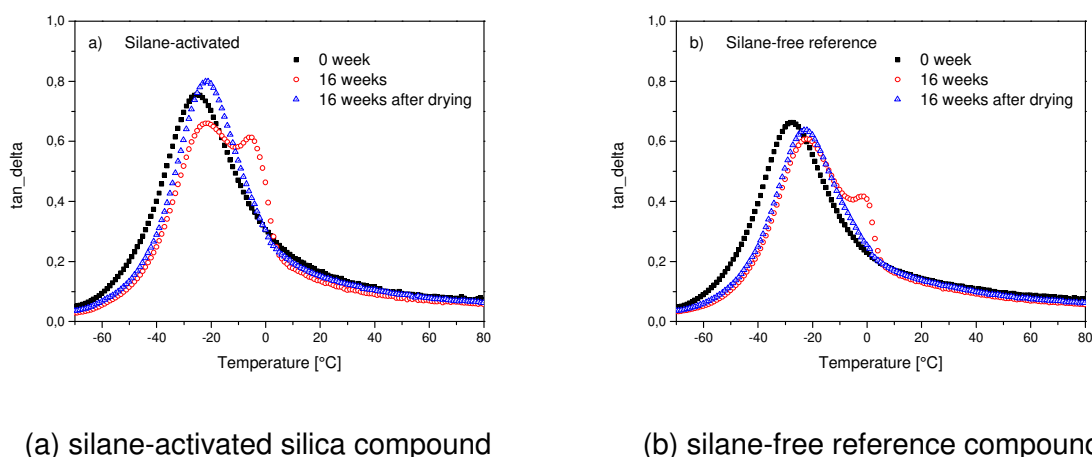


Figure 51. Dependence of  $\tan \delta$  curves on water storage and subsequent drying for the silane-activated silica compound and for the silane-free reference compound (a) before water storage (black squares), (b) after 16 weeks water storage (red circles), (c) after 16 weeks water storage and subsequent drying (blue triangles)

In Figure 52 the dependencies of storage ( $G'$ ) and loss ( $G''$ ) moduli on temperature are comparatively shown for three vulcanizates prior and after 16 weeks water storage at 80 °C, as well as after drying subsequent to the storage in water (16 weeks/80 °C). The incremental changes in  $G'$  and  $G''$  between the original samples before the exposure to water (black squares) and the vulcanizates which were dried subsequent to the storage in water (blue triangles) are possibly due to an increase of the crosslink densities caused by the residual curative during the thermal process in hot water at 80 °C. A comparison of the hydrated sample (red circles) with the sample which was subsequently dried (blue triangles), shows that water has a huge influence on the intensities of  $G'$  and  $G''$ . Notable differences in  $G'$  and  $G''$  which show below 0 °C can be attributed to an increase of the stiffness by frozen water as frozen water molecules act as filler in the vulcanizates. At temperatures well above 0 °C liquid water molecules act as a plasticizer which increases the mobility of the rubber chains thereby decreasing the stiffness and the loss energy. The plasticizer effect of water in non-

crystalline (synthetic) polymers has been observed by Slade<sup>[167]</sup>. This effect was mainly applied in polymeric food materials.

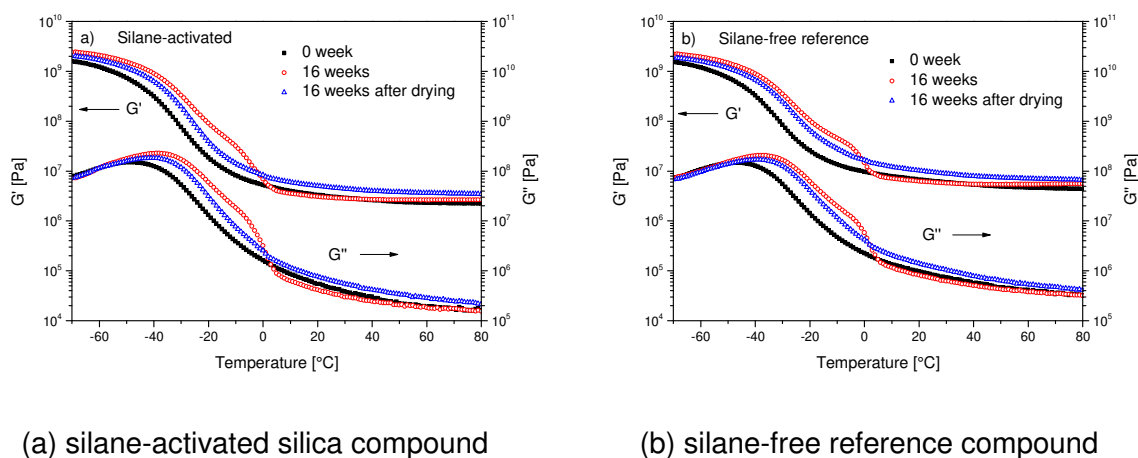


Figure 52. Dependencies of the storage moduli  $G'$  and the loss moduli  $G''$  on water storage and subsequent drying for the silane-activated silica compound and for the silane-free reference compound (a) before water storage (black squares), (b) after 16 weeks water storage at 80 °C (red circles), (c) after 16 weeks water storage and subsequent drying (blue triangles)

### 3.4.6 Hydrolysis of the silanized silica vulcanizate

In order to find out whether the hydrolysis occurs in the silanized silica vulcanizate during water storage, gas chromatography with mass spectrometry detection was used according to the experimental design shown in Figure 71 (see experimental part, Chap. 5.2.1.7).

Firstly, the volatiles of the two vulcanizates (the silane-activated and the silane-free) were determined before water storage. The chromatograms are shown in Figure 53. The volatiles were subsequently identified by mass spectrometry, which breaks each molecule into ionized fragments and detects these fragments using their mass-to-charge ratio. Besides an intensive ethanol peak which was only found in the silanized sample the other peaks are identical for the two vulcanizates. These peaks could be assigned to fragments of oil, plasticizer, accelerator etc. The huge ethanol peak which is released from the silane-activated vulcanizate is probably due to residual silane which was not consumed during the silanization.



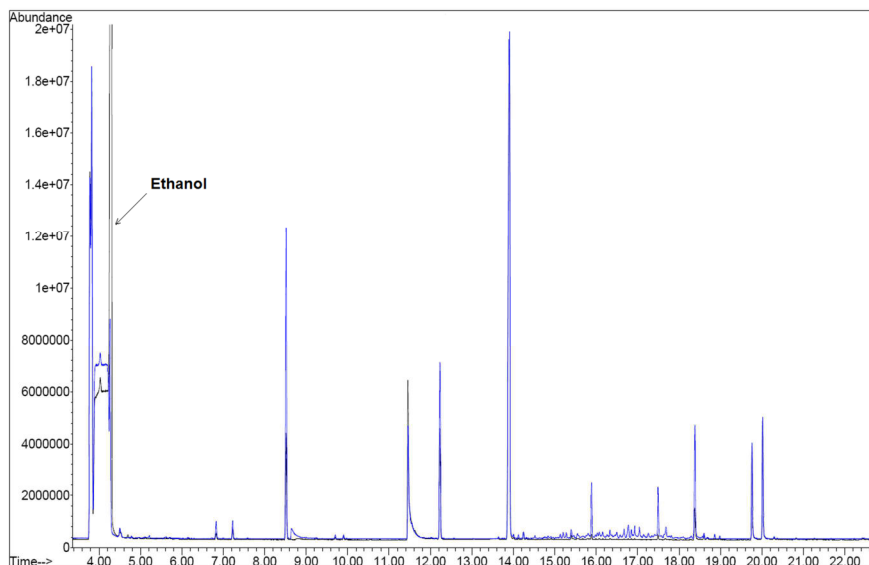


Figure 53. GC-MS-Total-Ion chromatogram of the volatiles from the silane-activated vulcanizate (black line) and the silane-free reference vulcanizate (blue line) at 80 °C

Secondly, the volatiles of the two vulcanizates were determined after water storage for 1 week at 80 °C. The components in the gas phase were directly injected by the headspace sampler (Figure 54), whereas the components in the liquid phase were extracted by hexane and then analyzed by gas chromatography (Figure 55). Under these experimental conditions, no additional peak could be observed subsequent to the storage in water. This clearly shows that the silane-activated vulcanizate was not hydrolyzed during water storage.

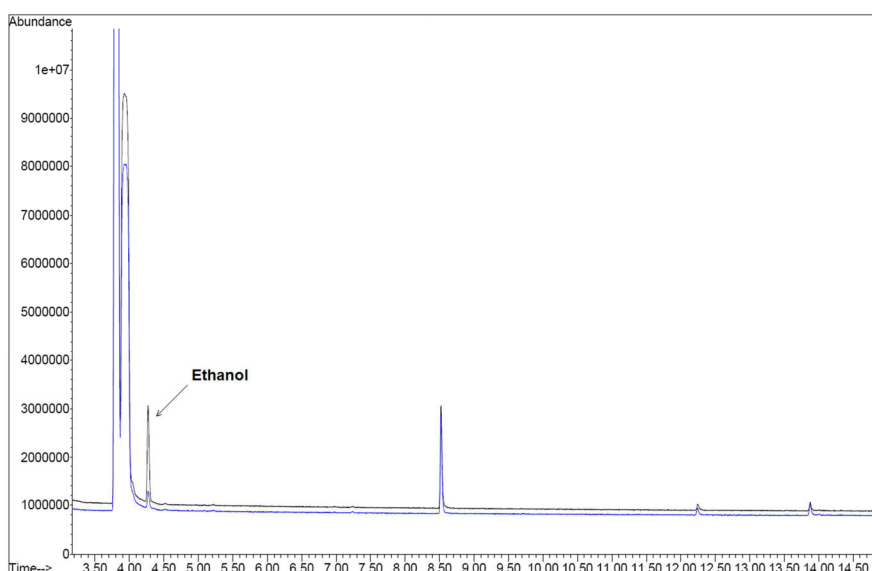


Figure 54. GC-MS-Headspace-Total-Ion chromatogram of the components in the gas phase of the silane-activated vulcanizate (black line) and the silane-free reference vulcanizate (blue line) after water storage at 80 °C for 1 week

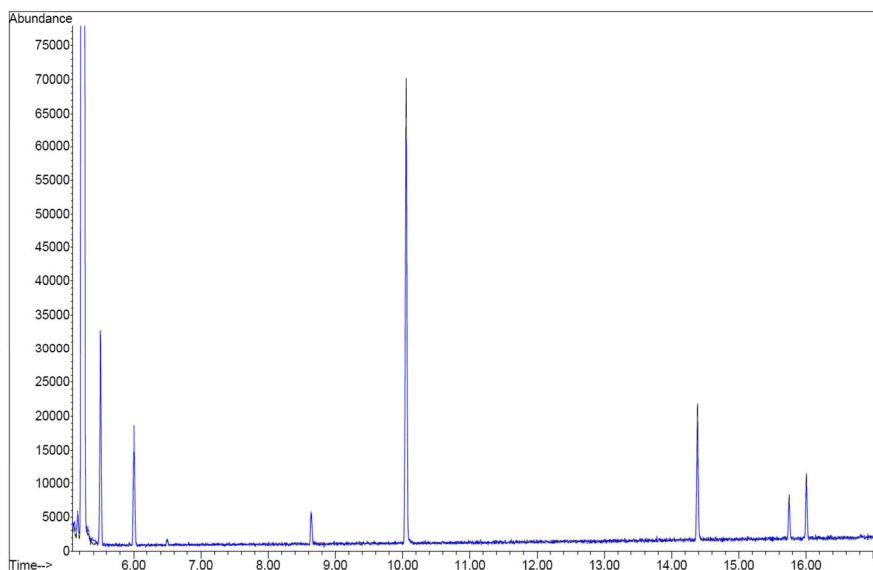
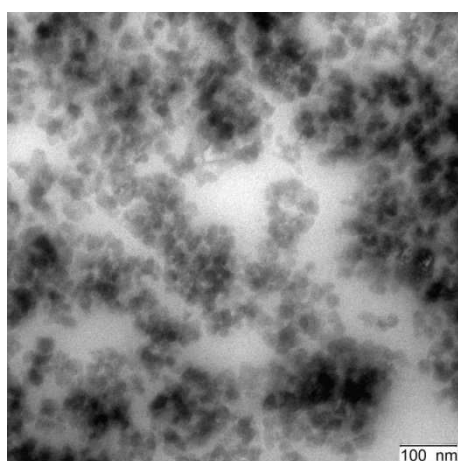
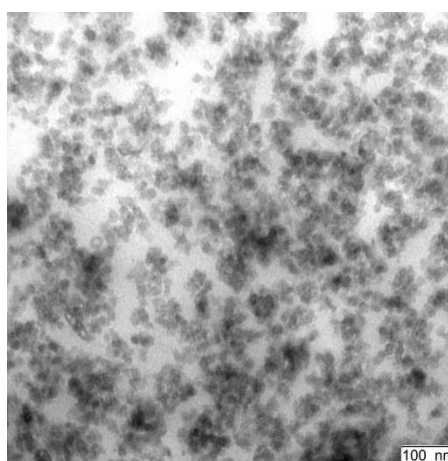


Figure 55. GC-MS-Total-Ion chromatogram of the components in the liquid phase of the silane-activated vulcanizate (black line) and the silane-free reference vulcanizate (blue line) after water storage at 80 °C for 1 week

TEM analysis was carried out to get an idea regarding the influence of water on silica dispersion of the silane-activated vulcanizate. In Figure 56 TEM micrographs are shown of the compound before and after water storage. It can be seen that the dark spots in Figure 56 (a) that prior to water storage silica aggregates strongly in the rubber matrix. By the exposure to water the dark spots become smaller as shown in Figure 56 (b). Also tiny gaps can be seen on the surface of the spots. These observations indicate that silica-silica interaction is reduced by the influence of water.



(a) Before water storage



(b) After water storage

Figure 56. Transmission electron micrographs of the silane-activated silica compound: (a) before water storage (b) after the storage in water for 16 weeks

To the best of our knowledge, the findings about the influence of water storage on the performance of vulcanizates which were summarized above are absolutely new. These results are not only important from a scientific point of view but also from a practical one, as tires are regularly exposed to the swelling with water.

### 3.5 Influence of water on vulcanizates which contain other fillers

In the previous section, it was shown that water has a huge effect on silica loaded vulcanizates regarding the swelling in water and the dynamic mechanical properties. The impact of water, which was detected by DMA measurements was of special interest, in particular as the exposure to water caused an additional  $\tan \delta$  peak in the temperature range 0 – 5 °C. As silica is highly polar and hydrophilic the question comes up how vulcanizates perform, which are loaded with other fillers e.g. the hydrophobic carbon black or with a silica filled vulcanizate, which also contains hydroxylated nano size particles. In order to answer these questions the investigations on the influence of water on tire tread properties was extended with an additional compound study. Four compounds were included in this study the composition of which is given in Table 15.

Table 15. Composition\* of the vulcanizates which contain different fillers (unfilled, carbon black, silica and silica plus Nanoprene®)

Ingredients	1	2	3	4
Buna® VSL 4526-2 HM	96	96	96	96
Buna® CB 25	30	30	30	30
Ultrasil® VN3 GR	-	-	80	80
Carbon black N220	-	74	-	-
Nanoprene® BM75OH	-	-	-	15
Si 75®	-	-	6.4	6.4
Vivatec® 500	10	10	10	10
Zinc oxide	3.0	3.0	3.0	3.0
Stearic acid	2.0	2.0	2.0	2.0
Vulkanox® 4020	2.0	2.0	2.0	2.0
Antilux® 500	1.0	1.0	1.0	1.0
Vulkacit® CZ	1.6	1.6	1.6	1.6
Vulkacit® D	1.5	1.5	1.5	1.5
Sulfur	2.0	2.0	2.0	2.0

\* All weights are in phr (parts in weight per 100 g rubber).

#### 3.5.1 Influence of water on the weight increase of vulcanizates

The dependence of the water uptake was determined as a function of water storage time at a fixed storage temperature of 80 °C (Figure 57). The plots refer to the unfilled (No.1), carbon

black filled (No.2), silica/silane filled (No.3) and silica/Nanoprene® BM75OH/silane filled (No.4) vulcanizates.

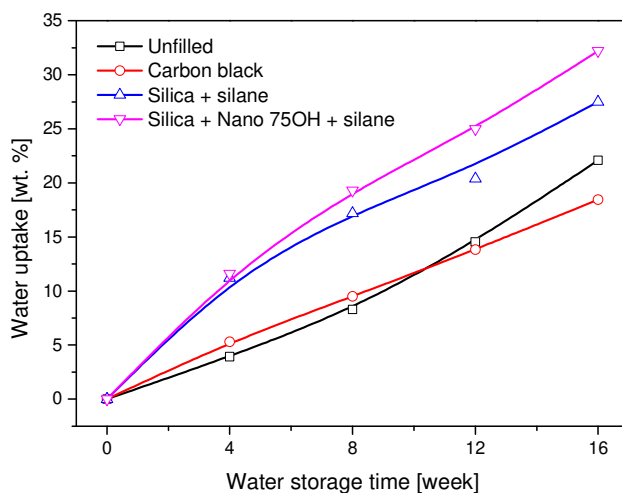


Figure 57. Dependence of the water uptake on storage time at 80 °C of vulcanizates which are unfilled (black squares), carbon black filled (red circles), silica/silane filled (blue triangles) and silica/Nanoprene® BM75OH/silane filled (pink triangles)

As can be seen in Figure 57 for all four vulcanizates the water uptake increases with the water storage time. The water content of the carbon black filled vulcanizate (No.2) increases in a linear manner during 16 weeks. The results which were obtained for the unfilled vulcanizate (No.1) are very close to the results with the carbon black filled vulcanizate (No.2). However, the water uptakes of the silanized silica compound (No.3), and of the silanized silica/Nanoprene® BM75OH filled vulcanizate (No.4) were approximately double over that of the unfilled and carbon black filled vulcanizates (No.1 and No.2) after 4 weeks storage time. It can be also seen that the incorporation of silica/Nanoprene® BM75OH/silane filled vulcanizate (No.4) results in an additional increase of the water swelling in comparison with the silica/silane loaded compound (No.3).

As expected the unfilled compound (No.1) and the carbon black loaded compound (No.2) showed the lowest degree of water swelling. The low weight increases of these two compounds can be attributed to the hydrophobic character of both compounds. The weight increases are significantly lower than for the two silica containing compounds (No.3) and (No.4) which are much more hydrophilic. The surprising fact is that the silanized compound (No.4) which also contains nano size particles showed a slightly higher degree of swelling than compound (No.3) which did not contain nanoparticles. The reasons for this small

difference may be due to an incremental increase of hydrophilicity by the hydroxyl groups of the nanoparticles or to an increased number of hydrophilic sites on the silica surface which are due to an improved silica dispersion by the nanoparticles.

### 3.5.2 Dynamic mechanical properties of the original vulcanizates

Figure 58 shows the dependencies of the mechanical loss factor ( $\tan \delta$ ) on temperature for the indicated four compounds. Peaks in the  $\tan \delta$  value indicate the occurrence of transitions in the segmental mobility of the rubber chains. In the temperature range from  $-70$  to  $+80$  °C all the compounds showed a single peak between  $-27$  to  $-25$  °C which corresponds to the  $T_g$ s of the investigated four compounds (Figure 58). A comparison of the  $\tan \delta$  curves of the carbon black loaded compound (No. 2) and the silica-containing compounds (No. 3 and No. 4) shows that at temperatures  $< 15$  °C the  $\tan \delta$  values of compound No. 2 are lower, and at temperatures  $> 40$  °C the  $\tan \delta$  values are higher. These results confirm the well-known fact that carbon black loaded tire treads are inferior regarding wet skid and rolling resistance.

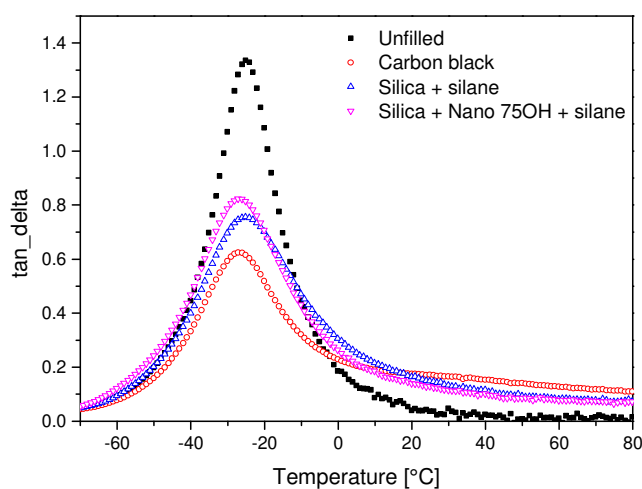


Figure 58. Temperature dependence of  $\tan \delta$  for the unfilled (black squares), carbon black (red circles), silica/silane (blue triangles) and silica/Nanoprene® BM75OH/silane (pink triangles) filled rubber compounds

The dependencies of the storage ( $G'$ ) and loss ( $G''$ ) moduli on temperature are shown in Figure 59. It is worth noting that at temperatures  $> 40$  °C compound No.4 which contains the silanized silica/Nanoprene®-hybrid system exhibits lower  $G''$  and  $\tan \delta$  values than compound No.3 which is a reflection of improved rolling resistance.

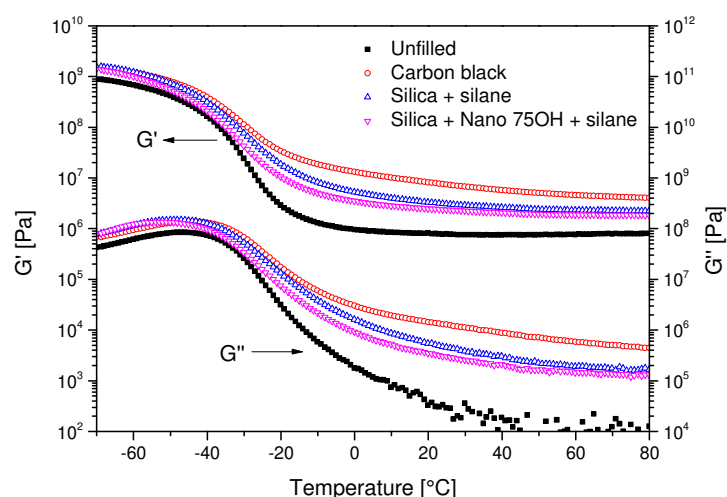


Figure 59. Temperature dependences of the storage moduli  $G'$  and the loss moduli  $G''$  for the unfilled (black squares), carbon black (red circles), silica/silane (blue triangles) and silica/Nanoprene<sup>®</sup> BM75OH/silane (pink triangles) filled rubber compounds

### 3.5.3 Influence of water on dynamic mechanical properties

The 4 vulcanizates were stored in water at 80 °C, and the storage time was varied. Subsequently the dynamic mechanical properties were determined in the temperature range from -70 to 80 °C. From the DMA measurements the temperature dependences of the storage modulus  $G'$ , the loss modulus  $G''$  and  $G''/G'$  ( $\tan \delta$ ) were obtained.

Figure 60 (a, b, c and d) shows the damping curves of the four vulcanizates subsequent to water storage. As can be seen in Figure 60 (a), the plot of the unfilled vulcanizate (No.1) shows a single  $\tan \delta$  peak which corresponds to the dynamic glass transition temperature ( $T_g$ ) of the polymer matrix under the indicated testing conditions. The  $T_g$  peak shifts to higher temperatures with increasing water storage times. Also the intensity of  $T_g$  peak decreases with increasing water storage time.

The plots for the carbon black loaded vulcanizate (No. 2) are shown in Figure 60 (b). After water storage only one  $\tan \delta$  peak is observed for the carbon black loaded vulcanizate. This peak shifts to higher temperatures after water storage. Contrary to the unfilled vulcanizate (No.1) the width and the intensity of the  $\tan \delta$  peak of the carbon black filled vulcanizate increase continuously with the increase of water storage time. A closer inspection of the  $\tan \delta$  curve after 16 weeks water storage at 80 °C reveals a shoulder on the  $T_g$ -peak which is located in the temperature range around -10 to 5 °C. This shoulder could indicate a restricted mobility of the polymer chains by ice clusters which are distributed in the rubber matrix.

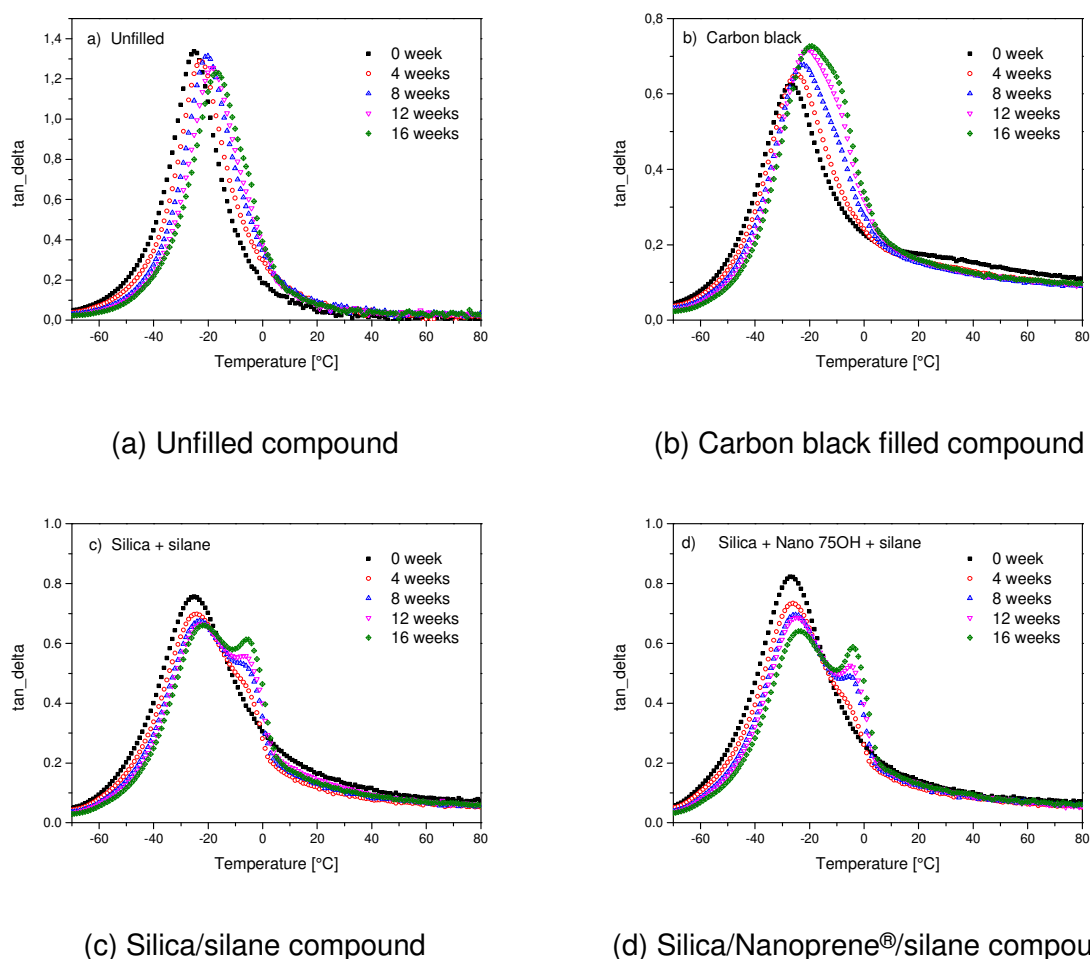


Figure 60. Temperature dependence of  $\tan \delta$  on water storage time at 80 °C for the (a) unfilled compound, (b) carbon black filled compound, (c) silica/silane compound, (d) silica/Nanoprene<sup>®</sup> BM75OH/silane compound

In the literature a lower intensity of a  $\tan \delta$  peak value is attributed to the confinement of polymer chains by filler. That also indicates an improvement in the interfacial reinforcement in the filled composites<sup>[153]</sup>. As a result, the reasons for the increase of the  $\tan \delta$  peak height can be due to: (1) an increase of water content inside the vulcanizates, (2) a filler effect of frozen water clusters which are contained in a separate phase inside the vulcanizates. A potential explanation could be there is sufficient water that aggregates and freezes around the segments, leading to a restriction of the segmental motion. Moreover, the  $\tan \delta$  value around 0 °C increases significantly indicating the increase of wet skid resistance. The  $\tan \delta$  at 60 °C is reduced which is an indication for the improvement of rolling resistance of a tire tread. This aspect will be discussed in the context of the results regarding  $G'$  and  $G''$ .

Figure 60 (c) shows the  $\tan \delta$  curves of the silica/silane filled vulcanizate (No.3) before and after water storage which has been discussed in the previous section (see Chap. 3.4.3). In



contrast to the carbon black filled compound, a second  $\tan \delta$  peak of the silica loaded compound appears obviously by the exposure of the vulcanizate to water. The damping process of silica/Nanoprene<sup>®</sup> BM75OH/silane vulcanizate (No.4) is analogous to the results of the silica filled vulcanizate (see Figure 60 d), but it expresses a more significant separation between the two  $\tan \delta$  peaks which is certainly due to the presence of hydroxyl groups on Nanoprene<sup>®</sup> BM75OH particles. The second  $\tan \delta$  peak in the silica/Nanoprene<sup>®</sup>/silane filled vulcanizate also increases with the weight of absorbed water, and contributes to the improvement of wet skid performance in a tire tread.

Water results in a reduction of the  $\tan \delta$  peak which represents the phase transition of the polymer matrix at around  $-25\text{ }^{\circ}\text{C}$  and in an appearance of the water peak at the range of  $-5$  to  $0\text{ }^{\circ}\text{C}$  for the silica filled compounds, e.g. the silica/silane compound (No.3), silica/Nanoprene<sup>®</sup> BM75OH/silane compound (No.4), and the silane-free silica compound (see Chap. 3.4.3). The height difference of the first  $\tan \delta$  peak (around  $-25\text{ }^{\circ}\text{C}$ ) before and after water storage at  $80\text{ }^{\circ}\text{C}$  correlates with the height difference of the second  $\tan \delta$  peak ( $-5$  to  $0\text{ }^{\circ}\text{C}$ ) is depicted in Figure 61.

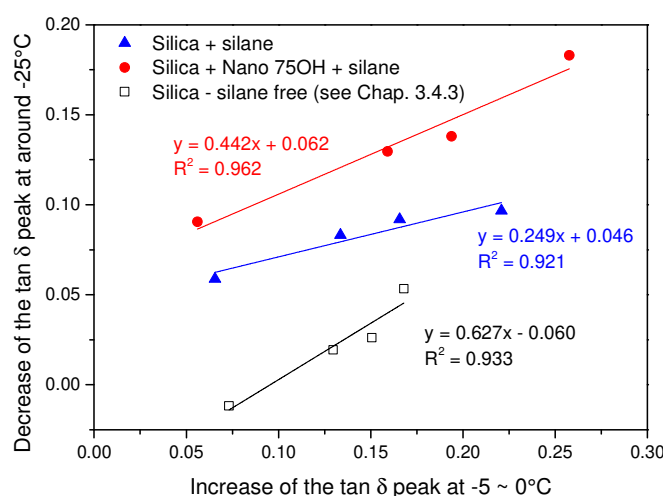


Figure 61. Comparison of the height difference of the first  $\tan \delta$  peak before and after water storage with the height difference of the second  $\tan \delta$  peak

As can be seen with the increase of the water storage time the decrease of the first  $\tan \delta$  peak and the increase of the second  $\tan \delta$  peak can be expressed as good linear fittings. The silica/Nanoprene<sup>®</sup> BM75OH/silane compound (No.4) displays the most pronounced value in the height differences of both the  $\tan \delta$  peaks. The silane-free silica compound which contains a higher water uptake than the silica/silane compound (see Chap. 3.4.2)

shows the lowest difference of the  $\tan \delta$  peak heights. That means the difference of the  $\tan \delta$  peak heights is independent in the water uptake but depends on the extent of the polymer-filler interaction. Hence, the Nanoprene<sup>®</sup> BM75OH modified compound exhibits a better polymer-filler interaction.

Figure 62 (a, b, c and d) show the temperature sweep of  $G'$  for the indicated vulcanizates.

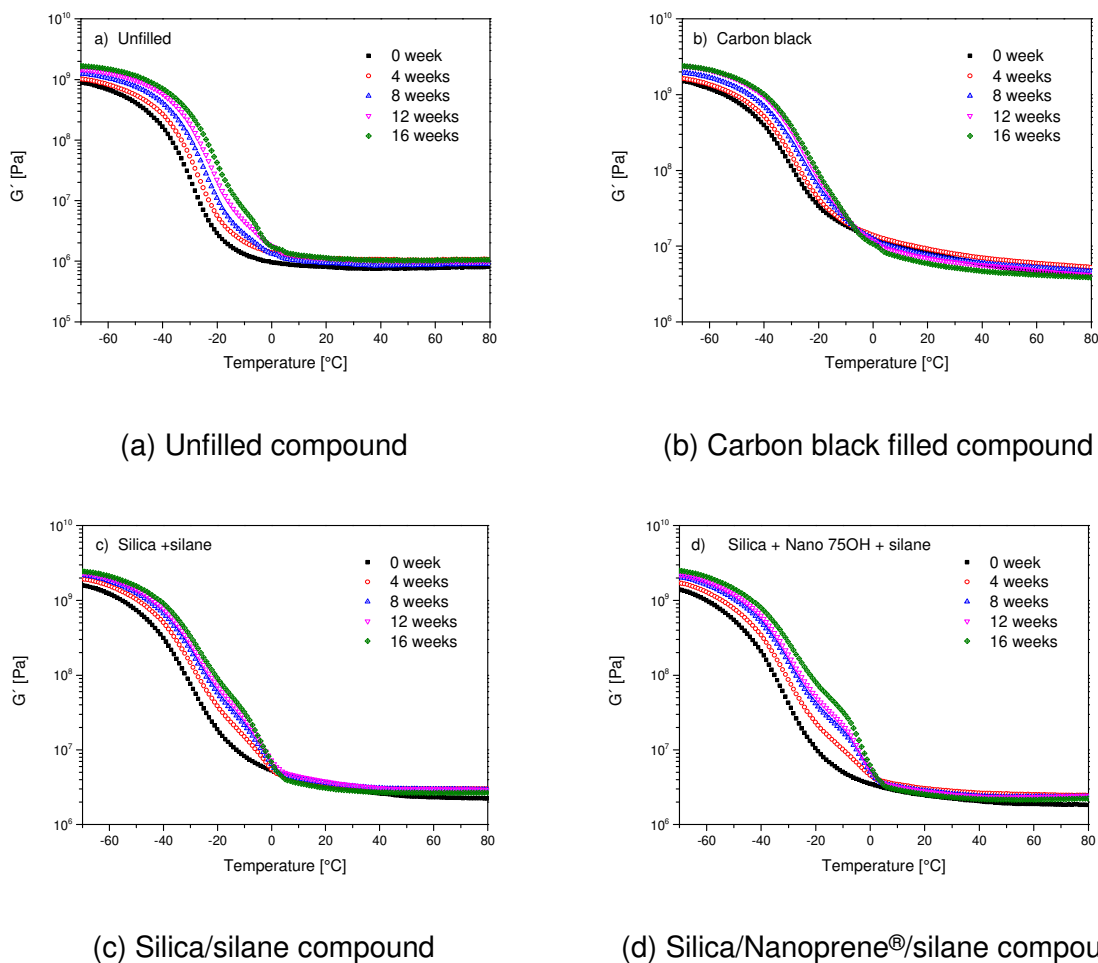


Figure 62. Dependence of the storage moduli  $G'$  on water storage time at 80 °C for the (a) unfilled compound, (b) carbon black filled compound, (c) silica/silane compound, (d) silica/Nanoprene<sup>®</sup> BM75OH/silane compound

As can be seen from the figures for temperatures  $< 0$  °C water swelling results in an increase of  $G'$  for all the vulcanizates.  $G'$  increases gradually with the water storage time. As water is frozen in this temperature range the adsorbed water results in an increase of the effective filler volume. It is well established that an increase in filler loading will cause an increase in  $G'$ <sup>[162,163]</sup>. In addition, it is easily observed that the water swollen silica filled vulcanizates (No.3 and 4) exhibit a small peak shoulder in the temperature range of -10 to 0 °C (see

Figure 62 c and d). This shoulder is mainly due to water which is physisorbed at the hydrophilic parts of the silica surface even when the silica particles are attached to the rubber matrix by covalent sulfur bounds.

In the carbon black filled compound (Figure 62 b) no separate peaks but small shoulders which are due to the influence of water can be detected. This indicates that water molecules only have a small influence on the segmental movement in carbon black filled compounds.

In the unfilled compound the water content is around 22.1 wt.% after 16 weeks of water storage. At temperatures  $> 0\text{ }^{\circ}\text{C}$  the water is randomly distributed in the rubber matrix. And the effect of water on  $G'$  is rather small. At temperatures  $< 0\text{ }^{\circ}\text{C}$  water forms ice crystals. As these crystals are contained in a separate phase they act like filler particles which reduce the chain mobility and affect the transition process. The effect of reduced chain mobilities shows as a weak peak shoulder of the  $\tan \delta$  peak at  $-10$  to  $0\text{ }^{\circ}\text{C}$  (Figure 60 a).

The temperature sweeps of  $G''$  of the water containing samples are shown in Figure 63 (a, b, c and d). In the low temperature region ( $< 0\text{ }^{\circ}\text{C}$ ) in which water is frozen there is an increase of  $G''$  for all vulcanizates. This effect can be explained by the presence of ice crystals which increases the filler volume fraction. The  $G''$  plots of the silica/silane and silica/Nanoprene<sup>®</sup> BM75OH/silane filled samples (No.3 and 4) after water storage show a peak shoulder in the temperature range of  $-10$  to  $0\text{ }^{\circ}\text{C}$  which is analogous to the  $G'$  plots. The water influences on  $G'$  and  $G''$  of the silica/Nanoprene<sup>®</sup> BM75OH/silane compound seem more pronounced than for the silica/silane compound since the distances between the temperature sweep curves in the temperature range of  $-20$  to  $0\text{ }^{\circ}\text{C}$  are wider. In parallel to  $G'$ , there is still not any additional peak shoulders in the unfilled and carbon black filled samples (No.1 and 2). This means that the increase of energy dissipation during phase transition of water appears only when the water molecules reduce the mobility of the polymer chains. In the high temperature region ( $> 0\text{ }^{\circ}\text{C}$ ) the adsorbed water is liquid in the vulcanizates and acts as plasticizer. The reduction of both  $G''$  and  $\tan \delta$  at  $60\text{ }^{\circ}\text{C}$  indicates the improvement of rolling resistance by water for the filled rubber compounds.

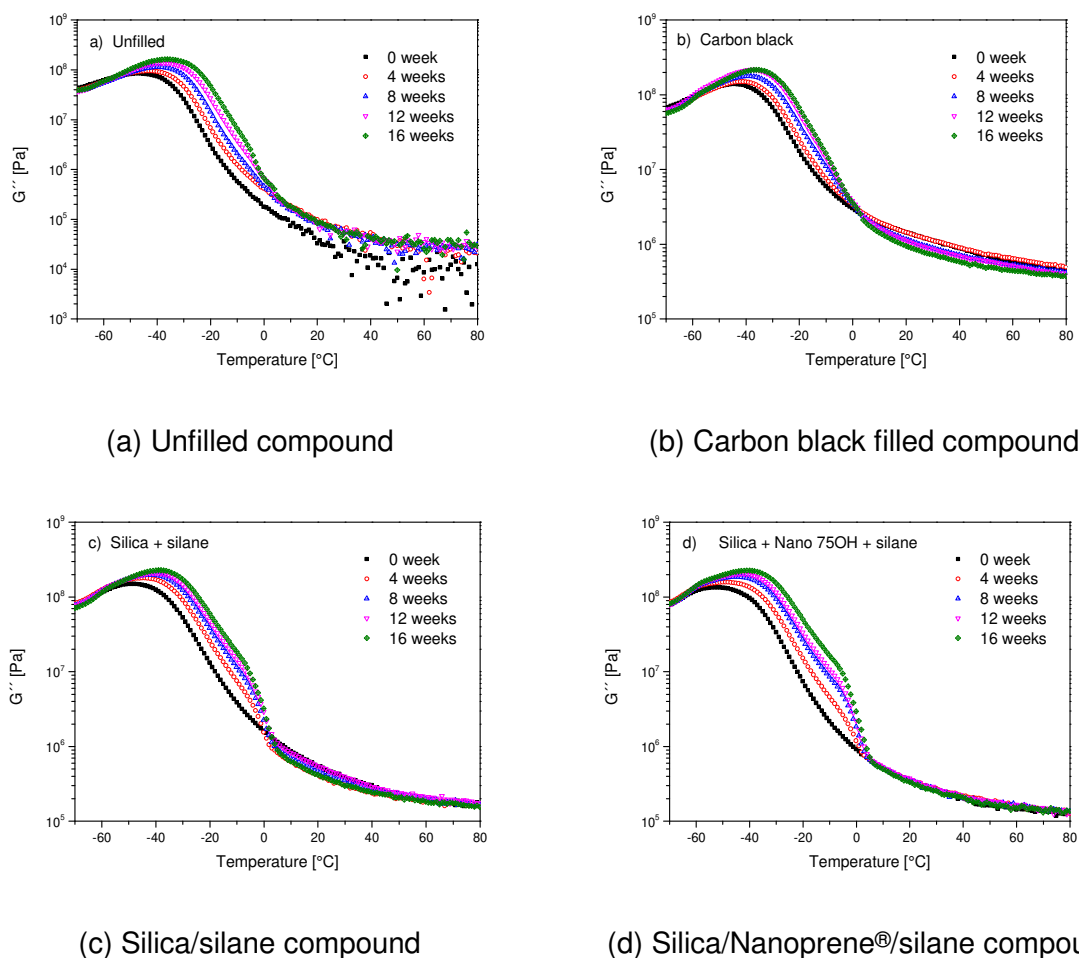


Figure 63. Dependence of the loss moduli  $G''$  on water storage time at 80 °C for the (a) unfilled compound, (b) carbon black filled compound, (c) silica/silane compound, (d) silica/Nanoprene<sup>®</sup> BM75OH/silane compound

### 3.5.4 Influence of water on the Payne effect

It is well known that the non-linear viscoelastic dependency on the strain amplitude is an important feature for the properties of filled rubber compounds, known as the Payne effect. In order to investigate whether water affects the Payne effect, the dependencies of  $G'$  on the strain amplitude were determined at room temperature (23 °C) for the carbon black filled (No.2), silica/silane filled (No.3) and silica/Nanoprene<sup>®</sup> BM75OH/silane filled (No.4) vulcanizates before and after water storage. The results will be discussed in this section.

The amplitude of Payne effect can be influenced by different filled systems due to the difference of filler-filler interaction. Figure 64 shows the strain sweep curves of the carbon black, silica/silane and silica/Nanoprene<sup>®</sup> BM75OH/silane filled compounds prior to water treatment. The carbon black filled compound (No.2) exhibits a much higher  $G'$  at low strain

amplitudes than the compounds with the other fillers. For the carbon black loaded vulcanizate  $G'$  is reduced considerably when the strain is increased above 0.2 %. The value of  $G'$  for the carbon black filled compound at low strain amplitude was found much higher than the silica filled compounds. In the literature, the Payne effect which is observed in carbon black filled vulcanizates is well documented. It is attributed to the strain induced break up of the carbon black network. With the addition of Nanoprene® BM75OH in the silica filled compound the Payne effect was further reduced as it was discussed in Chap. 3.2.3.

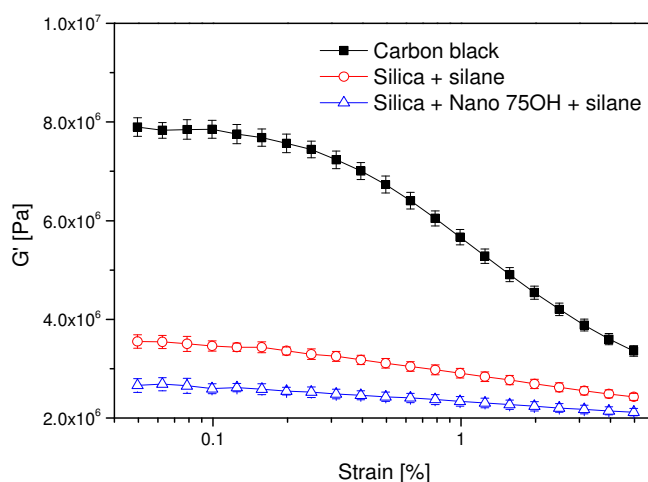


Figure 64. Payne effect measurement of different filled systems at the test temperature of 23 °C

In the case of the carbon black filled compound (No.2) which was stored in deionized water at 80 °C up to 16 weeks, the results on the Payne effect are shown in Figure 65.

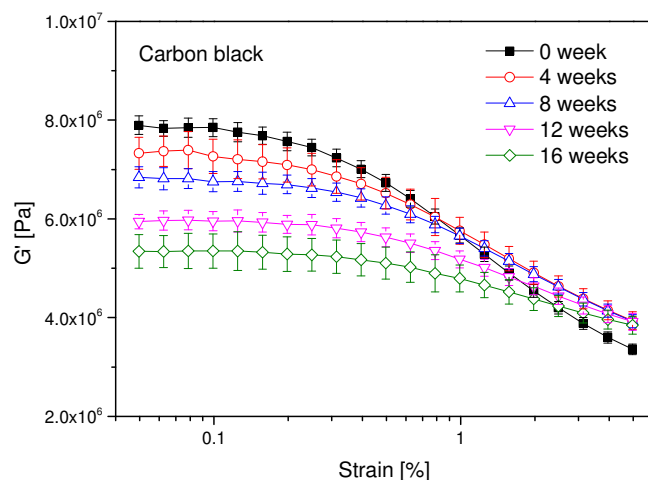


Figure 65. Strain amplitude dependency of  $G'$  on water storage time at the test temperature of 23 °C for carbon black filled compound

It is evident that water has a significant influence on the Payne effect of the carbon black filled vulcanizate. The storage modulus at low strain amplitude ( $G'_0$ ) decreases with an increasing content of water. This is an indication for the disaggregation of carbon black aggregates by water which reduces the van der Waals bonds of the carbon black aggregates. Furthermore, the high strain modulus ( $G'_\infty$ ) of the carbon black filled compound increases from about 3.3 to 4.0 MPa by the swelling with water. It is well known that the hydrodynamic effect, filler-rubber interactions and the crosslink density of the matrix have no influence on the dependence of  $G'$  on strain (see Chap. 2.4). The filler-rubber interaction is not changed by the water storage since no additional linkage between filler and rubber can be produced by the presence of water. However, as the hydrodynamic effect in filled rubber compound depends on the filler volume fraction and the shape of the filler particles, the absorbed water which can not affect the shape of the filler particles but can reduce the total filler volume fraction in the swollen specimen results in a decrease of the moduli at high strain amplitudes (see Equ. (12)).

In addition, the crosslink density is increasing by the thermal storage temperature at 80 °C and this effect will cause an increase of the moduli at high strain amplitudes. With further increase the water storage time from 4 week to 16 week, the crosslink density which is influenced only by the thermal aging process increases more slightly. As a consequence, if the influences of the competitive processes for the carbon black filled vulcanizate, the hydrodynamic effect which leads to the reduction of  $G'_\infty$  after water storage and the increase of polymer crosslink density which results from thermal aging and which leads to the increase of  $G'_\infty$ , are equivalent the values of  $G'_\infty$  after water storage of 4 weeks to 16 weeks could be the same.

In the case of the silica/silane filled and the silica/Nanoprene® BM75OH/silane filled compounds (No.3 and 4), as shown in Figure 66 and Figure 67 respectively, water is adsorbed on the surface of silica. This effect reduces the silica-silica interaction and results in a decrease of the Payne effect. In contrast to the carbon black compound, the hydrodynamic effect of the silica filled compounds should be much higher due to the higher water uptake resulting in a softening effect on the moduli at all strain amplitudes.

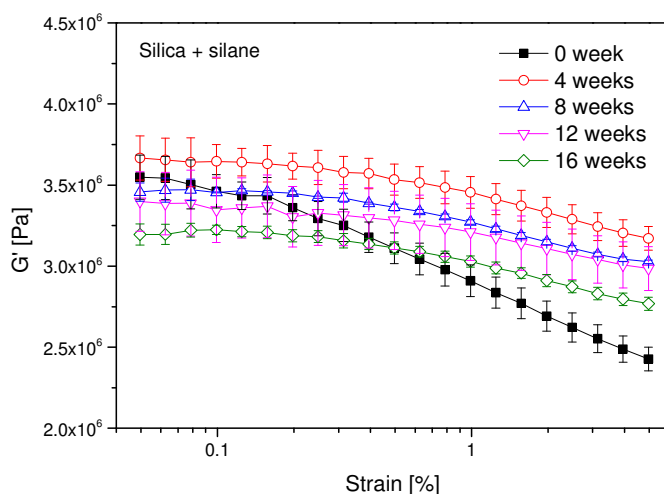


Figure 66. Strain amplitude dependency of  $G'$  on water storage time at the test temperature of 23 °C for silica/silane filled compound

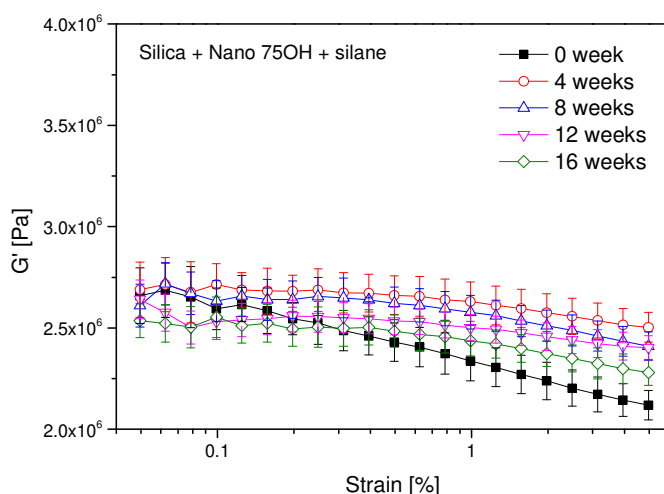


Figure 67. Strain amplitude dependency of  $G'$  on water storage time at the test temperature of 23 °C for silica/Nanoprene® BM 75OH/silane compound

To get an impression of the available hydrophilic area of the filler particles which can be occupied by water, the degrees of surface coverage of water on pure filler particles were calculated. The results are summarized in Table 16. The estimated water content of the silica and Nanoprene® BM75OH surface are in the range of 2 – 5 wt.% based on the pure filler. The weights of absorbed water after 4 weeks at 80 °C are more than 10 wt.% in the silica/silane and silica/Nanoprene® BM75OH/silane vulcanizates. On the basis of these figures at least one layer of water molecules which is physisorbed on the filler surface after

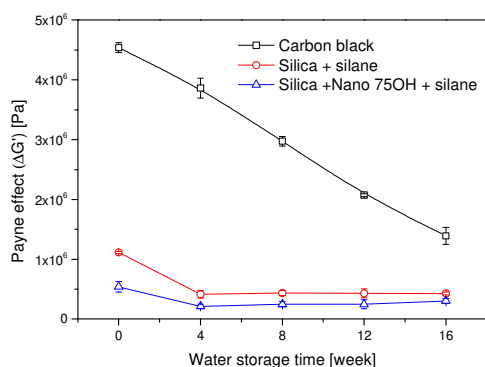
immersion in water for 4 weeks/80 °C can be rationalized for. On the other hand, the silica/silane and silica/Nanoprene® BM75OH/silane vulcanizates were modified by bifunctional coupling agent. Not only silica-rubber bonds but also silica-silica bonds can be formed by the use of Si 75®. The chemisorption of silica-silica bonds cannot be affected by water. In both cases, absorbed water can reduce the filler aggregation but cannot affect the chemical interaction of the fillers.

Table 16. Evolution of water content on silica and Nanoprene® BM75OH surface

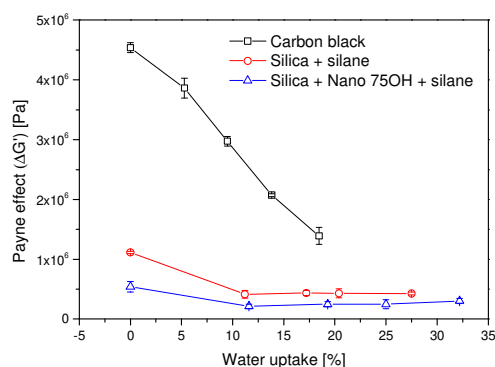
Samples	Diameter [nm]	Projected surface area [nm <sup>2</sup> ]	Surface area [m <sup>2</sup> /g]	Coverage ratio of H <sub>2</sub> O* [wt.%]
H <sub>2</sub> O	0.4	0.1256	3750	-
Silica (VN3)	14	-	160	4.3
Nano 75OH	51	-	125	2.6

\* Coverage ratio in wt.% corresponds to the total projected surface area of H<sub>2</sub>O occupied on the surface of filler.

The dependency of the Payne effect versus water storage time, respectively water uptake are shown in Figure 68 (a) and (b).



(a) Payne effect vs. time



(b) Payne effect vs. water uptake

Figure 68. Dependency of the Payne effect on (a) the water storage time (b) water uptake at a fixed storage temperature of 80 °C for the carbon black (black squares), silica/silane (red circles) and silica/Nanoprene® BM75OH/silane (blue triangles) filled rubber compounds

As can be seen from these figures the magnitude of the Payne effect decreases linearly with an increase of the water content from 0 to 18.5 wt.% for the carbon black filled compound



(No.2), whereas the Payne effect of the silica/silane compound (No.3) decreases from 1.1 MPa (referred to 0 wt.% water) to 0.43 MPa (referred to 11.2 wt.% water). Additional amounts of adsorbed water have no influence on the Payne effect. The Payne effect of the silica/Nanoprene<sup>®</sup> BM75OH/silane compound is analogous to that of the silica filled compound, which decreases slightly during water storage and then levelled off after 4 weeks. The Payne effect which is observed with the silica/Nanoprene<sup>®</sup> BM75OH filler, however, is the lowest from the fillers studied, indicating that Nanoprene<sup>®</sup> BM75OH reduces the filler aggregation and improves silica dispersion. This is clear evidence that Nanoprene<sup>®</sup> is most efficient in the reduction of silica/silica interaction and the improvement of silica dispersion.

## 4 Conclusions

Rubber compounds which are based on silane activated silica represent the state-of-the-art tire tread vulcanizates in Europe. The incorporation of hydroxyl modified nanoscale rubber particles in the compounds results in further performance improvements of the tread compounds. As the contribution of the nanoparticles to the reinforcing effect of silica is not yet understood the main target of this thesis is an elucidation of the mechanisms by which the nanoscale rubber particles cause these improvements.

A series of nanoparticles with different functional groups was provided by Lanxess. For the characterization of the functionalized nanoparticles, Fourier transform infrared spectroscopy and differential scanning calorimetry were employed. The FTIR spectra and the  $T_g$  values of the indicated Nanoprene<sup>®</sup> grades confirmed that the Nanoprene<sup>®</sup> grades are all polybutadiene based. The functional groups have an influence on the  $T_g$  due to the different volumes and the flexibilities of the side groups. Further, as the same mass fraction of the functional monomers was used in the synthesis process, the molar content of the functional groups is inversely proportional to the molecular weight of the functional monomers.

In the first step of the thesis the silanization rates of silica and of hydroxyl modified nanoparticles were determined. A new test method was developed by using headspace gas chromatography to analyze the silanizations of Nanoprene<sup>®</sup> grades and their kinetics in model reactions. In order to avoid side reactions which can occur with the silanes used in the tire industry, the model silane triethoxy(octyl)silane (OCTEO) was utilized. It was found that the more acid silanol groups of silica react significantly faster than the hydroxyl groups of the nanoparticles. At complete silane conversion the ratio of silanization was around 95/5 in favour of the silanol groups.

For the study of the reinforcing mechanisms of the Nanoprene<sup>®</sup> grades in silica loaded hybrid systems a compound study was performed by firstly evaluating the commercial grade of hydroxylated Nanoprene<sup>®</sup> (Nanoprene<sup>®</sup> BM75OH). A compound study was performed in which 5 rubber compounds were included. The results clearly showed that the silica dispersion which was achieved by the silanization reaction was as good as that, which was achieved by the addition of the nanoparticles without silanization. For a silanized compound which contained silica and hydroxyl modified nanoparticles the best results regarding silica dispersion, resistance towards filler flocculation, mechanical, and dynamic mechanical properties were obtained.

Swelling experiments with toluene which were performed on these 5 compounds showed that the addition of the nanoparticles decreases the swelling. Additional interactions between polymer and filler are the cause for this reduction. Due to the slow silanization of the hydroxyl groups the higher number of crosslinks was attributed to an increased number of crosslinks between the silica surface and the rubber matrix. The root cause for these increases was attributed to a better accessibility of the silanol groups within the silica clusters as a consequence of the improvements in silica dispersion by the nanoparticles.

In dynamic mechanical analysis the dependence of the shear modulus  $G'$  on the shear amplitude was investigated. The vulcanizates showed a reduction of  $G'$  with increasing shear amplitude which is due to a break down of the filler network (Payne effect). A comparison of a silanized silica loaded vulcanizate with a silanized silica compound which also contained nanoparticles showed a reduction of the Payne effect by the nanoparticles. This result on the improvement of silica dispersion by hydroxyl modified nanoparticles was consistent with the results of the other experiments described above.

Summarizing the results obtained, it can be concluded that in a ready made silica based vulcanizate which also contained hydroxylated nanoparticles and which was silanized there are unreacted silanol groups on the silica surface and unreacted hydroxyl groups on the surface of the nanoparticles. As a consequence of hydrogen bonding between the hydroxyl and the silanol groups mixed clusters of the inorganic and the organic nano-filler are formed. From this perspective the clusters can be referred to as a new class of hybrid fillers.

Additional experiments in which the vulcanizates were exposed to water storage yielded the following results:

After water storage at 80 °C/16 weeks the weight increase of the silica-loaded vulcanizates was significantly higher than that of unfilled (22.1 wt.%) or carbon black loaded (18.5 wt.%) vulcanizates. Without silanization the water content of the silica loaded vulcanizate was 32.3 wt.%. The water content of the respective silanized silica compound was only 27.5 wt.%. The differences demonstrated the highly hydrophilic character of the silica containing vulcanizates in comparison with the unfilled and the carbon black loaded vulcanizates. The water swelling data also showed a reduction in the weight increase after water storage by the silanization reaction. This effect is consistent with a reduction of the hydrophilic nature of silica by the silanization reaction.

For the silica containing vulcanizates an activation energy between 37.9 – 44.5 kJ/mol was determined for the temperature dependence of the water uptake. The activation energy did

not depend on whether the compound was silanized or not. The activation energy compared well with literature data for the physisorption of water on silica (35 – 45 kJ/mol). On the basis of identical activation energies it was concluded that the rate determining step in the water uptake was rather the physisorption of water on the silica surface than the diffusion of water through the hydrophobic rubber matrix.

After water storage at 80 °C/16 weeks neither in the gas nor in the aqueous phase volatile products could be detected by GC which were caused by hydrolysis. This negative result was found for both silica compounds and did therefore not depend on the silanization reaction. By this study the high hydrolytic stability of the chemical bonds between the silica surface and the rubber matrix which were formed by the silanization reaction could be confirmed.

From TEM evidence it was concluded that silica aggregation was reduced by the exposure of the vulcanizates to water. The storage in water not only reduced silica aggregation but also caused gaps on the surface of the silica particles. It was therefore concluded that water was preferentially adsorbed within and around the silica clusters rather than in a random manner within the rubber matrix.

A DMA-temperature sweep revealed that at temperatures below 0 °C the presence of water increased  $G'$  and  $G''$ . In this temperature range frozen water performed like a filler. In the temperature range -5 and 0 °C water generated an additional  $\tan \delta$  peak. This peak was assigned to a stiffening of the rubber molecules which were chemically attached to the silica surface by the adsorption of water molecules on hydrophilic areas of the silica surface. The height of the “water peak” increased with the weight increase of absorbed water. At temperatures well above 0 °C water is liquid and performed like a plasticizer. As a consequence, in this temperature range the mobility of the rubber chains was increased. This effect causes a decrease of the stiffness and of the loss energy. As a consequence of water adsorption  $\tan \delta$  decreases at temperatures  $> 40$  °C, which is an indication for the reduction of rolling resistance.

A DMA amplitude sweep showed that water caused a reduction of filler agglomeration (Payne effect). The reduction of the Payne effect by water did not depend on the nature of the fillers (carbon black, silanized silica, or hybrid-filler). This result shows that there is further potential for the performance improvement of tire treads in particular for silica loaded tire treads if water can be replaced by an appropriate nonvolatile compounding ingredient.

The full reversibility of the effects, which were caused by the swelling with water was established by DMA measurements on vulcanizates, which were first immersed in water and subsequently dried. Due to the reversibility of the water effects it was concluded that water adsorption occurred by physisorption rather than by chemisorption.

An emphasis of this thesis was on hydroxyl modified nanoparticles. In another aspect, Lanxess provided nanoparticles with other functional groups. The functional monomers which were used for the synthesis of these nanoparticles included: acrylic acid, 2-vinylpyridin, 4-vinylpyridin, glycidyl methacrylate, and 2-dimethylamino ethyl methacrylate. The nanoparticles were evaluated in a comparative compound study the basis of which was a silanized silica compound. This study revealed that the additional incorporation of nanoparticles caused improvements over the respective reference silica compound which did not contain any nanoparticles. The improvements which were obtained with the hydroxyl modified nanoparticles, however, were superior over the improvements with nanoparticles with other functional groups.

## 5 Experimental part

### 5.1 Materials

#### 5.1.1 Rubbers

The solution-polymerized styrene butadiene rubber grade Buna<sup>®</sup> VSL 4526-2 MH (S-SBR) and the solution high-cis polybutadiene polymer grade Buna<sup>®</sup> CB 25 (BR) were both from Lanxess Deutschland GmbH. The SBR rubber has a vinyl content of 44.5 wt.%, a styrene content of 26 wt.% and is extended with TDAE type oil (27.3 wt.%). The density of Buna<sup>®</sup> VSL 4526-2 MH is 0.96 g/cm<sup>3</sup>. Buna<sup>®</sup> CB 25 has a cis-1,4 content of min. 96 wt.% and a density of 0.91 g/cm<sup>3</sup>.

#### 5.1.2 Fillers

The inorganic fillers used in this work were precipitated silica (Ultrasil<sup>®</sup> VN3) obtained from Evonik Degussa GmbH, and carbon black N220 supplied by Columbian Carbon. Their chemical characteristics are shown in Table 17. The hydroxylated Nanoprene<sup>®</sup>-grade BM75OH and the Nanoprene<sup>®</sup>-grades with other functional groups were obtained from Lanxess Deutschland GmbH. Details on these grades are given in Chap. 2.1.

Table 17. Characteristic data of Ultrasil<sup>®</sup> VN3 and of CB N220

Name	Ultrasil <sup>®</sup> VN3	CB N220
Primary particle size [nm]	14	21
CTAB surface area [m <sup>2</sup> /g]	160	111
BET surface area [m <sup>2</sup> /g]	170	119
DBP adsorption [m <sup>2</sup> /g]	200	114
Moisture content [%]	5.5	< 1
pH value	6.2	7-10
Silanol group (total) density [nm <sup>-2</sup> ]	12.3	-
Silanol group (isolated) density [nm <sup>-2</sup> ]	9.8	-
Iodine Adsorption Number [g/kg]	-	121

### 5.1.3 Chemicals

The solvents which were used for gas chromatography, extraction, and equilibrium swelling as well as the suppliers and technical data are listed in Table 18.

Table 18. Solvents

Solvents	Producer, technical data
Ethanol	Sigma-Aldrich, $\geq 99.5\%$ , d 0.789 g/ml
Isopropanol	Sigma-Aldrich, $\geq 99.7\%$ , d 0.785 g/ml
Dodecane	Acros Organics, $\geq 99\%$ , d 0.753 g/ml
Triethoxy(octyl)silane (OCTEO)	Sigma-Aldrich, $\geq 97.5\%$ , d 0.88 g/ml
n-Hexane	Sigma-Aldrich, $\geq 95\%$ , d 0.659 g/ml
Toluene	Fluka Chemie AG, $\geq 99\%$ , d 0.865 g/ml

The chemicals which were used for the preparation of the rubber compounds and the suppliers are listed in Table 19.

Table 19. Chemicals used for the preparation of the rubber compounds

Chemicals	Producer, technical data
Si 75 <sup>®</sup>	Evonik Degussa GmbH, silane coupling agent
Vivatec <sup>®</sup> 500	Klaus Dahleke K.G., aromatic oil
Zinc oxide	Grillo Zinkoxid GmbH, 99.6 %, activator
Stearic acid	Henkel KG, Edenor ST 4A, mixture of palmitin and stearic acid with low amount of oil (stearic iodine number 4), activator
Vulkanox <sup>®</sup> 4020	Lanxess Deutschland GmbH, antioxidant
Antilux <sup>®</sup> 500	Rhein Chemie Rheinau GmbH, anti-sun check waxes and antiozonants
Vulkacit <sup>®</sup> CZ (CBS)	Lanxess Deutschland GmbH, vulcanization accelerator
Vulkacit <sup>®</sup> D (DPG)	Lanxess Deutschland GmbH, vulcanization accelerator
Sulfur	Solvay Barium Strontium GmbH, $\geq 99.95\%$

## 5.2 Methods and apparatus employed

### 5.2.1 Gas chromatography-mass spectrometry (GC-MS)

#### 5.2.1.1 Technical parameters of GC-MS

The silanization was monitored by the release of ethanol with an automated head space analyzer attached to gas chromatography with mass spectrometry detection. Two separated peaks were detected for ethanol and isopropanol (internal standard) as under the conditions shown in Table 20. The areas of the two peaks were determined by integration with Agilent Chemstation. The ratio of the peak areas was used for the establishment of calibration curves.

Table 20. Technical parameters of gas chromatography

Parameter	Technical data
GC:	Agilent 7697A
Detector:	Agilent mass selective detector (MSD) 5975
Ionization:	Electron impact, 70 eV
Ion source temp.:	250 °C
Scan rate:	4.21/sec.
Range of mass detection:	15 to 350 m/z
Capillary column:	Varian CP8960 VF 5 MS, 60 m × 0.25 mm × 0.25 μm
Carrier gas:	Helium
Oven temp.:	40 °C to 250 °C
Heating rate:	10 °C/min
Injection source:	Headspace, Agilent 7697A
Injection temp.:	120 °C, 140 °C, and 160 °C
Vial shaking:	71 shakes/min

#### 5.2.1.2 Preparation of standard solutions

The quantification of ethanol was achieved by the method of internal standardization. For the establishment of calibration curves a series of standard solutions was prepared by starting with concentrated solutions of ethanol and isopropanol in dodecane and subsequent dilution with dodecane. The standard stock solution which contained  $10^4$  ppm of ethanol was obtained by diluting 1.0 g ethanol in a 100 ml volumetric flask with dodecane. Dodecane was



chosen as the liquid phase due to its chemical stability and the high boiling point (215 – 217 °C). Isopropanol was used as internal standard. The standard solutions, each with a known concentration of ethanol (0.8 ppm, 4 ppm, 12 ppm, 20 ppm, 40 ppm, 60 ppm, 80 ppm, and 100 ppm) and a constant concentration of isopropanol (60 ppm), were obtained by diluting appropriate standard stock solutions with dodecane. For GC-headspace analysis, 4 ml aliquots of the standard solutions were pipetted into a 20 ml headspace vial and immediately sealed with a Teflon-lined septum and an aluminum crimp cap. Each standard was measured 3 – 5 times in a separate vial and the mean value was used.

### 5.2.1.3 Sample preparation for silanization analysis

For the GC-headspace analysis, a vial was charged with either 50 mg Nanoprene® or silica which were dispersed in 4 ml diluent (dodecane) containing  $10^3$  ppm triethoxy(octyl)silane and 60 ppm internal standard. The vial was immediately sealed with a Teflon-lined septum and an aluminum crimp cap. Then the vial was shaken for one night in order to sufficiently swell Nanoprene®. The reaction was started to by putting the vials in an oven (Thermo Scientific Heraeus oven). The reactions were stopped according to a fixed time schedule by cooling down the samples with ice water. Finally the vials were loaded onto the headspace sampler for analysis. The equilibrium temperature used was the same as the reaction temperature. For each determination a separate vial was measured, and each sample was tested 3 times to obtain the mean value.

### 5.2.1.4 Determination of equilibrium time

There are many instrumental parameters of headspace sampler that can affect the sensitivity, precision, and accuracy of GC analysis. These include time (vial equilibration, loop fill, and injection), temperatures (oven, transfer line and loop), pressure (carrier gas and vial), shake speed, and so on<sup>[168]</sup>. An oven temperature of 120 °C, which is the same as the silanization temperature, was selected as the equilibrium temperature. The optimal vial equilibration between the gas phase and the solution was determined by experiments using a 100 ppm working standard of ethanol or isopropanol in the dilution solvent of dodecane. The equilibrium time in headspace was varied from 5 to 120 min and the other parameters were maintained at the same conditions. Figure 69 shows the response of the peak area as a function of the equilibrium time.

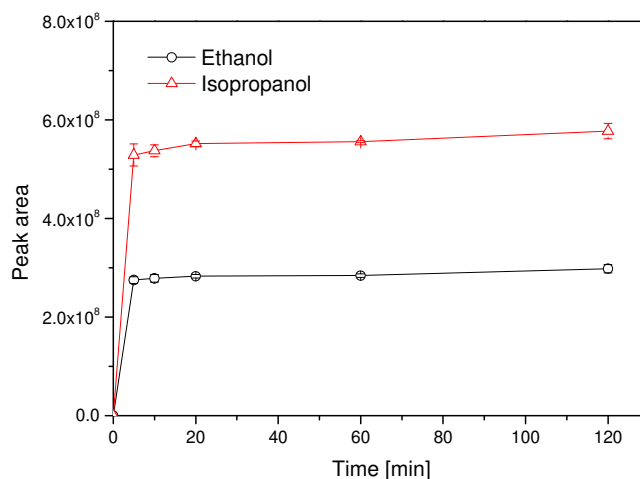


Figure 69. Dependence of the residence time on the peak area of released ethanol and isopropanol

When equilibrium is achieved, the concentration of volatile components diffused into the gas phase should reach a constant. The results indicate that the minimum time to achieve the vapor-liquid equilibrium at the temperature of 120 °C is 20 min for the ethanol and isopropanol solutions. In the analytical procedure for the quantitative determination of the released ethanol the equilibration time was hold constant (20 min/120 °C).

After the determination of all the GC experimental parameters, it is possible to use solutions of different concentrations for the construction of a calibration curve.

#### 5.2.1.5 Calibration curve

In the previous chapters the influence of the relevant parameters in the HSGC-analysis were evaluated. On this basis the parameters for the set-up of a calibration curve were established.

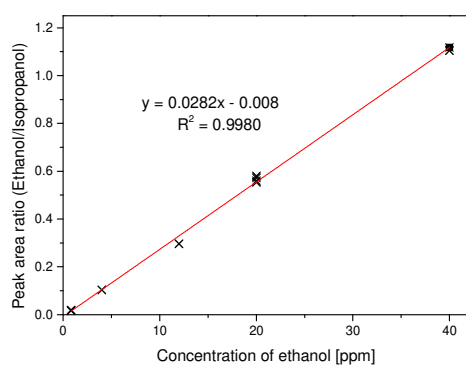
The amount of substance in a sample is proportional to the area under the chromatographic peak of that substance. However, the proportionality constant or the response factor between the analyte and standard is different for each substance and detector. Therefore, to do quantitative analysis by gas chromatography, the dependence of the proportionality constant on the concentrations of each substance in the mixture should be determined by constructing calibration lines. In this study the calibration curves were developed for quantitative analysis of ethanol.

The response factor  $f_i$  is expressed by the following equation<sup>[169]</sup>:

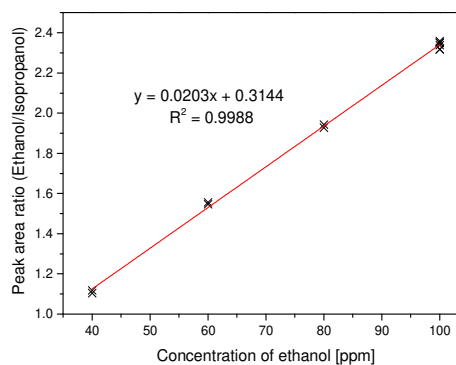
$$f_i = \frac{C_{ET}}{C_{st}} \cdot \frac{A_{st}}{A_{ET}} \quad \text{Equ. (46)}$$

where  $C_{ET}$  and  $C_{st}$  are the concentrations of ethanol and isopropanol,  $A_{ET}$  and  $A_{st}$  are the signals (peak areas) of ethanol and isopropanol. The response factor under given detector conditions is constant since the response of a given component is proportional to the mass of the injection<sup>[170]</sup>. By means of the separately determined response factor the amount of ethanol which was evolved during the silanization reaction could be determined.

A variety of calibration solutions were prepared which contained a fixed amount of the internal standard isopropanol. In the calibration solutions the concentration of ethanol was varied. After the vial equilibration time of 20 min at 120 °C, the results of the internal standard calibration curves for ethanol are graphically demonstrated in Figure 70 (a) and (b). Ideally, for a given volume of compound injected into the chromatograph, the peak area is linearly dependent on the concentration of the sample. In order to obtain a good linear relationship, two calibration curves were established for the quantification of the amount of evolved ethanol. Figure 70 (a) is valid for the detection of low ethanol concentrations between 0.8 ppm up to a threshold of 40 ppm. For the determination of higher ethanol concentrations between 40 and 100 ppm the calibration Figure 70 (b) is valid. These two calibration curves follow exactly a linear response with a correlation coefficient ( $R^2$ ) of 0.9980 and 0.9988, respectively.



(a) low concentrations



(b) high concentrations

Figure 70. Calibration line with concentrations (a) between 0.8 and 40 ppm; (b) between 40 and 100 ppm. Equilibrium for 20 min, at 120 °C

The calibration curves were also evaluated at 140 °C and 160 °C using the same run for measuring the peak areas of the standard analytes, and two calibration curves were established at each temperature with the threshold of 40 ppm. The calibration curves and the correlation coefficients which were obtained at temperatures of 120 °C, 140 °C and 160 °C are summarized in Table 21. As can be seen in this table the correlation coefficients  $R^2$  of all the calibration functions are  $> 0.99$ . On the basis of these results it can be concluded that the analytical method for the quantitative determination of ethanol is satisfactory<sup>[171]</sup>. These calibration functions were used for the investigation of the silanization kinetics of the different Nanoprene® grades and for the investigation of the silanization kinetics at different temperatures.

### 5.2.1.6 Limit of detection and limit of quantitation

Limit of detection (LOD) and limit of quantitation (LOQ) are important characteristics used to describe the lowest concentration of an analyte that can be reliably determined by an analytical procedure<sup>[172]</sup>. These limits have to be measured for each method and each measurand. The DIN 32645 standard defines these two terms and describes the calculation procedure based on the results of chemical analysis<sup>[173]</sup>. The definition of LOD is the minimum concentration of analyte in the test sample that can be measured with a stated probability. The definition of LOQ is the minimum concentration at which the analyte can not only be reliably detected but at which some predefined goals for bias and imprecision are met. In general, the LOQ is approximately three times higher than the LOD<sup>[174]</sup>.

Table 21. Calibration functions and detection and quantitation limits

Temp.	Calibration function	Concentration profiles [ppm]	Correlation coefficient $R^2$	LOD [ppm]	LOQ [ppm]
120 °C	$y=0.0282x - 0.0080$	0.8~40	0.998	1.7	5.8
	$y=0.0203x + 0.3144$	40~100	0.999	3.4	10.9
140 °C	$y=0.0249x - 0.0099$	0.8~40	0.999	1.3	4.7
	$y=0.0198x + 0.1907$	40~100	0.995	12.9	34.9
160 °C	$y=0.0241x + 0.0018$	0.8~40	0.999	1.0	3.7
	$y=0.0191x + 0.1974$	40~100	0.993	14.5	38.1

The detection and quantitation limits were carried out using a statistical software (Validat® 5.59.1629) based on the data of the standard analytes. There are two methods to calculate

the limits according to DIN 32645, the blank value method and the calibration line method. The results achieved in this work are from the calibration line method, which is more statistical than the blank value method. In this case, the blank value is estimated by extrapolation of the calibration line. The detection and quantitation limits of ethanol at different testing conditions are summarized in Table 21. For example, at 120 °C the LOD and LOQ are 1.7 ppm and 5.8 ppm, respectively (basis on the calibration curve for low concentrations). This means that the calibration curve for low ethanol concentrations allows the accurate determination of ethanol in the range from 5.8 ppm to 40 ppm. At ethanol concentrations which are higher than 40 ppm, the high concentration calibration function has to be used for the quantification of ethanol.

### 5.2.1.7 Identification of hydrolysis products by GC

In order to find out whether hydrolysis occurred in the silanized silica compound during water storage at 80 °C, gas chromatography with mass spectrometry detection was used to study the hydrolysis process. The experimental setup is depicted in Figure 71.

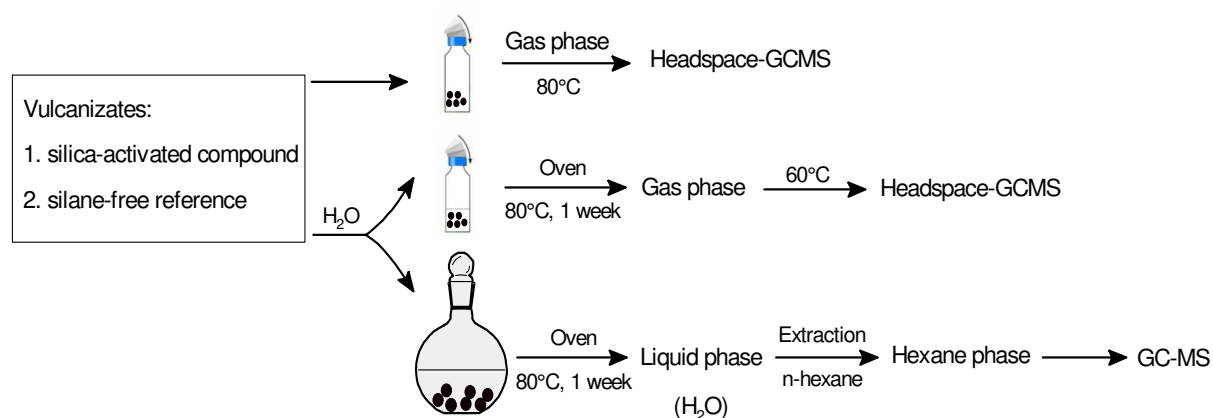


Figure 71. Schematic representation of the experiment setup for the determination of hydrolysis products

On the one hand, the volatiles of the silane-activated and silane-free reference vulcanizates at 80 °C were analyzed by GCMS-headspace. On the other hand, the vulcanizates immersed in water were stored in an oven for 1 week at 80 °C in a closed vial. The emission profile in the gas phase was directly analyzed by GCMS-headspace after water storage. The components remaining in the water phase were extracted by n-hexane and the n-hexane extracts were measured by GC-MS.

### 5.2.2 Mixing process

The compounds were prepared in three mixing steps corresponding to the procedure presented in Table 22.

Table 22. Mixing procedure

Mixing steps	Procedure
1st stage:	GK 1.5E: 80 rpm, chamber temp. 80 °C; fill factor 0.56
0'-1'	polymers
1'-2'	1/2 silica; silane; ZnO; Nanoprene®
2'	raise ram and clean
2'-3'	1/2 silica; oil
3'	raise ram and clean
3'-8'	mix @ 155 °C
8'	dump; pass through a wide nip on an open mill one time
2nd stage:	GK 1.5E: 80 rpm, chamber temp. 80 °C; fill factor 0.56
0'-1'	batch stage 1
1'-6'	mix @ 155 °C
6'	dump; pass through a wide nip on an open mill one time
3rd stage:	GK 1.5E: 40 rpm, chamber temp. 50 °C
0'-0.5'	batch stage 2
0.5'-2'	ingredients 3rd stage
2'	dump and homogenize on open mill

An internal mixer was used (Werner & Pfleiderer, GK 1.5 E). In the first mixing step when the rubbers, filler, zinc oxide, silane and Nanoprene® were added the mixing temperature was raised to 150 – 160 °C and held in this temperature range for 5 min. After the dumping of the compounds they were stored at ambient temperature overnight. Subsequently a second mixing step mix was used during which the temperature was again raised to 150 – 160 °C for 5 min. The compounds were dumped, homogenized and cooled using an open mill (Berstorff type 150 × 230 RR) and stored overnight. In the third mixing step the vulcanizing package (consisting of sulfur and accelerators) was added.

### 5.2.3 Vulcanization process

The vulcanization rate was monitored with a Monsanto Rheometer (Type MDR 2000 E) at a temperature of 160 °C, a frequency of 1.67 Hz and +/- 0.5 % amplitude in accordance with DIN 53529 and  $t_{90}$  was determined (time when 90 % conversion was achieved) for each compound. The vulcanized test specimens were prepared in a heating press (J. Wickert & Söhne Type WPL 63/3,5/3) under 300 bar pressure at a curing temperature of 160 °C. The vulcanization time was  $t_{90}$  as previously determined with the Monsanto Rheometer.

### 5.2.4 Rheological characterization (filler flocculation analysis)

Uncured samples which were taken after mixing step one and after mixing step two were used to study the filler flocculation and the subsequent break-down of the filler network. For these studies a rubber process analyzer (RPA 2000, Alpha Technology) was used. In order to study filler flocculation  $G'$  was monitored at 160 °C at a constant oscillation of 1 % for 60 min. Subsequently, the filler network was destroyed by the increase of the shear amplitude from 1 % to 400 % strain. The frequency was kept constant at 1 Hz for both experiments.

### 5.2.5 Mooney viscosity

Mooney viscosity and Mooney relaxation measurements were performed with an Alpha Technologies MV 2000E, at 100 °C, according DIN 53523.

### 5.2.6 Tensile testing

Stress/strain tests were performed at ambient temperature with a material tester (Zwick 1445, Ulm, Germany) using optical strain control with a crosshead speed of 200 mm/min (DIN 53504). The measurements were done 5 times and mean values were used.

### 5.2.7 Hardness

The Shore A hardness of the vulcanizates was determined in five different places on the sample according to DIN 53505 after 3 sec (Zwick digitest, Germany). The thickness of the vulcanized specimens was 6 mm.

### **5.2.8 Rebound resilience**

For the measurements of rebound resilience, the specimens with cylindrical shapes were used (diameter: 60 mm; thickness: 6 mm): The measurements were performed according to DIN 53512 with the Zwick rebound tester 5109.01.

### **5.2.9 Compression set**

The compression set tests were performed at 23 °C and 70 °C for 72 hours according to DIN 53517.

### **5.2.10 DIN abrasion**

DIN abrasion test were performed with Frank 11565 according to DIN 53516. The specimens were abraded by friction. The abrading distance on the surface on the surface of the drum was 40 m and the speed was 40 rpm.

### **5.2.11 Equilibrium swelling experiments**

A sorption-desorption method was used to measure the swelling behaviour of the vulcanizates. Dry specimens were punched out in a circular shape of diameter 10 mm with known weight and were immersed in toluene in closed diffusion bottles at 20 °C on a shaker. For the determination of equilibrium swelling three samples were periodically taken out from the toluene and the excess liquid on the specimen surface was removed by blotting with a filter paper, and weighed immediately with an electronic balance. The process was continued until the weight of the swollen samples reached the equilibrium. The crosslink density was determined by means of Flory-Rehner equation (Equ. (25), Chap. 2.5.3). The values of the Flory-Huggins interaction parameter  $\chi$  for cured rubber with different solvents can be found in the chemistry handbooks<sup>[175, 176]</sup>. For toluene  $\chi = 0.4$  was used in the calculations. The swelling ratio of the vulcanizates was also obtained from equilibrium swelling data to predict the degree of crosslinking. The swelling ratio (Q) was calculated by Equ. (27).

### **5.2.12 Dynamic mechanical analysis (DMA)**

Dynamic mechanical analysis was performed with a Rheometric Dynamic Analyzer RDA II (Rheometric Scientific GmbH, Germany). The shape of the test specimens was rectangular with 40 mm, 10 mm and 2 mm.



The temperature sweeps were measured in a temperature range from -70 to +80 °C at a constant strain amplitude of 0.5 %. The heating rate was 1 K/min under liquid nitrogen flow. The amplitude sweeps were performed at 23 °C in which the strain amplitude was increased in logarithmic steps from 0.05 to 5 %. All dynamic mechanical measurements were done using a frequency of 10 Hz.

### 5.2.13 Water storage

Water storage was performed on rectangular vulcanized specimens with the size: 40 mm, 10 mm and 2 mm. In the experimental design the storage time and also the storage temperature were varied. The samples were hung in deionized water at different temperatures (20, 40, 60, and 80 °C), as shown in Figure 72. The water storage time was from 4 to 16 weeks. The weight of the samples was determined before and after water storage. Before the weight determination of the wet samples water was removed from the surface of the specimens with a filter paper. The water uptake was calculated using the Equ. (44) in Chap. 3.4.2.

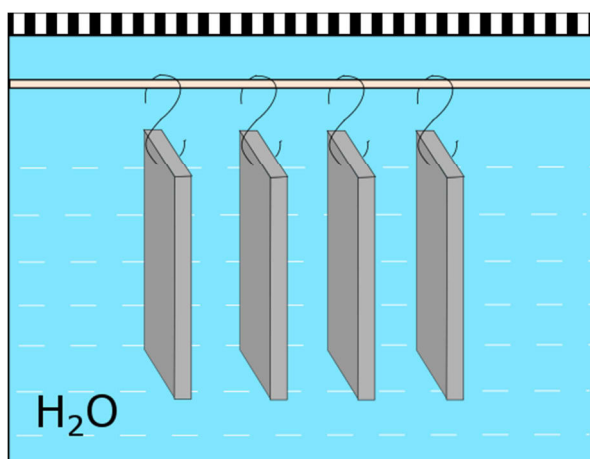


Figure 72. Schematic layout of experimental setup for water storage

In order to study the reversibility of water swelling the wet samples were dried to constant weight in a vacuum oven at room temperature before the samples were characterized by DMA measurement.

### 5.2.14 Differential scanning calorimetry (DSC)

DSC measurements were performed by using a DSC 2920CE from TA-Instruments. Two cooling-heating cycles between -100 to +100 °C with a rate of 10 °C/min were applied. The

first cycle used to erase previous thermal history. The glass transition temperature ( $T_g$ ) was determined at the inflection point of the endotherm curve from the second heating cycle.

#### **5.2.15 ATR-FTIR spectroscopy**

The ATR-FTIR spectra were measured by means of Thermo Nicolet Nexus micro scale IR spectrometry equipped with a horizontal 45° germanium (Ge) crystal ATR device. The samples were pressed on horizontal surface of the Ge crystal at room temperature. The spectra were the results of 256 scans with a resolution of 2  $\text{cm}^{-1}$  in the spectral range of 4000 – 550  $\text{cm}^{-1}$ .

#### **5.2.16 Transmission electron microscopy (TEM)**

Electron micrographs were obtained by transmission electron microscopy. The microtome cuts were prepared at -100 °C a FC 4 microtome (Zeiss EM902) with the thickness of 100 nm. Transmission electron microscopy was performed with an electron microscope imaging (ESI) of Zeiss Libra® 120.

## 6 Literature

- [1] Hickman, H. L. *American Alchemy: The History of Solid Waste Management in the United States*; Forester Press: United States, 2003, 364-365.
- [2] Blank, S. D. *AICCM Bulletin*, 1988, 14 (3-4), 53-93.
- [3] Goodyear, C. U.S. Patent 3,633, 1844.
- [4] Harp, S. L. *A World History of Rubber*; John Wiley & Sons, Inc.: UK, 2016, 1-5.
- [5] Myers, R. *The Basics of Chemistry*; Greenwood Publishing Group: London, 2003, 299-301.
- [6] Mihara, S. *Reactive processing of silica-reinforced tire rubber: new insight into the time and temperature dependence of silica rubber interaction*; Dissertation, University of Twente, Netherlands, 2009.
- [7] Vanooij, W. J.; Harakuni, P. B.; Buytaert, G. *Rubber Chemistry and Technology*, 2009, 82 (3), 315-339.
- [8] Datta, R. N. *Rubber Curing Systems*; Rapra Rev. Rep.: United Kingdom, 2001, 12 (12), 32-35.
- [9] Bhowmick, A. K. *Current Topics in Elastomers Research*; CRC Press: New York, 2008, 445-447.
- [10] Sengloyluana, K.; Sahakaroa, K.; Dierkes, W. K.; Noordermeer, J. W. M. *European Polymer Journal*, 2014, 51 (1), 69-79.
- [11] Zhu, Z.; Thompson, T.; Wang, S.; von Meerwall, E. D.; Halasa, A. *Macromolecules*, 2005, 38 (21), 8816-8824
- [12] Gauthier, C.; Reynaud, E.; Vassoille, R.; Ladouce-Stelandre, L. *Polymer*, 2004, 45 (8), 2761-2771.
- [13] Rodgers, B. *Rubber Compounding: Chemistry and Applications, Second Edition*; CRC Press: New York, 2016, 251-253.
- [14] Montes, H.; Lequeux, F.; Berriot, J. *Macromolecules*, 2003, 36 (21), 8107-8118.
- [15] Morozov, I.; Svistkov, A.; Lauke, B.; Heinrich, G. *KGK, Kautschuk Gummi Kunststoffe*, 2006, 59, 642-647.
- [16] Wang, M, J. *KGK, Kautschuk Gummi Kunststoffe*, 2008, 61, 33-42.
- [17] Robertson, C. G.; Roland, C. *Rubber Chemistry and Technology*, 2008, 81 (3), 506-522.
- [18] Kraus, G. *Reinforcement of Elastomers*; Interscience Publishers: New York, 1965, 2-3.
- [19] Degussa AG, DE patent 2447614 C2, 1974.
- [20] Takeshita, M.; Mukai, U.; Sugawara, T. U.S. patent 4820751 A, 1988.

- [21] Rauline, R. U.S. patent 5227425 A, 1992.
- [22] Rauline, R. E.P. patent 0 501227A1, Michelin & Cie, 1992.
- [23] Barrand, J.; Bokar, J. SAE Int. J. Passeng. Cars - Mech. Syst., 2009, 1 (1), 9-17.
- [24] Limper, A. Mixing of Rubber Compounds; Carl Hanser Verlag: Munich, 2012, 95-96.
- [25] Obrecht, W.; Steger, L. ATZautotechnology, 2008, 8 (7), 42-45.
- [26] Obrecht, W.; Jeske, W. U.S. patent 6399706B1, 2002.
- [27] Obrecht, W. International Polymer Science and Technology, 2010, 37 (2), 33-35.
- [28] Obrecht, W.; Summer, A. J. M. U.S. patent US 6809146 B2, 2004.
- [29] Obrecht, W.; Köhler, B.; Jeske, W. U.S. patent US 7134466 B2, 2006.
- [30] Obrecht, W. E.P. patent WO 2008132061 A2, 2008.
- [31] Obrecht, W. U.S. patent 20100197829 A1, 2010.
- [32] Obrecht, W. U.S. patent 8084547 B2, 2011.
- [33] Sulpizi, M.; Gaigeot, M.; Sprik, M. Journal of Chemical Theory and Computation, 2012, 8 (3), 1037-1047.
- [34] Rimstidt, J. D.; Barnes, H. L. Geochimica et Cosmochimica Acta, 1980, 44 (11), 1683-1699.
- [35] Otegui, J.; Schwartz, G. A.; Cervený, S.; Colmenero, J.; Loichen, J.; Wenstermann, S. Macromolecules, 2013, 46 (6), 2407-2416.
- [36] Lange, H. Kolloid Zeitschrift & Zeitschrift für Polymere, 1968, 233, 24-30.
- [37] Müller, H. G. Colloid Polym. Sci., 1989, 267 (12), 1113-1116.
- [38] Obrecht, W.; Steger, L. Kunststoffe International, 2009, 10, 38-42.
- [39] Cataldo, F. Effect of Nanorubber in Black-filled Rubber Compounds; Tire Technol. Int. 2011, 22-27.
- [40] Steinhauser, N.; Obrecht, W.; Hardy, D.; Groß, T. U.S. patent 8173741B2, 2012.
- [41] Obrecht, W.; Steger, L. Improvement of Tire Performance by New Polymer-Nano-Additives; Proceedings of Tire Expo, Hamburg, Germany, 2009.
- [42] Jeske, W.; Obrecht, W. C.A. patent 2312171A1, 2000.
- [43] Obrecht, W. E.P. patent 1307504, 2000.
- [44] Obrecht, W. E.P. patent 218665, 2008.
- [45] Recker, C. E.P. patent 1520732 A1, 2004
- [46] Obrecht, W. U.S. patent 8119728B2, 2012.
- [47] Chern, C. S. Principles and Applications of Emulsion Polymerization; John Wiley & Sons, Inc.: Canada, 2008, 5-8.
- [48] Früh, T.; Boivin, C.; Ziser, T. Presentation "Organische Nanopartikel - Steuerung der Materialeigenschaften", Rhein Chemie Rheinau GmbH, 2007.
- [49] Fox, T. G.; Flory, P. J. Journal of Applied Physics, 1950, 21, 581-591.

- [50] DIN 53240, Determination of hydroxyl value (HN).
- [51] Katz, H. S.; Mileski, J. V. Handbook of Fillers for Plastic; Van Nostrand Reinhold: New York, 1987, 167-169.
- [52] Xanthos, M. Functional Filler for Plastics; Wiley-VCH: Germany, 2010, 395-398.
- [53] Otterstedt, J. E.; Brandreth, D. A. Small Particles Technology; Plenum Press: New York and London, 1998, 443-445.
- [54] Dogan, A. U.; Dogan, M.; Onal, M.; Sarikaya, Y.; Aburub, A.; Wurster, D. E. Clays and Clay Minerals, 2006, 54 (1), 62-66.
- [55] Parmentier, F.; Persello, J. U.S. patent 5009874 A, 1988.
- [56] Rodgers, B. Rubber Compounding: Chemistry and Applications, Second Edition; CRC Press: New York, 2016, 256-257.
- [57] Chakraborty, S.; Shah, D. Rubber World, Sept. 1, 2013.
- [58] Goerl, U.; Hunsche, A.; Mueller, A.; Koban H. G. Rubber Chemistry and Technology, 1997, 70 (4), 608-623.
- [59] Derouet, D.; Forgeard, S.; Brosse, J. C.; Emery, J.; Buzare, J. Y. Journal of Polymer Science: Part A, Polymer Chemistry, 1998, 36 (3), 437-453.
- [60] Luhmer, M.; d'Espinose, J. B.; Hommel, H.; Legrand, A. P. Magnetic Resonance Imaging, 1996, 14 (7-8), 911-913.
- [61] Blume, A.; Gallas, J. P.; Janik, M.; Thibault-Starzyk, F.; Vimont, A. KGK, Kautschuk Gummi Kunststoffe, 2008, 61, 359-362.
- [62] Blume, A.; El-Roz, M.; Thibault-Starzyk, F. KGK, Kautschuk Gummi Kunststoffe, 2013, 10, 63-70.
- [63] El-Roz, M.; Thibault-Starzyk, F.; Blume, A. KGK, Kautschuk Gummi Kunststoffe, 2014, 5, 53-57.
- [64] Zhao, X. S.; Lu, G. Q.; Whittaker, A. K.; Millar, G. J.; Zhu, H. Y. J. Phys. Chem. B, 1997, 101 (33), 6525-6531.
- [65] Wang, M. J.; Wolff, S.; Donnet, J.-B. Rubber Chem. Technol., 1991, 64 (4), 559-576.
- [66] Dirote, E. V. Trends in Nanotechnology Research; Nova Science Publishers, Inc.: New York, 2004, 57-58.
- [67] Mark, J. E.; Erman, B.; Eirich, F. R. Science and Technology of Rubber; Academic Press: United States, 1994, 439-440.
- [68] Visakh, P. M.; Thomas, S.; Chandra, A. K.; Mathew, A. P. Advances in Elastomers I: Blends and Interpenetrating Networks; Springer-Verlag Berlin Heidelberg: New York, 2013, 106-107.
- [69] Laidler, K. J. Journal of Chemical Education, 1984, 61 (6), 494-498.
- [70] Liu, Y.; Li, Y.; Li, X. M.; He, T. Langmuir, 2013, 29 (49), 15275-15282.

- [71] Buszewski, B.; Nondek, L.; Jurášek, A.; Berek, D. *Chromatographia*, 1987, 23 (6), 442-446.
- [72] Krasnoslobodtsev, A. V.; Smirnov, S. N. *Langmuir*, 2002, 18 (8), 3181-3184.
- [73] Schmidt, H.; Scholze, H.; Kaiser, A. *Journal of Non-Crystalline Solids*, 1984, 63 (1-2), 1-11.
- [74] Hertl, W. J. *Phys. Chem.*, 1968, 72 (4), 1248-1253.
- [75] Vilmin, F.; Bottero, I.; Travert, A.; Malicki, N.; Gaboriaud, F.; Trivella, A.; Thibault-Starzyk, F. *J. Phys. Chem. C*, 2014, 118 (8), 4056-4071.
- [76] Wolff, S. *Rubber Chemistry and Technology*, 1996, 69 (3), 325-346.
- [77] Blume, A. *KGK, Kautschuk Gummi Kunststoffe*, 2011, 64 (4), 38-43.
- [78] Roy, S.; Dixit, C. K.; Woolley, R.; MacCraith, B. D.; O'Kennedy, R.; McDonagh, C. *Langmuir*, 2010, 26 (23), 18125-18134.
- [79] Kinkel, J. N.; Unger, K. K. *Journal of Chromatography A*, 1984, 316, 193-200.
- [80] Payne, A. R. *Journal of Applied Polymer Science*, 1965, 9 (6), 2273-2284.
- [81] Payne, A. R. *Rubber Chemistry and Technology*, 1966, 39 (2), 365-374.
- [82] Fröhlich, J.; Niedermeier, W.; Luginsland, H. D. *Composites: Part A*, 2005, 36, 449-460.
- [83] Wang, M. J. *Rubber Chemistry and Technology*, 1998, 71 (3), 520-589.
- [84] Flory, P. J. *Chem. Rev.*, 1944, 35 (1), 51-75.
- [85] Flory, P. J. *Transactions of the Faraday Society*, 1961, 57, 829-838.
- [86] Treloar, L. R. G. *Rep. Prog. Phys.*, 1973, 36, 755-826.
- [87] Manchado, M. L.; Herrero, B.; Arroyo, M. *Polymer International*, 2004, 53 (11), 1766-1772.
- [88] Guth, E.; Gold, O. *Phys. Rev.*, 1938, 53, 322-328.
- [89] Guth, E. *Journal of Applied Physics*, 1945, 16 (11), 20-25.
- [90] Payne, A. R. *Journal of Applied Polymer Science*, 1962, 21, 368-372.
- [91] Niedermeier, W.; Fröhlich, J.; Luginsland, H. D. *KGK, Kautschuk Gummi Kunststoffe*, 2002, 55 (7-8), 356-366.
- [92] Medalia, A. I. *Rubber Chemistry and Technology*, 1973, 46 (4), 877-896.
- [93] Heinrich, G.; Klüppel, M.; Vilgis, T. A. *Current Opinion in Solid State and Materials Science*, 2002, 6 (3), 195-203.
- [94] Funt, J. M. *Rubber Chemistry and Technology*, 1988, 61 (5), 842-865.
- [95] Thomas, S. Maria, H. J. *Progress in Rubber Nanocomposites*; Woodhead Publishing: United Kingdom, 2016, 85-87.
- [96] Rodgers, B. *Rubber Compounding: Chemistry and Applications*, Second Edition; CRC Press: New York, 2016, 277-279.

- [97] Wolff, S.; Wang, M. J. *Rubber Chemistry and Technology*, 1992, 65 (2), 329-342.
- [98] Clément, F.; Bokobza, L.; Monnerie, L. *Rubber Chemistry and Technology*, 2005, 78 (2), 211-231.
- [99] Robertson, C. G.; Lin, C. J.; Rackaitis, M.; Roland, C. M. *Macromolecules* 2008, 41 (7), 2727-2731.
- [100] Böhm, G. G. A.; Nguyen, M. N. *Journal of Applied Polymer Science*, 1995, 55 (7), 1041-1050.
- [101] Lin, C. J.; Hergenrother, W. L.; Alexanian, E.; Böhm, G. G. A. *Rubber chemistry and technology*, 2002, 75 (5), 865-890.
- [102] Stöckelhuber, K. W.; Svistkov, A. S.; Pelevin A. G.; Heinrich, G. *Macromolecules*, 2011, 44 (11), 4366-4381.
- [103] Ghosh, P.; Katare, S.; Patkar, P.; Caruthers, J. M.; Venkatasubramanian, V.; Walker, K. A. *Rubber Chemistry and Technology*, 2003, 76 (3), 592-693.
- [104] Flory, P. J. *Principles of Polymer Chemistry*; Cornell University Press: United States, 1953, 457-459.
- [105] Galimberti, M. *Rubber-Clay Nanocomposites: Science, Technology, and Applications*; John Wiley & Sons: New York, 2011, 275-278.
- [106] Oenslager, G. *Industrial & Engineering Chemistry*, 1933, 25 (2): 232-237.
- [107] Heideman, G. *Reduced zinc oxide levels in sulphur vulcanization of rubber compound*; Dissertation, University of Twente, Netherlands, 2004.
- [108] Dogadkin, B. A. *J. Appl. Polym. Sci.*, 1958, 30 (121), 351-361.
- [109] Da Costa, H. M.; Visconte, L. L. Y.; Nunes, R. C. R.; Furtado, C. R. G. *J. Appl. Polym. Sci.*, 2003, 90 (6), 1519-1531.
- [110] Guzam, M. *Novel Vulcanization Ingredients: Towards Greener Rubber Formulations*; Dissertation, University Ramon Llull, Barcelona, 2012.
- [111] Ignatz-Hoover, F. *Rubber World*, 1999, 220 (5), 24-29.
- [112] Datta, R. N. *Rubber Curing Systems*; *Rapra Rev. Rep.*: United Kingdom, 2001, 12 (12), 3-5.
- [113] Coran, A. Y. *J. Appl. Polym. Sci.*, 2003, 87 (1), 24-30.
- [114] Görl, U. *Gummi Fasern Kunststoffe*, 1998, 51 (5), 416-424.
- [115] Luginsland, H. D.; Kalscheuren, H., *KGK, Kautschuk Gummi Kunststoffe*, 2000, 53 (1-2), 10-23.
- [116] Luginsland, H. D.; Röben, C. *Gummi Fasern Kunststoffe*, 2015, 68 (11), 734-737.
- [117] Hasse, A.; Klockmann, O.; Wehmeier, A.; Luginsland, H. D. *KGK, Kautschuk Gummi Kunststoffe*, 2002, 55 (5), 236-243.

- [118] Young, R. J.; Lovell, P. A. Introduction to Polymers, Third Edition; CRC press: New York, 2011, 526-530.
- [119] Flory, P. J. J. Chem. Phys., 1942, 10 (1), 51-61.
- [120] Flory, P. J. Proc. R. Soc. London, 1976, A351, 351-380.
- [121] Mark, J. E. Physical Properties of Polymers Handbook; Springer: New York, 2007, 502-507.
- [122] Wall, F. T.; Flory, P. J. J. Chem. Phys. 1951, 19 (12), 1435-1439.
- [123] Kraus, G. J. Appl. Polym. Sci., 1963, 7 (3), 861-871.
- [124] Da Costa, H. M.; Nunes, R. C. R.; Visconte, L. L. Y.; Furtado, G. R. G. KGK, Kautschuk Gummi Kunststoffe, 2001, 54 (5), 242-249.
- [125] Marzocca, A. J.; Rodriguez Garraza, A. L.; Mansilla, M. A. Polymer Testing, 2010, 29 (1), 119-126.
- [126] Heinrich, G. Advanced Rubber Composites; Springer-Verlag Berlin Heidelberg: Germany, 2011, 38-44.
- [127] Abedali, A. H. Journal of Civil Engineering and Construction Technology, 2015, 6 (3), 15-26.
- [128] Dick, J. S. Basic Rubber Testing: Selecting Methods for a Rubber Test Program; ASTM International: USA, 2003, 41-43.
- [129] Mogi, E.; Mizone, T.; Hase, H.; Nishitani, K.; Mizutani, T.; Takahashi, H. Review of Automotive Engineering, 2008, 29, 149-155.
- [130] Byers, J. T. Rubber Chemistry and Technology, 2002, 75 (3), 527-548.
- [131] Hall, D. E.; Cal Moreland, J. Rubber Chemistry and Technology, 2001, 74 (3), 525-539.
- [132] Shanmugharaj, A. M.; Bhowmick, A. K. Journal of applied polymer Science, 2003, 88 (13), 2992-3004.
- [133] Whelan, A.; Lee, K. S. Developments in Rubber Technology - 4; Elsevier Applied Science: London and New York, 1987, 36-38.
- [134] Maghami, S. Silica-Filled Tire Tread Compounds; Ph.D Thesis, University of Twente, 2016.
- [135] Rodgers, B. Rubber Compounding: Chemistry and Applications, Second Edition; CRC Press: New York, 2016, 60-65.
- [136] Hays, D. The Physics of Tire Traction: Theory and Experiment; Springer Science Business Media: New York, 1974, 227-230.
- [137] Roland, C. M. Viscoelastic Behavior of Rubbery Materials; Oxford University Press: New York, 2011, 69-70.
- [138] Williams, M. L.; Landel, R. F.; Ferry, J. D. J. Amer. Chem. Soc. 1955, 77 (14): 3701-3707.

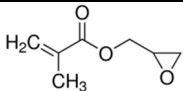
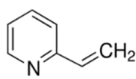
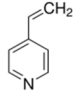
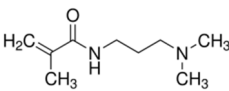
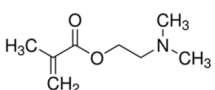
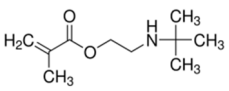
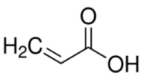
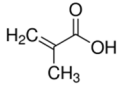
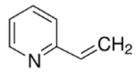
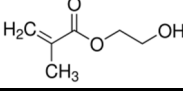


- [139] Nordsiek, K. H. KGK, Kautschuk Gummi Kunststoffe, 1985, 38 (3), 178-185.
- [140] Groenewoud, W. M. Characterisation of Polymers by Thermal Analysis; Elsevier: Netherland, 2001, 17-18.
- [141] Krüger, A. Carbon Materials and Nanotechnology; WILEY-VCH Verlag GmbH & Co. KGaA: Weinheim, 2010, 374-376.
- [142] Kromidas, S.; Kuss, H. J. Quantification in LC and GC: A Practical Guide to Good Chromatographic Data; Wiley-VCH Verlag GmbH & Co. KGaA: Weinheim, 2009, 238-240.
- [143] Wilson, I. D.; Poole, C. F. Handbook of Methods and Instrumentation in Separation Science, Volume 1; Elsevier: USA, 2009, 233-236.
- [144] Stuart, B. Gas Chromatography; LGC (Teddington) Limited: UK, 2003, 27-29.
- [145] Cassada, D. A.; Zhang, Y.; Snow, D. D.; Spalding, R. F. Anal. Chem., 2000, 72 (19), 4654-4658.
- [146] Pauls, R. E.; McCoy, R. W.; Journal of Chromatographic Science, 1981, 19 (11), 558-561.
- [147] Polmanteer, K. E.; Lentz, C. W. Rubber chemistry and technology, 1975, 48 (5), 795-809.
- [148] Meera, A. P.; Said, S.; Grohens, Y.; Thomas, S. J. Phys. Chem. C, 2009, 113 (42), 17997-18002.
- [149] Pathak, S.; Lim, E. J.; Abadi, P. P. S. S.; Graham, S.; Cola, B. A.; Greer, J. R. ACS Nano, 2012, 6 (3), 2189-2197.
- [150] Suzuki, N.; Ito, M.; Yatsuyanagib, F. Polymer, 2005, 46 (1), 193-201.
- [151] Kumar, P. V. A., Varghese, K. T.; Thomas, S. Ind. Eng. Chem. Res., 2012, 51 (19), 6697-6704.
- [152] Huggins, M. L. J. Phys. Chem., 1942, 46 (1), 151-158.
- [153] Bindu, P.; Thomas, S. J. Phys. Chem. B, 2013, 117 (41), 12632-12648.
- [154] Strobl, G. The Physics of Polymers; Springer-Verlag Berlin Heidelberg: Germany, 2007.
- [155] Ladouce, L.; Bomal, Y.; Flandin, L.; Labarre, D. Rubber Chemistry and Technology, 2003, 76 (1), 145-159.
- [156] Seo, B.; Kang, J.; Jang, S.; Kang, Y.; Kin, W. Journal of Nanoscience and Nanotechnology, 2013, 13 (3), 2179-2188.
- [157] Isayev, A. I.; Palsule, S. Encyclopedia of Polymer Blends, Volume 2: Processing; Wiley-VCH Verlag GmbH & Co. KGaA: Germany, 2011, 167-169.
- [158] Choi, S. S. J. Appl. Polym. Sci., 2002, 83 (12), 2609-2616.
- [159] Natchimuthu, N. Rubber Chemistry and Technology, 2010, 83 (2), 123-132.

- [160] Jitkarnka, S.; Chusaksri, B.; Supaphol, P.; Magaraphan, R. J. *Anal. Appl. Pyrolysis*, 2007, 80 (1), 269-276.
- [161] Santoso, M.; Giese, U.; Schuster, R. H. *KGK, Kautschuk Gummi Kunststoffe*, 2007, 60 (4), 192-198.
- [162] Jordana, J.; Jacobb, K. I.; Tannenbaum, R.; Sharafb, M. A.; Jasiuk, I. *Materials Science and Engineering: A*, 2005, 393, 1-11.
- [163] Song, Y. S.; Youn, J. R. *Carbon*, 2005, 43 (7), 1378-1385.
- [164] Takino, H.; Nakayama, R.; Yamada, Y.; Kohjiya, S.; Matsuo, T. *Rubber Chemistry and Technology*, 1997, 70 (4), 584-594.
- [165] Zhuravlev, L. T. *Colloids Surf. A*, 2000, 173, 1-38.
- [166] Yanagihara, H.; Yamashita, K.; Endo, A.; Daiguji, H. *J. Phys. Chem. C*, 2013, 117 (42), 21795-21802.
- [167] Levine, H.; Slade, L. *Water Science Reviews*; Cambridge University Press: Cambridge, 1988, 79-185.
- [168] Li, Z.; Han, Y. H.; Martin, G. P. *Journal of Pharmaceutical and Biomedical analysis*, 2002, 28 (3), 673-682.
- [169] Kolb, B.; Ettre, L. S. *Static Headspace-Gas Chromatography: Theory and Practice*; John Wiley & Sons, Inc.: Canada, 2006.
- [170] Heftmann, E. *Chromatography: Fundamentals and applications of chromatography and related differential migration methods*; Elsevier B. V.: Netherlands, 2004, 349-351.
- [171] Sen, Z. *Innovative Trend Methodologies in Science and Engineering*; Springer International Publishing AG: Switzerland, 2017, 57-58.
- [172] Armbruster, D. A.; Pry, T. *Clin Biochem Rev.*, 2008, 29 (1), 49-52.
- [173] DIN 32645. *Chemical analysis - Decision limit, detection limit and determination limit under repeatability conditions - Terms, methods, evaluation.*
- [174] Taylor, J. K. *Quality Assurance of Chemical Measurements*; Lewis Publishers: United State, 1987, 79-82.
- [175] Kleemann, W.; Weber, K., *Formeln und Tabellen für die Elastomerverarbeitung*; Gupta Verlag: Germany, 1994, 126-133.
- [176] Allan, F. M. Barton, *Handbook of Polymer-Liquid Interaction Parameters and Solubility Parameters*; CRC Press LLC: USA, 1990.

## 7 Annexes

Table 23. Nanoprene® grades and the functional monomer for polymerization

Nanoprene® grade	Functional monomer	Chemical Formula	ACS No.	Structure
OBR 1504 D	Glycidyl methacrylate (GDMA)	C <sub>7</sub> H <sub>10</sub> O <sub>3</sub>	106-91-2	
OBR 1504 F	2-Vinylpyridine (2-VP)	C <sub>7</sub> H <sub>7</sub> N	100-69-6	
OBR 1504 G	4-Vinylpyridine (4-VP)	C <sub>7</sub> H <sub>7</sub> N	100-43-6	
OBR 1504 H	N-[3-(Dimethylamino)propyl] methacrylamide (DMAPMA)	C <sub>9</sub> H <sub>18</sub> N <sub>2</sub> O	5205-93-6	
OBR 1504 I	2-(Dimethylamino)ethyl methacrylate (DMAEMA)	C <sub>8</sub> H <sub>15</sub> NO <sub>2</sub>	2867-47-2	
OBR 1504 K	2-(tert-Butylamino)ethyl methacrylate (BAEMA)	C <sub>10</sub> H <sub>19</sub> NO <sub>2</sub>	3775-90-4	
OBR 1504 L	Acrylic acid (AA)	C <sub>3</sub> H <sub>4</sub> O <sub>2</sub>	79-10-7	
OBR 1504 M	Methacrylic acid (MAA)	C <sub>4</sub> H <sub>6</sub> O <sub>2</sub>	79-41-4	
OBR 1504 N	2-Vinylpyridine (2-VP)	C <sub>7</sub> H <sub>7</sub> N	100-69-6	
BM75OH*	2-Hydroxyethyl methacrylate (HEMA)	C <sub>6</sub> H <sub>10</sub> O <sub>3</sub>	868-77-9	

\* The commercial Nanoprene® grade.

Table 24. Concentration of released ethanol evaluated by headspace gas chromatography

Nanoprene® grades	Temp. [°C]	Concentration of ethanol [ $\times 10^{-6}$ mol]			
		20 min	60 min	180 min	300 min
Silica	120	8.88±0.48	9.81±0.29	9.78±0.53	9.67±0.59
	140	9.59±0.20	10.0±0.12	10.6±0.54	11.2±0.05
	160	8.77±0.43	9.78±0.19	-	-
OBR 1504 D	120	0.42±0.02	0.60±0.03	0.88±0.09	1.32±0.07
	140	0.48±0.01	0.83±0.03	1.51±0.06	4.74±0.16
	160	0.91±0.03	3.37±0.12	-	-
OBR 1504 F	120	1.08±0.02	1.87±0.03	3.98±0.20	5.10±0.41
	140	1.24±0.01	2.61±0.11	5.79±0.10	7.85±0.08
	160	3.46±0.30	7.95±0.55	-	-
OBR 1504 G	120	0.85±0.02	1.30±0.01	2.29±0.11	2.98±0.08
	140	1.02±0.01	1.74±0.03	3.72±0.03	6.34±0.42
	160	2.49±0.12	5.92±0.37	-	-
OBR 1504 H	120	0.32±0.01	0.34±0.01	0.39±0.02	0.46±0.09
	140	0.29±0.01	0.31±0.01	0.51±0.01	0.93±0.05
	160	0.31±0.02	0.57±0.06	-	-
OBR 1504 I	120	0.37±0.01	0.45±0.01	0.80±0.03	1.17±0.05
	140	0.37±0.01	0.59±0.04	1.43±0.10	4.27±0.34
	160	0.67±0.01	1.87±0.05	-	-
OBR 1504 K	120	0.51±0.01	0.72±0.01	1.12±0.02	1.54±0.07
	140	0.53±0.03	0.89±0.02	1.60±0.02	3.31±0.33
	160	0.97±0.03	2.12±0.03	-	-
OBR 1504 L	120	8.20±0.37	10.0±0.52	12.6±0.35	13.9±0.47
	140	9.20±0.40	14.3±0.08	15.6±0.03	19.6±0.53
	160	11.0±0.34	18.5±0.34	-	-
OBR 1504 M	120	7.84±0.60	9.57±0.67	10.7±0.29	13.4±0.39
	140	8.30±0.32	12.9±0.29	15.1±0.73	21.3±1.53
	160	11.2±0.35	18.6±0.34	-	-
OBR 1504 N	120	1.61±0.04	2.58±0.09	4.10±0.20	6.25±0.29
	140	2.03±0.08	3.88±0.03	7.28±0.07	9.67±0.25
	160	4.67±0.34	9.56±0.18	-	-
BM 75OH	120	0.53±0.02	0.97±0.03	2.31±0.04	3.75±0.04
	140	0.63±0.01	1.41±0.08	3.92±0.02	6.86±0.11
	160	1.30±0.06	4.86±0.42	-	-

Table 25. Conversion of functional groups of silica and Nanoprene®

Nanoprene® grades	Temp. [°C]	Conversion of functional groups [%]			
		20 min	60 min	180 min	300 min
Silica	120	6.8±0.36	7.5±0.22	7.5±0.40	7.4±0.45
	140	7.3±0.15	7.7±0.09	8.1±0.42	8.6±0.04
	160	6.0±0.33	6.7±0.15	-	-
OBR 1504 D	120	1.6±0.07	2.3±0.11	3.3±0.32	5.0±0.28
	140	1.8±0.04	3.2±0.13	5.7±0.24	18.0±0.62
	160	3.5±0.10	12.8±0.45	-	-
OBR 1504 F	120	3.0±0.05	5.3±0.08	10.2±0.50	14.2±1.00
	140	3.5±0.03	7.3±0.32	16.2±0.29	22.0±0.23
	160	9.7±0.83	22.3±1.53	-	-
OBR 1504 G	120	2.4±0.06	3.7±0.02	6.4±0.30	8.3±0.23
	140	2.9±0.03	4.9±0.09	10.4±0.09	17.7±1.29
	160	7.0±0.33	16.6±1.03	-	-
OBR 1504 H	120	1.4±0.02	1.6±0.02	1.8±0.04	2.0±0.18
	140	1.3±0.05	1.4±0.04	2.3±0.04	4.2±0.23
	160	1.4±0.10	2.6±0.28	-	-
OBR 1504 I	120	1.6±0.03	1.9±0.03	3.3±0.09	4.9±0.14
	140	1.5±0.03	2.5±0.15	6.0±0.43	17.9±1.41
	160	2.8±0.05	7.8±0.20	-	-
OBR 1504 K	120	2.6±0.06	3.6±0.07	5.6±0.11	7.6±0.39
	140	2.6±0.12	4.4±0.10	7.9±0.08	16.3±1.43
	160	4.8±0.13	10.5±0.16	-	-
OBR 1504 L	120	18.0±0.71	22.0±1.00	27.1±0.67	30.7±0.90
	140	17.7±0.77	27.5±0.15	30.0±0.07	37.6±1.03
	160	21.2±0.65	35.6±0.65	-	-
OBR 1504 M	120	18.0±1.37	22.0±1.52	27.1±0.67	30.7±0.89
	140	19.1±0.73	29.7±0.67	34.6±1.50	49.0±3.52
	160	21.5±0.78	35.6±0.77	-	-
OBR 1504 N	120	4.5±0.12	7.2±0.25	11.5±0.59	17.5±0.81
	140	5.7±0.23	10.9±0.08	20.4±0.19	27.1±0.70
	160	13.1±0.95	26.8±0.51	-	-
BM 75OH	120	1.8±0.05	3.3±0.07	7.9±0.10	12.8±0.10
	140	2.1±0.03	4.8±0.27	13.4±0.05	23.5±0.38
	160	4.5±0.22	16.6±1.51	-	-

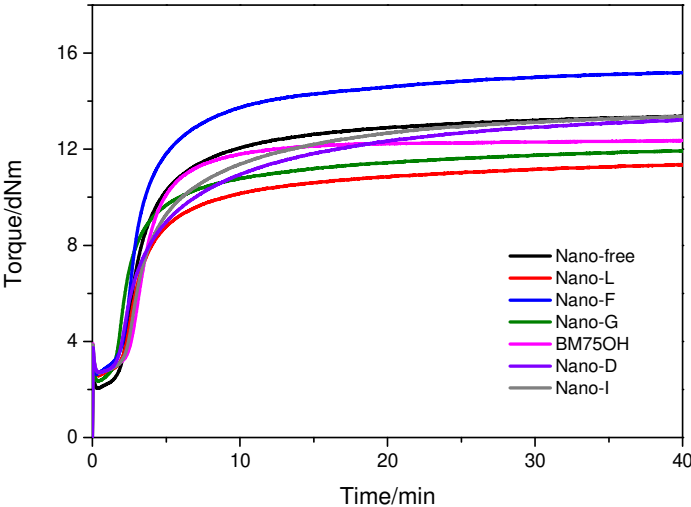


Figure 73. Influence of different functionalized nanoparticles on the rheological characteristics at 160 °C

---

**Abbreviations**

a	Radius
ASTM	American Society for Testing Materials
ATR	Attenuated total reflectance
BR	Polybutadiene (butadiene rubber)
C	Kraus parameter
CBS	N-cyclohexyl-2-benzothiazolesulfenamide
CTAB	Cetyltrimethylammonium bromide
DIN	Deutsche Industrie-Norm (German Industrial Standards)
DMA	Dynamical mechanical analysis
DPG	Diphenylguanidine
DSC	Differential scanning calorimetry
$E_a$	Activation energy
EP(D)M	Ethylene propylene rubber
f	Shape factor
$\Delta F$	Change of free energy
$\Delta F_m$	Ordinary free energy
$\Delta F_{el}$	Elastic free energy
$Fe^{2+}$	Ferrous ion
FM	Functional monomer
FTIR	Fourier transform infrared spectroscopy
G	Modulus
$G_0$	Modulus of the gum rubber
$G^*$	Dynamic shear modulus
$G'$	Dynamic storage modulus or elastic modulus
$G''$	Dynamic loss modulus or viscous modulus
GC	Gas chromatography
GCMS	Gas chromatography with mass spectrometry detection
Ge	Germanium
HN	Hydroxyl number
HPLC	High performance liquid chromatography
HSGC	Headspace gas chromatography
IIR	Isobutylene isoprene rubber (butyl-rubber)
k	Boltzmann constant
$k_a$	Reaction rate constant

## Abbreviations

---

KOH	Potassium hydroxide
$M_{100}$	Stress modulus at 100 % elongation
$M_{300}$	Stress modulus at 300 % elongation
$M_c$	Average molecular weight of a network chain
ML	Mooney viscosity (with large rotor)
MBT	2-Mercaptobenzothiazole
MBTS	2,2'-Dithiobenzothiazole
$M_n$	Average number molecular weight of polymer
$n_i$	Mole number
N	Avogadro's number
NBR	Acrylonitrile butadiene rubber,
NR	Nature rubber
OH	Hydroxyl group
OCTEO	Triethoxy(octyl)silane
P	Pressure
phr	Parts in weight per 100 g rubber
Q	Equilibrium swelling value
R	Gas constant
RPA	Rubber process analyzer
Si	Silicium
S-SBR	Solution poly(styrene-co-butadiene) rubber
SMO	Sorbitan monooleate
t	Time
T	Temperature
TESPD	Bis[3-(triethoxysilyl)-propyl]disulfide
TESPT	Bis[3-(triethoxysilyl)-propyl]tetrasulfide
$\tan \delta$	Loss factor ( $G''/G'$ )
TEM	Transmission electron microscopy
$T_g$	Glass transition temperature
$t_{90}$	Time when 90 % conversion is achieved
$\nu$	Crosslink density
$\nu_i$	Volume fraction
$\nu_e$	Effective number of chains in the network
$\nu_0$	Total number of cross-linkages
V	Volume of the swollen network



---

$V_0$	Volume of the unswollen polymer
$V_{r_0}$	Volume fraction of unfilled rubber
$V_{r_f}$	Volume fraction of filled rubber
$w$	Weight fraction of monomer
$W_i$	Weight of the sample
$x$	Number of segments
$\delta$	Phase angle
$\eta$	Viscosity
$\eta_0$	Viscosity of the gum rubber
$\phi$	Filler volume fraction
$\sigma$	Stress
$\sigma_0$	The maximum stress
$\varepsilon$	Strain
$\varepsilon_0$	The maximum strain
$\omega$	Radian frequency
$\chi$	Polymer solvent interaction parameter
$\rho$	Density
$\varphi_1$	Molar volume of the solvent
$\Delta\mu$	Chemical potential

## Acknowledgments

The work described in this thesis was performed in Deutsches Institut für Kautschuktechnologie e.V. (DIK) under the supervision of Prof. Dr. U. Giese and Prof. Dr. C. Vogt from March 2014 until August 2017.

First of all I would like to express my deepest gratitude to my supervisor Prof. Dr. U. Giese for his excellent guidance, worthwhile discussions, ideas, and his advice which supported me to finish my PhD work. I am sure that his teaching and coaching during this period will help me in my future career.

I would also like to thank Prof. Dr. C. Vogt from the Institute of Analytic Chemistry for the acceptance as supervisor of this work.

Many thanks goes also to Prof. Dr. W. Obrecht from whom I learned a lot in rubber chemistry and technology. I would like to thank him for his recommendation for the funding by Lanxess (Arlanxeo), for the useful discussions and suggestions concerning my work and for the support showed over these years.

I would like to express my thanks to Prof. Dr. J. Caro from the Institute of Physical Chemistry and Electrochemistry for the acceptance as chair of the examination board.

I truly appreciate and thank Dr. T. Frueh whose valuable discussions, ideas and advice really helped me during my PhD work.

I really appreciate and admire the work done together with my colleagues at the DIK: Mr. J. Hamann, Mr. J. Heier, Mrs. S. Bauder, Dr. A. Diekmann, Mr. B. Matschke, Mr. P. Erren, Mr. T. Giesecke, and Dr. H. Wittek.

I would also like to address my thanks to Lanxess (Arlanxeo) Deutschland GmbH for the financial support of this work.

Last but not the least, my special thanks goes to all of my friends and my family who always supported me during my stay even though I was far away from China.

## Curriculum vitae

### Personal data:

Name: Xu

First name: Minghan

Date of birthday: 28.04.1986

Place of birthday: Jilin, China

Nationality: Chinese

### Education background:

09/2005-06/2009	Bachelor of Engineering in Polymer Materials Science and Engineering at Qingdao University of Science and Technology, China.
09/2009-06/2012	Master of Science in Polymer Chemistry and Physics at Qingdao University of Science and Technology, China.

### Work experience:

12/2011-02/2014	Analytical lab specialist at Lanxess Chemical Co., Ltd. (China) in High Performance Rubber Research & Develop Center, Qingdao, China.
03/2014-2017	Dissertation at Leibniz Universität Hannover, Institute for inorganic chemistry. The work was done in Deutsches Institut für Kautschuktechnologie e.V. in Hannover, based on research projects financed by Lanxess Deutschland GmbH.

Hanover, 2017

Minghan Xu

Oral presentations:

“Influence of Water Storage on Silica Loaded Tire Tread Vulcanizates”

Minghan Xu, Ulrich Giese, Werner Obrecht

16th International Seminar on Elastomers (ISE), 14.06.-17.06.2016, Qingdao, China

“Influence of Water on Dynamic Mechanical Properties of Silica Loaded Tire Tread Vulcanizates”

Minghan Xu, Ulrich Giese, Werner Obrecht, Thomas Frueh

12th Fall Rubber Colloquium (Kautschuk-Herbst-Kolloquium, KHK), 22.11.-24.11.2016, Hanover, Germany

Publications:

“Influence of Water on Dynamic Mechanical Properties of Silica Loaded Tire Tread Vulcanizates”

Minghan Xu, Ulrich Giese, Werner Obrecht, Thomas Frueh

Kautschuk Gummi Kunststoffe, 2017, 4 (17), 47-53.